UNIVERSIDADE ESTADUAL DE CAMPINAS
Instituto de Física Gleb Wataghin

Christyan Costa de Oliveira

Analog Models for the BTZ Black Hole

Modelos Análogos para o Buraco Negro de BTZ

Campinas
2023

Christyan Costa de Oliveira

Analog Models for the BTZ Black Hole

Modelos Análogos para o Buraco Negro de BTZ

Tese apresentada ao Instituto de Física Gleb Wataghin da Universidade Estadual de Campinas como parte dos requisitos para a obtenção do título de Doutor em Física.

Thesis presented to the Gleb Wataghin Institute of Physics of the University of Campinas in partial fulfillment of the requirements for the degree of Doctor in Physics.

Supervisor/Orientador: Prof. Dr. Ricardo Antonio Mosna
Co-supervisor/Coorientadora: Prof. Dra. Carola Dobrigkeit Chinellato

Este trabalho corresponde à versão final da Tese defendida por Christyan Costa de Oliveira e orientada pelo Prof. Dr. Ricardo Antonio Mosna.

Campinas
2023

Ficha catalográfica
Universidade Estadual de Campinas
Biblioteca do Instituto de Física Gleb Wataghin
Lucimeire de Oliveira Silva da Rocha - CRB 8/9174

OL4a Oliveira, Christyan Costa de, 1992-
Analog models for the BTZ black hole / Christyan Costa de Oliveira. – Campinas, SP : [s.n.], 2023.

Orientador: Ricardo Antonio Mosna.
Coorientador: Carola Dobrigkeit Chinellato.
Tese (doutorado) – Universidade Estadual de Campinas, Instituto de Física Gleb Wataghin.

1. Modelos análogos. 2. Buracos negros de Banados-Teitelboim-Zanelli. I. Mosna, Ricardo Antonio, 1974-. II. Chinellato, Carola Dobrigkeit, 1952-. III. Universidade Estadual de Campinas. Instituto de Física Gleb Wataghin. IV. Título.

Informações Complementares

Título em outro idioma: Modelos análogos para o buraco negro de BTZ
Palavras-chave em inglês:
Analogue models
Banados-Teitelboim-Zanelli black holes
Área de concentração: Física
Titulação: Doutor em Ciências
Banca examinadora:
Ricardo Antonio Mosna [Orientador]
Alberto Vazquez Saa
Pedro Cunha de Holanda
Roldão da Rocha Júnior
Vilson Tonin Zanchin
Data de defesa: 15-03-2023
Programa de Pós-Graduação: Física

Identificação e informações acadêmicas do(a) aluno(a)
- ORCID do autor: https://orcid.org/0000-0001-7799-5366
- Currículo Lattes do autor: http://lattes.cnpq.br/9492903929113502

MEMBROS DA COMISSÃO EXAMINADORA DA TESE DE DOUTORADO DO ALUNO CHRISTYAN COSTA DE OLIVEIRA - RA 190930 APRESENTADA E APROVADA AO INSTITUTO DE FÍSICA GLEB WATAGHIN, DA UNIVERSIDADE ESTADUAL DE CAMPINAS, EM 15/03/2023.

COMISSÃO JULGADORA:

- Prof. Dr. Ricardo Antonio Mosna – Presidente e orientador (IMECC/UNICAMP)

- Prof. Dr. Alberto Vazquez Saa (IMECC/UNICAMP)

- Prof. Dr. Pedro Cunha de Holanda (IFGW/UNICAMP)

- Dr. Roldão da Rocha Júnior (Universidade Federal do ABC)

- Dr. Vilson Tonin Zanchin (Universidade Federal do ABC, Centro de Ciências Naturais e Humanas)

OBS.: Ata da defesa com as respectivas assinaturas dos membros encontra-se no SIGA/Sistema de Fluxo de Dissertação/Tese e na Secretaria do Programa da Unidade.

CAMPINAS

2023

Acknowledgments

I would like to express my deepest gratitude to my supervisor, Dr. Ricardo A. Mosna, for his invaluable guidance during my academic formation journey and especially in the years I spent working on this thesis. I am also grateful to Dr. Carola D. Chinellato for her assistance and coorientation during this period.

I am also grateful to Dr. João P. M. Pitelli for his help in finding, understanding and interpreting the results obtained along this research.

Special thanks to M. Richartz for insightful discussions and feedback, which were fundamental to clarify the exposition of the results in this thesis.

I am also thankfull to all the administrative staff and the librarians of the Gleb Wataghin Institute of Physics for their technical support.

I would also like to thank the State University of Campinas (UNICAMP) for providing the infrastructure and the academic environment necessary for the completion of this work.

This endeavor would not have been possible without the financial support from the Conselho Nacional de Desenvolvimento Científico e Tecnológico (CNPq, Brazil), under Grant No. 142529/2018-4.

Lastly, I thank my family for the support along this journey.

Resumo

Uma analogia bem formulada pode em alguns casos ser uma ferramenta de raciocínio bastante eficiente. Quando devidamente aplicada, pode ressaltar conexões que seriam difíceis de enxergar por outro modo. Nesta tese, aplicamos métodos comumente associados à área de pesquisa em Modelos Análogos à Gravitação (Analog Gravity) para analisar alguns aspectos da propagação de ondas no buraco negro de Bañados, Teitelboim e Zanelli (BTZ).

A área de Modelos Análogos à Gravitação ocupa-se de estabelecer conexões (tanto teóricas como experimentais) entre sistemas gravitacionais e sistemas de outras áreas da física, com o objetivo de entender mais profundamente ambos os sistemas.

Inicialmente apresentamos uma breve visão geral a respeito dos conceitos básicos envolvidos no estudo de Modelos Análogos à Gravitação, e apresentamos o espaço-tempo que pretendemos analisar (o espaço-tempo de BTZ).

Em seguida, apresentamos um modelo análogo para o espaço-tempo de BTZ, o qual é baseado no escoamento unidirecional de um fluido heterogêneo. Mais adiante, analisamos a excitação dos modos característicos de oscilação (modos quase-normais) do campo escalar no espaço-tempo de BTZ em termos do modelo análogo obtido.

Finalmente, apresentamos um modelo análogo baseado no bocal de Laval — um bocal com secção transversal variável que inicialmente converge e posteriormente diverge, formando uma garganta na região central, e que comumente é usado para acelerar o ar — e analisamos o efeito que a imposição de condições de contorno de Robin no infinito espacial exerce sobre a dinâmica no seu interior. Estudamos ainda os efeitos causados por estas condições de contorno por meio do modelo análogo apresentado.

Abstract

A well-designed analogy can sometimes provide a very effective way of reasoning. When properly applied, it may highlight conections that are difficult to see otherwise. In this thesis, we employ the methods of the Analog Gravity research program to analyse some aspects of wave propagation in the Bañados, Teitelboim and Zanelli (BTZ) black hole.

The Analog Gravity program deals with establishing connections (both theoretical and experimental) between gravitational systems and systems belonging to other areas of physics, aiming to achieve in this way a deeper understanding of both sides.

Initially, in this work, we give a brief overview of the basic concepts involved in the study of analog models of gravity and present the spacetime we intend to emulate (the BTZ spacetime).

After that, we introduce a novel analog model of the BTZ spacetime based on the unidirectional flow of a nonhomogeneous fluid. Then we analyse the excitation of the characteristic oscillation modes (the quasinormal modes) of the scalar field in the BTZ spacetime in terms of the obtained analog model.

Finally, we introduce an analog model based on the Laval nozzle — which is a convergent-divergent nozzle with a throat in the middle, usually employed to accelerate air — and analyse the effect that imposing Robin boundary conditions at the BTZ spatial infinity has on the dynamics in the spacetime bulk. We study these effects by means of the analog model presented here.

Contents

Chapter 1

Introduction

In a broad sense, an analogy can be defined as the process of using the known features of a particular subject to explain and understand the features of another subject. It is a powerful cognitive tool for individuals to approach reality in everyday life since it relies on previously accumulated experiences to draw inferences when one faces new scenarios. However, when naively employed, an analogy might lead to misleading conclusions, and, in a time of increasing spreading of misinformation, this can ultimately cause irreversible harm to individuals and to society as a whole.

In the context of science, where criteria are arguably more rigorous, this tool of reasoning (analogy) has a wide range of applications. A particularly fruitful area where arguments based on analogy have thrived is the so-called *Analog Gravity* (also referred to as *analog models of gravity*) [1]. The Analog Gravity research program is based on the observation that the propagation of classical or quantum fields in curved spacetimes can be mapped into the propagation of perturbations in background states of systems belonging to other branches of physics. The time evolution of perturbations is governed by a wave-like equation determined by a (Lorentzian) *effective metric* which, in turn, fully depends on the background.

Since the background is governed by equations of motion unrelated to the Einstein field equations of General Relativity (GR) [2, 3, 4, 5], the approach based on an analog model naturally leads us to think deeply about the fundamental differences among features resulting uniquely from the curved spacetime structure (which are generally referred to as *kinematical* features) and features resulting from the Einstein field equations (which are generally referred to as *dynamical* features). In particular, this approach leads us to consider the fundamental role and differences between Lorentzian Geometry, the Einstein equivalence principle, and GR as a whole. For instance, one can show that aspects such as Hawking radiation [6] and horizons, which are generally thought of as intrinsic to GR, are, in fact, general features of quantum field theory in curved spacetimes [7, 8, 9, 10], not fundamentally related with gravity.

The seminal work establishing the beginning of the modern period of analog gravity is Unruh's paper [7], published in 1981. The physical system implemented was a perfect fluid, and the goal was to probe fundamental issues — such as the trans-Planckian problem [11, 12, 13] — regarding Hawking radiation within a context where the microscopic degrees of freedom of the underlying background were fully understood. The initial motivation to explore the similarities between this system and gravity can be summarized, in the words of the author, by:

> "This system forms an excellent theoretical laboratory where many of the unknown effects that quantum gravity could exert on black hole evaporation can be modelled. (...) At distances of 10^{-8} cm, the assumptions which I use of a smooth background flow are no longer valid just as in gravity one expects the concept of a smooth spacetime on which the various relativistic fields propagate to breakdown at scales of 10^{-33} cm."

After the publication of [7], more developments in the same direction were pursued [13, 14, 15, 16, 17, 18, 19]. Aside from that, many other analog models of gravity, implementing both classical and quantum systems, were discovered in the following years. For instance, we mention models based on: surface waves in a shallow basin [20]; Bose-Einstein condensates [21, 22, 23, 24], nonlinear electrodynamics [25], etc. For an extensive list, we refer the reader to the already mentioned review [1] and the works [26], [27] and references therein.

Finally, in the last decades, the efforts on the experimental side culminated in the observation of phenomena such as analog Hawking radiation [28, 29, 30, 31, 32, 33]; superradiant amplification [34]; and the quasinormal ringing of an analog black hole [35, 36]. For an account of the current state of affairs and future prospects of experiments in analog gravity, we refer the reader to [37].

Although the efforts of the last years have significantly turned towards the experimental side, it is still worth considering analog models from a theoretical perspective since thought experiments and toy models often provide insightful grounds to test GR effects by means of systems governed by simpler laws. It is with this spirit that we approach the problems considered in this thesis, but before presenting the specific subject of this work, we still have to discuss some essential points in order to put things in perspective.

The description of wave propagation in GR is usually formulated in the context of *globally hyperbolic* spacetimes. For this kind of spacetime, the wave motion is completely determined by a wavelike equation together with proper initial conditions. However, when one drops the assumption of global hyperbolicity, the wave time evolution is no longer uniquely determined from the equations of motion together with proper initial conditions. Indeed, spatial infinity now plays a fundamental role in the dynamics, and appropriate boundary conditions are required in order to fully describe the motion in bulk. A spacetime lacking global hyperbolicity is also referred to as a *nonglobally* hyperbolic spacetime.

As an example of nonglobally hyperbolic spacetime, we mention the anti-de Sitter space (AdS) [5, 3], a maximally symmetric solution of General Relativity with a negative cosmological constant. In AdS spacetime, null geodesics can reach spatial infinity for a finite value of the affine parameter, which means that information can effectively flow through spatial infinity. In work [38], the authors characterized the non-dynamical boundary conditions at the conformal boundary of the two-dimensional anti-de Sitter space, AdS_2, using an analog model based on a perfect fluid flowing radially into/from a sink/source. They showed that the boundary conditions at the AdS_2 conformal boundary are encoded into the phase difference between circularly symmetric waves falling into the sink/source and waves reflected. By regularizing the velocity profile of the fluid in the vicinity of the sink/source — which at the analog spacetime level corresponds to deforming AdS_2 at its infinity —, it was found that appropriate boundary conditions are automatically imposed according to the specific form of the function used to perform the regularization [39].

Another interesting example of nonglobally hyperbolic spacetime is the Bañados, Teitelboim and Zanelli (BTZ) black hole [40], which is a solution to (2+1)-dimensional GR with a negative cosmological constant. The rotating BTZ black hole has many properties in common with the Kerr black hole [2, 4, 41]. For instance, it is stationary and axisymmetric and (in the non-extremal case) has an inner and an outer horizon [42, 43, 44]. Nevertheless, instead of asymptotically flat, the asymptotic structure of the BTZ black hole is ruled by the AdS_3 geometry. The BTZ black hole also has a timelike conformal boundary at its spatial infinity, so that information can reach spatial infinity in finite time, reflecting the lack of global hyperbolicity of this spacetime.

Our focus in this thesis is to emulate the effects resulting from the presence of the BTZ conformal boundary on wave propagation by means of properly designed analog models. The main physical observables we will consider are the *quasinormal modes* (QNMs) [45, 46, 47], characteristic vibrations that depend only on the background spacetime parameters. For asymptotically flat black holes, the effective potential describing wave propagation vanishes at spatial infinity so that we have a plane wave behavior for the field there. Hence, in this case, we can define QNMs as mode solutions of an eigenvalue problem obeying ingoing (plane wave) boundary conditions at the horizon and outgoing (plane wave) boundary conditions at infinity.

On the other hand, for asymptotically curved black holes (which is the case o the BTZ spacetime), aside from the difficulty imposed by the lack of global hyperbolicity, the effective potential does not vanish at spatial infinity, and no plane wave (neither ingoing nor outgoing) boundary conditions can be fulfilled there. Thus we cannot distinguish ingoing modes from outgoing modes at spatial infinity [48, 49]. Hence the definition of QNMs, in this case, will necessarily involve the prescription of boundary conditions describing the state of the field and the energy flux at infinity. In the particular case of the BTZ black hole, the spatial infinity corresponds to a timelike conformal boundary, and the necessity of boundary conditions highlights the fundamental role played by the boundary in the description of the dynamics in bulk.

We are going to use two different physical systems as analog models to investigate scalar wave propagation in the BTZ black hole. First, we will consider the canonical case of acoustic waves propagating in an inviscid barotropic fluid. We will show that when the fluid pressure p and density ρ obey the simplest non-trivial equation of state

$$p = c\rho, \tag{1.1}$$

with the sound speed c being a constant, we can find profiles for the physical quantities (v, ρ, p) so that acoustic waves in the fluid are equivalent to massless scalar waves propagating in the static BTZ black hole.

The second system we use to model the BTZ geometry is an isentropic gas flowing within a Laval nozzle. The Laval nozzle is a convergent-divergent nozzle with a throat in the middle, usually employed to accelerate air. When the ends of the nozzle are submitted to a sufficiently strong pressure difference, a transonic flow is achieved [50, 51]. In such a case, an acoustic horizon (the point where gas velocity equals sound speed) forms at the nozzle throat. In a Laval nozzle, all the physical quantities describing the fluid (p, ρ, v, c, ...) can be determined from the cross-sectional area A of the nozzle. Thus, by judiciously prescribing an area profile, one can emulate the effective potential for massive scalar waves traveling in spherically symmetric spacetimes [52, 53].

We have organized this thesis in the following manner. First, in Chapter 2, we present a general view of the Analog Gravity framework. As a prototypical system, we consider the propagation of acoustic waves in the bulk of an inviscid fluid in motion. We derive the effective geometry to which the waves couple and discuss how the concepts of GR can be carried to other physical contexts. We also discuss how the effective geometry inherits some properties from physical spacetime.

In Chapter 3, we review some basic concepts concerning the geometry of the BTZ black hole and the quasinormal modes of the scalar field propagating in this spacetime. In particular, we show how the boundary conditions at spatial infinity influence the dynamics in the spacetime bulk.

In Chapter 4, we introduce an analog model for the BTZ black hole by performing appropriate coordinate transformations on the effective metric presented in Chapter 2. We find that our model effectively maps the BTZ conformal boundary into a location at finite distance in laboratory. After that, we numerically solve the nonlinear equations of motion of fluid dynamics to study the excitation and decay of quasinormal modes in the analog BTZ spacetime. The material in this chapter was published in [54].

In Chapter 5, we consider acoustic waves in the Laval nozzle and find a nozzle form such that the sound propagation mimics the propagation of a conformally coupled scalar field on the BTZ black hole. We find that the corresponding nozzle has a finite size, with the BTZ spatial infinity being effectively mapped onto one of the nozzle ends. We show that one can emulate the implementation of Robin boundary conditions (RBCs) at the BTZ conformal boundary by properly extending the nozzle. The material in this chapter is based on our work [55].

In Appendix A, we present a work written in parallel with the research for the main subject of this thesis. In the work [56], we study the energy flux through spatial infinity of a scalar field propagating in an asymptotically anti-de Sitter spacetime. We show that in the general case when there is a superposition of field modes, the boundary conditions of Dirichlet and Neumann types are the only boundary conditions compatible with the assumption that the spacetime is isolated.

Appendix B gives a brief introduction to the theory of scalar field propagation in nonglobally hyperbolic spacetimes. We start by introducing the basic tools of the formalism and then apply them to the case of the BTZ spacetime.

Chapter 2

General Features of Analog Models

In this chapter, we present a general view of the basic concepts and mathematical machinery of the Analog Gravity research program. We start by deriving the canonical result that acoustic waves propagating in the bulk of a nonhomogeneous fluid are equivalent to a scalar field propagating in an (effective) spacetime endowed with a metric determined by the background state of the fluid. After that, we discuss how the kinematical and dynamical aspects of General Relativity (GR) relate to the description in terms of the effective geometry obtained. We also discuss the causal structure of the analog spacetime and how some concepts of GR (as horizons and ergoregions) can be naturally defined at the analog spacetime level. Finally, we present a general approach unifying the description of systems that can be treated in terms of effective/analog geometries. The material in this chapter is widely known in the field and our exposition is strongly based on the references [1, 26, 8].

2.1 The Effective Metric

The fundamental equations of motion for a classical fluid with velocity field given by $\vec{v}(t, \vec{x})$ and density $\rho(t, \vec{x})$ are [57] the equation of continuity

$$\frac{\partial \rho}{\partial t} + \nabla \cdot (\rho \vec{v}) = 0, \tag{2.1}$$

and the Euler equation

$$\rho \frac{d\vec{v}}{dt} = \rho \left[\frac{\partial \vec{v}}{\partial t} + (\vec{v} \cdot \nabla)\vec{v} \right] = \vec{F}, \tag{2.2}$$

where $\vec{F}$ represents the net force acting upon a volume element of the fluid.

We assume the fluid to be nonviscous so that the internal surface forces are only those due to pressure p. Additionally, we consider the Newtonian gravitational potential, ϕ, and an external bulk force due to an arbitrary potential, Φ, so that the total force is given by

$$\vec{F} = -\nabla p - \rho\nabla\phi - \rho\nabla\Phi. \tag{2.3}$$

Further assuming that the flow is irrotational ($\nabla \times \vec{v} = 0$), and the fluid is barotropic (this means that pressure depends only on the density), we can rewrite the Euler equation (2.2) as

$$\frac{\partial\vec{v}}{\partial t} = -\frac{\nabla p}{\rho} - \nabla\left[\frac{1}{2}\vec{v}^2 + \phi + \Phi\right]. \tag{2.4}$$

Taking $\psi(t, \vec{x})$ as the velocity potential ($\vec{v} = -\nabla\psi$) and defining enthalpy by

$$h(p) = \int_0^p \frac{dp'}{\rho(p')}, \qquad \text{so that} \qquad \nabla h = \frac{\nabla p}{\rho}, \tag{2.5}$$

the Euler equation can be recasted as the Bernoulli equation

$$-\frac{\partial\psi}{\partial t} + \frac{1}{2}(\nabla\psi)^2 + h + \phi + \Phi = 0. \tag{2.6}$$

Given an initial profile for the density ρ and velocity potential ψ, and a barotropic equation of state, $p = p(\rho)$, the dynamics of the fluid is completely determined by Eqs. (2.1) and (2.6). In order to find the equation of motion for acoustic disturbances in the fluid, we linearize these equations around a background solution. We do this by considering the full solution of Eqs. (2.1) and (2.6) as being the sum of a contribution due to the background state (with physical quantities denoted by $\psi_0, \vec{v}_0, \rho_0, \dots$), plus a contribution due to the linear acoustic perturbations (with physical quantities denoted by $\psi_{(1)}, \vec{v}_{(1)}, \rho_{(1)}, \dots$), plus a contribution due to second order perturbations, and so on. Of course, we assume that the amplitudes of the perturbations are small when compared to the amplitude of background physical quantities.

Linearizing the equation of continuity yields

$$\frac{\partial\rho_0}{\partial t} + \nabla\cdot(\rho_0\vec{v}_0) = 0, \tag{2.7}$$

$$\frac{\partial\rho_{(1)}}{\partial t} + \nabla\cdot\left[\rho_{(1)}\vec{v}_0 + \rho_0\vec{v}_{(1)}\right] = 0. \tag{2.8}$$

From the barotropic condition, it follows

$$h(p) = h(p_0 + \epsilon p_{(1)} + O(\epsilon^2)) = h_0 + \epsilon \frac{p_{(1)}}{\rho_0} + O(\epsilon^2). \tag{2.9}$$

Substituting this relation in the linearized Bernoulli equation (2.6), gives

$$-\frac{\partial \psi_0}{\partial t} + \frac{1}{2} (\nabla \psi_0)^2 + h_0 + \phi + \Phi = 0 \tag{2.10}$$

$$-\frac{\partial \psi_{(1)}}{\partial t} + \frac{p_{(1)}}{\rho_0} - \vec{v}_0 \cdot \nabla \psi_{(1)} = 0. \tag{2.11}$$

Here we are assuming that the variations of the fluid physical variables do not affect the external potentials ϕ and Φ, that is, we do not allow back-reaction. Putting differently, in the present case, linear disturbances are insensitive to variations in the external potentials.

From Eq. (2.11), we have

$$p_{(1)} = \rho_0 \left[\frac{\partial \psi_{(1)}}{\partial t} + \vec{v}_0 \cdot \nabla \psi_{(1)} \right], \tag{2.12}$$

and using the barotropic assumption, it follows

$$\rho_{(1)} = \left(\frac{\partial \rho}{\partial p} \right)_0 p_{(1)} = \left(\frac{\partial \rho}{\partial p} \right)_0 \rho_0 \left[\frac{\partial \psi_{(1)}}{\partial t} + \vec{v}_0 \cdot \nabla \psi_{(1)} \right], \tag{2.13}$$

where the subscript '0' in the derivative $(\partial \rho / \partial p)_0$ means that we evaluate it with respect to the background state of the flow.

Substituting this last result into the linearized equation of continuity Eq. (2.8), we find the wave equation for acoustic perturbations

$$-\frac{\partial}{\partial t} \left\{ \left(\frac{\partial \rho}{\partial p} \right)_0 \rho_0 \left[\frac{\partial \psi_{(1)}}{\partial t} + \vec{v}_0 \cdot \nabla \psi_{(1)} \right] \right\} + \nabla \cdot \left\{ \rho_0 \nabla \psi_{(1)} - \vec{v}_0 \left(\frac{\partial \rho}{\partial p} \right)_0 \rho_0 \left[\frac{\partial \psi_{(1)}}{\partial t} + \vec{v}_0 \cdot \nabla \psi_{(1)} \right] \right\} = 0. \tag{2.14}$$

Given a background state solving the Eqs. (2.7) and (2.10), we determine the propagation of the perturbation in the velocity potential $\psi_{(1)}$ by solving Eq. (2.14). Having obtained $\psi_{(1)}$, we can use Eqs. (2.12) and (2.13) to find the disturbances in the pressure and density, respectively. Thus it follows that Eq. (2.14) fully determines the time evolution of acoustic waves in the fluid.

To recast the wave equation (2.14) in a form suitable to direct application of the Lorentzian differential geometry mathematical machinery, we define the auxiliar 4×4 symmetric matrix[1]

$$f^{\mu\nu}(t,\vec{x}) = \frac{\rho_0}{c^2}\left[\begin{array}{ccc} -1 & \vdots & -v_0^j \\ \cdots & \cdot & \cdots\cdots\cdots\cdots\cdots\cdots \\ -v_0^j & \vdots & \left(c^2\delta^{ij} - v_0^i v_0^j\right) \end{array}\right], \tag{2.15}$$

where c stands for the local speed of sound and is given by

$$c^{-2} = \left(\frac{\partial\rho}{\partial p}\right)_0 . \tag{2.16}$$

Introducing $(3+1)$-dimensional coordinates $x^{\mu\nu} \equiv (t, x^i)$, the wave equation (2.14) can be rewritten as[2]

$$\partial_\mu\left(f^{\mu\nu}\partial_\nu\psi_{(1)}\right) = 0. \tag{2.17}$$

In this form, the acoustic wave equation remarkably resembles the equation of motion for a minimally coupled massless scalar field propagating in a curved spacetime

$$\Box\psi = \frac{1}{\sqrt{-g}}\partial_\mu\left(\sqrt{-g}g^{\mu\nu}\partial_\nu\psi\right) = 0, \tag{2.18}$$

where $\Box = \nabla_\mu\nabla^\mu$ denotes the d'Alembert operator, and ∇_μ stands for the covariant derivative.

In order to accomplish the correspondence between these equations, a necessary condition is

$$\sqrt{-g}g^{\mu\nu} = f^{\mu\nu}. \tag{2.19}$$

Assuming that Eq. (2.19) holds, we find

$$g = \frac{\rho_0^4}{c^2}, \tag{2.20}$$

[1]Greek indices run from 0 to 3, and latin indices run from 1 to 3.

[2]All over the text, we will denote the partial derivative with respect to the μ-th coordinate in the traditional form

$$\partial_\mu = \frac{\partial}{\partial x^\mu}.$$

and the inverse effective metric

$$g^{\mu\nu}(t,\vec{x}) = \frac{1}{\rho_0 c}\begin{bmatrix} -1 & \vdots & -v_0^j \\ \cdots & . & \cdots\cdots\cdots\cdots\cdots\cdots \\ -v_0^j & \vdots & \left(c^2\delta^{ij} - v_0^i v_0^j\right) \end{bmatrix}. \tag{2.21}$$

Inverting $g^{\mu\nu}$, we finally find the *effective metric*[3]

$$g_{\mu\nu}(t,\vec{x}) = \frac{\rho_0}{c}\begin{bmatrix} -(c^2 - v_0^2) & \vdots & -v_0^j \\ \cdots\cdots\cdots\cdots & . & \cdots \\ -v_0^j & \vdots & \delta^{ij} \end{bmatrix}_{4\times 4}. \tag{2.22}$$

We note that the effective metric has a signature $(-,+,+,+)$, which makes $g_{\mu\nu}$ in fact a Lorentzian metric. Along the text, we will sometimes refer to the spacetime with geometry described by Eq. (2.22) as the analog spacetime.

The description in terms of Eq. (2.18) with metric given by Eq. (2.22) is completely equivalent to the description given in terms of Eq. (2.14). Nevertheless, the formulation in terms of the effective metric makes an approach inspired in the physics of fields propagating in curved spacetimes much more attainable.

It might be enlightening to look at the derivation of the obtained description in the opposite direction. Indeed, if we start with an effective metric, we can ask what constraints a particular fluid has to satisfy in order to reproduce the respective effective geometry. From Eq. (2.22) we can in principle identify the fluid degrees of freedom. After that, we have to check if these quantities obey the fluid equations of motion Eqs. (2.1) and (2.2). By judiciously adding an external driving potential, we can always fulfil the Euler equation, Eq. (2.2). Thus, the realization of the effective geometry will be constrained only by the equation of continuity, Eq. (2.1). In fact, by implementing this kind of reasoning we were able to find analog models to the equatorial sections of the Schwarzschild and Reissner-Nordström black holes in [58].

It is important to point out that the discussion developed in this section entails two relevant distinct spacetimes:

[3] In the particular case of acoustic waves, this metric is also commonly referred in the literature as "acoustic metric" and "Unruh's metric". We opt to use "effective metric" because of its applicability to analog models based on physical systems of any kind.

(i) the physical spacetime, with geometry described by the Minkowski metric

$$\eta_{\mu\nu} = \begin{pmatrix} -c_{\text{light}} & 0 & 0 & 0 \\ 0 & 1 & 0 & 0 \\ 0 & 0 & 1 & 0 \\ 0 & 0 & 0 & 1 \end{pmatrix}, \tag{2.23}$$

where c_{light} stands for the speed of light. The fluid elements move in Newtonian space plus time and couple only to this metric (i.e., fluid elements do not "feel" the effective metric). Aside from that, we point out that since we derived the dynamics of propagation from classical equations of motion — Eqs. (2.1) and (2.2) —, we are, in fact, assuming that the fluid motion is completely non-relativistic, $|\vec{v}| \ll c_{\text{light}}$.

(ii) the effective/analog spacetime, with geometry described by the effective metric Eq. (2.22). The acoustic waves couple only to this metric and do not "feel" the metric of the physical spacetime.

2.2 Kinematics and Dynamics

The equations governing the dynamics of the effective metric will depend on the underlying physics of the system being considered. In the specific case of acoustic waves propagating in an inviscid fluid, the fundamental physical laws are the equation of continuity, Eq. (2.1), Euler's equation, Eq. (2.2), and the barotropic equation of state, $p = p(\rho)$. On the other hand, metrics of spacetimes of GR obey the Einstein field equations [2, 3, 4, 5]. Thus, by means of analog geometries, we are, in general, only able to simulate kinematical aspects —such as the effects of an externally imposed geometry on the fields and trajectories of particles— of GR. The simulation of dynamical aspects is a much more subtle question, and we refer the interested reader to [26, 59] for further discussions.

Although not entirely equivalent to GR, the study of analog models of gravity can still lead to a deeper understanding of gravity specifically providing plenty of concrete physical contexts that allow one to distinguish intrinsic aspects of GR (resulting from Einstein field equations) from generic aspects of physics in curved spacetimes.

Arguably one of the most interesting results obtained by the approach based on analog models is the realization that the emission of Hawking radiation is a purely kinematical effect, which only depends on the existence of a horizon and does not depend on the Einstein field equations [10, 9].

2.3 Causal Structure

At any event in Minkowski spacetime, the definition of the notions of past, present, and future rely on the concept of light cone [60], which is the region generated by trajectories of light rays in the high wavelength (small frequency) limit. The light cone is fundamental to understanding the causal structure of the Minkowski spacetime. In general Lorentzian curved spacetimes, the local causal structure is the same as that of Minkowski space. However, light cones can now be warped by the underlying spacetime geometry. The light cone is now described by null geodesics of the spacetime metric.

Let us see how these notions are directly carried over to the analog spacetime described by the effective metric Eq. (2.22). First, we take ansatz

$$\psi(x^\mu) = A(x^\mu)\exp[i\omega\Theta(x^\mu)], \tag{2.24}$$

where $A(x^\mu)$ and $\Theta(x^\mu)$ are amplitude and phase functions, respectively, and ω is the frequency $\omega \sim \lambda^{-1}$ (In GR, the small wavelength scale is set by the curvature of spacetime, while in acoustics, this is fixed by the interatomic distance of fluid particles). Substituting Eq. (2.24) into Eq. (2.18), at leading order, we find the eikonal equation

$$g^{\mu\nu}\partial_\mu\Theta\partial_\nu\Theta = 0. \tag{2.25}$$

Hence the gradient of the phase, $k_\mu \equiv \partial_\mu\Theta$, is a null vector field normal to the family of constant-phase hypersurfaces $\Theta(x^\mu) = \text{const}$. Taking the derivative of Eq. (2.25) and using the identity[4] $\nabla_\nu k_\mu = \nabla_\mu k_\nu$, one can straightforwardly show that

$$k^\mu\nabla_\mu k^\nu = 0, \tag{2.26}$$

[4]This identity follows immediately from the fact that k_μ is a gradient.

and thus conclude that the integral curves of k_μ are null geodesics of spacetime. The vector field k_μ defines a *null congruence* [61], which is a family of null geodesics with tangent vectors given by k_μ.

In the eikonal limit, the wavefront propagates along a null congruence. In the case of sound waves governed by Eq. (2.18), this corresponds to the geometric acoustics limit in which sound rays propagate along null geodesics of the effective metric. Since null geodesics are invariant with respect to conformal transformations of the metric, from (2.22), we see that sound rays are insensitive to the background density of the fluid, and depend only on the local sound speed and velocity of the fluid.

For a detailed analysis of the eikonal wavefront propagation and a comparison with the full wavefront determined by the exact solution of Eq. (2.18), we refer the reader to [62] and [63]. For a discussion concerning general aspects such as global causal structure and maximal analytic extensions of analog spacetimes, we refer the reader to [64].

2.4 Horizons and Ergoregions

Because the Minkowski metric of the physical spacetime provides a natural definition of "at rest", we can define the notions of horizon, ergoregion, ergosurface, and trapped surface [2, 4] in a relatively simple manner, with much less work than that required to define these objects in GR.

First, let us consider the timelike vector induced by the Newtonian time $(\partial/\partial t)^\mu = (1, 0, 0, 0)$. Then

$$g_{\mu\nu}\left(\frac{\partial}{\partial t}\right)^\mu\left(\frac{\partial}{\partial t}\right)^\nu = g_{tt} = -(c^2 - v^2). \tag{2.27}$$

At a supersonic region ($|\vec{v}| > c$), a subsonic particle cannot appear stationary with respect to an observer located at a region such that $|\vec{v}| < c$. Thus any region of supersonic flow is an *ergoregion*. The boundary of an ergoregion is an ergosurface. The analog of this notion in GR is the ergosphere that surrounds a spinning black hole: a region where space moves with superluminal velocity with respect to distant observers [2, 41].

Let us now consider a region in space enclosed by a 2-surface and such that the fluid velocity points inwards and its normal component is greater than the speed of sound everywhere. A sound wave emitted from the interior of this region cannot escape and will be trapped inside the surface. Such a surface is said to be an *outer-trapped* surface. *Inner-trapped* surfaces can be defined similarly by demanding the fluid velocity to point outwards and to have a normal supersonic component everywhere. The acoustic *trapped region* is defined as the region containing outer-trapped surfaces, and the acoustic *apparent horizon* is the boundary of the trapped region. Finally, the acoustic *event horizon* is defined as the boundary of the region from which null geodesics cannot escape.

2.5 Generalization: Lagrangian approach

The existence of analog models with very distinct physical natures, ranging from condensed matter to fluid dynamics, suggests the existence of a deeper common structure shared by these systems. In fact, in this section, we will see that propagation of acoustic waves in a fluid is just one instance of a much larger class of systems that can be described in terms of an effective geometry.

Let us consider a scalar field, ϕ, with dynamics given by an arbitrary Lagrangian which depends on the field and its first derivatives, $\mathcal{L}(\partial_\mu\phi, \phi)$. First, we write the field as

$$\phi(t,\vec{x}) = \phi_0(t,\vec{x}) + \epsilon\phi_1(t,\vec{x}) + \frac{\epsilon^2}{2}\phi_2(t,\vec{x}) + \cdots, \tag{2.28}$$

where ϵ is a perturbation parameter (which we take being “small"); ϕ_0 is a background state; ϕ_1 is a linear perturbation; ϕ_2 is a second-order perturbation; and so on.

We want to study the dynamical evolution of linear perturbations on the background state, so we expand the Lagrangian around ϕ_0,[5]

$$\begin{aligned}\mathcal{L}(\partial_\mu\phi,\phi) =& \mathcal{L}(\partial_\mu\phi_0,\phi_0) + \epsilon\left[\left.\frac{\partial\mathcal{L}}{\partial(\partial_\mu\phi)}\right|_{\phi_0}\partial_\mu\phi_1 + \left.\frac{\partial\mathcal{L}}{\partial\phi}\right|_{\phi_0}\phi_1\right] + \frac{\epsilon^2}{2}\left[\left.\frac{\partial\mathcal{L}}{\partial(\partial_\mu\phi)}\right|_{\phi_0}\partial_\mu\phi_2 + \left.\frac{\partial\mathcal{L}}{\partial\phi}\right|_{\phi_0}\phi_2\right]\\ &+\frac{\epsilon^2}{2}\left[\left.\frac{\partial^2\mathcal{L}}{\partial(\partial_\mu\phi)\partial(\partial_\nu\phi)}\right|_{\phi_0}\partial_\mu\phi_1\partial_\nu\phi_1 + 2\left.\frac{\partial^2\mathcal{L}}{\partial(\partial_\mu\phi)\partial\phi}\right|_{\phi_0}\partial_\mu\phi_1\,\phi_1 + \left.\frac{\partial^2\mathcal{L}}{\partial\phi\partial\phi}\right|_{\phi_0}\phi_1\,\phi_1\right] + \mathcal{O}(\epsilon^3).\end{aligned} \tag{2.29}$$

Now we consider the action

$$S[\phi] = \int d^{d+1}x\,\mathcal{L}(\partial_\mu\phi,\phi), \tag{2.30}$$

[5]In this section, we consider a $(d+1)$-dimensional spacetime, with Greek indices ranging from 0 to d.

integrate by parts, and use the Euler-Lagrange equations,

$$\partial_\mu \left(\frac{\partial \mathcal{L}}{\partial(\partial_\mu \phi)} \right) - \frac{\partial \mathcal{L}}{\partial \phi} = 0, \tag{2.31}$$

to eliminate linear terms and obtain

$$\begin{aligned} S[\phi] =& S[\phi_0] \\ &+ \frac{\epsilon^2}{2} \int d^{d+1}x \left\{ \left(\frac{\partial^2 \mathcal{L}}{\partial(\partial_\mu \phi)\partial(\partial_\nu \phi)} \right) \bigg|_{\phi_0} \partial_\mu \phi_1 \partial_\nu \phi_1 + \left[\frac{\partial^2 \mathcal{L}}{\partial \phi \partial \phi} \bigg|_{\phi_0} - \partial_\mu \left(\frac{\partial^2 \mathcal{L}}{\partial(\partial_\mu \phi)\partial \phi} \right) \bigg|_{\phi_0} \right] \phi_1 \phi_1 \right\} \\ &+ \mathcal{O}(\epsilon^3). \end{aligned} \tag{2.32}$$

Hence the equation of motion for linear disturbances is

$$\partial_\mu \left[\left(\frac{\partial^2 \mathcal{L}}{\partial(\partial_\mu \phi)\partial(\partial_\nu \phi)} \right) \bigg|_{\phi_0} \partial_\nu \phi_1 \right] - \left[\frac{\partial^2 \mathcal{L}}{\partial \phi \partial \phi} \bigg|_{\phi_0} - \partial_\mu \left(\frac{\partial^2 \mathcal{L}}{\partial(\partial_\mu \phi)\partial \phi} \bigg|_{\phi_0} \right) \right] \phi_1 = 0, \tag{2.33}$$

which is a second-order differential equation with position-dependent coefficients (notice that these coefficients depend implicitly on the background ϕ_0).

In order to accomplish a geometrical interpretation, we proceed as in Sec. 2.1, and identify

$$\sqrt{-g} g^{\mu\nu} \equiv f^{\mu\nu} \equiv \left(\frac{\partial^2 \mathcal{L}}{\partial(\partial_\mu \phi)\partial(\partial_\nu \phi)} \right) \bigg|_{\phi_0}. \tag{2.34}$$

Taking the determinant of this equation

$$(-g)^{(d-1)/2} = -\det \left\{ \frac{\partial^2 \mathcal{L}}{\partial(\partial_\mu \phi)\partial(\partial_\nu \phi)} \right\} \bigg|_{\phi_0}, \tag{2.35}$$

so that

$$g^{\mu\nu}(\phi_0) = \left(-\det \left\{ \frac{\partial^2 \mathcal{L}}{\partial(\partial_\mu \phi)\partial(\partial_\nu \phi)} \right\} \bigg|_{\phi_0} \right)^{-1/(d-1)} \left\{ \frac{\partial^2 \mathcal{L}}{\partial(\partial_\mu \phi)\partial(\partial_\nu \phi)} \right\} \bigg|_{\phi_0}, \tag{2.36}$$

and the effective metric becomes

$$g_{\mu\nu}(\phi_0) = \left(-\det \left\{ \frac{\partial^2 \mathcal{L}}{\partial(\partial_\mu \phi)\partial(\partial_\nu \phi)} \right\} \bigg|_{\phi_0} \right)^{1/(d-1)} \left[\left\{ \frac{\partial^2 \mathcal{L}}{\partial(\partial_\mu \phi)\partial(\partial_\nu \phi)} \right\} \bigg|_{\phi_0} \right]^{-1}. \tag{2.37}$$

The equation of motion for linear perturbations is then

$$\left[\Box(g(\phi_0)) - V(\phi_0) \right] \phi_1 = 0, \tag{2.38}$$

where the notation for the d'Alembert operator, $\Box(g(\phi_0))$, emphasizes its dependence on the background state of the system. The background-dependent "mass term" is given by

$$V(\phi_0) = \left(-\det \left\{ \frac{\partial^2 \mathcal{L}}{\partial(\partial_\mu \phi)\partial(\partial_\nu \phi)} \right\} \Bigg|_{\phi_0} \right)^{-1/(d-1)} \times \left(\frac{\partial^2 \mathcal{L}}{\partial \phi \partial \phi} - \partial_\mu \left[\frac{\partial^2 \mathcal{L}}{\partial(\partial_\mu \phi)\partial \phi} \right] \right) \Bigg|_{\phi_0}. \tag{2.39}$$

The linearized equation Eq. (2.38) describes the propagation of perturbations on the fixed background ϕ_0. In fact, Eq. (2.38) is going to be *hyperbolic* — and, as such, will have wave-like solutions — if and only if the effective metric $g_{\mu\nu}(\phi_0)$ has Lorentzian signature [22]. Therefore, we conclude that any physical system with dynamics described by a Lagrangian depending only on a single scalar field and its first derivatives, and such that the metric given by Eq. (2.37) has Lorenzian signature, will allow a description of wave propagation in terms of an effective spacetime.

That the barotropic irrotational perfect fluid considered in Sec. 2.1 belongs to the class of systems introduced in this section results from the fact that (i) the equations of motion for the fluid can be derived from the Lagrangian [65]

$$\mathcal{L}(\phi, \partial_\mu \phi) = \rho \dot{\phi} + \frac{1}{2} \rho (\nabla \phi)^2 + u(\rho), \tag{2.40}$$

where $\vec{v} = -\nabla \phi$, and $u(\rho)$ is the internal energy density; and (ii) the corresponding effective metric for acoustic disturbances has a Lorentzian signature. [6]

[6]For a complete derivation of the effective (acoustic) metric Eq. (2.22) starting from the Lagrangian Eq. (2.40), we refer the reader to [65].

Chapter 3

The BTZ Black Hole and its Quasinormal Modes

In this chapter, we introduce the Bañados, Teitelboim and Zanelli (BTZ) black hole [40] and the quasinormal modes associated with the scalar field in this geometry. We first discuss the BTZ spacetime causal structure, and after that we calculate the mode solutions and obtain the equation that determines the quasinormal frequencies obeying various Robin boundary conditions (including those of Dirichlet and Neumann types). The concepts and results presented in this chapter will lay the ground for the development of the forthcoming chapters. The results in this chapter are by no means original [42, 43, 44, 45, 46, 66, 67].

3.1 The BTZ Black Hole

The rotating BTZ black hole is described by the metric [40]

$$ds^2 = -(N^\perp)^2 dt^2 + (N^\perp)^{-2} dr^2 + r^2(d\varphi^2 + N^\varphi dt)^2, \tag{3.1}$$

where

$$N^\perp = \left(-M + \frac{r^2}{l^2} + \frac{J^2}{4r^2}\right)^{1/2}, \qquad N^\varphi = -\frac{J}{2r^2} \qquad (|J| < Ml). \tag{3.2}$$

The metric Eq. (3.1) is stationary and axially symmetric, with Killing vectors ∂_t and ∂_φ. One can check that the metric Eq. (3.1) is a solution to the Einstein field equations in (1+2)-

dimensions,

$$R_{\mu\nu} - \frac{1}{2}g_{\mu\nu}R + \Lambda g_{\mu\nu} = 0, \tag{3.3}$$

with cosmological constant given by $\Lambda = -1/l^2$. The constants M and J are the mass and the angular momentum of the BTZ black hole [43, 44]. Note that M is a nondimensional quantity in the units used here.

The BTZ black hole share many properties with its (1+3)-dimensional counterparts. For instance, the surface where $g_{00} = 0$, i.e., the surface determined by

$$r = r_{\text{erg}}, \tag{3.4}$$

with $r_{\text{erg}} = M^{1/2}l$, is an *ergosphere*, so that an observer with $r < r_{\text{erg}}$ is dragged along by the black hole rotation and cannot remain static. Besides, the values

$$r_{\pm}^2 = \frac{Ml^2}{2}\left\{1 \pm \left[1 - \left(\frac{J}{Ml^2}\right)^2\right]^{1/2}\right\}, \tag{3.5}$$

for which the metric has coordinate singularities, determine an *event horizon* ($r = r_+$) and a *Cauchy horizon* ($r = r_-$).

In the next chapters, we will consider only the static ($J = 0$) BTZ spacetime. In this case, the metric Eq. (3.1) reduces to

$$ds^2 = -\left(-M + \frac{r^2}{l^2}\right)dt^2 + \frac{dr^2}{\left(-M + \frac{r^2}{l^2}\right)} + r^2 d\varphi^2, \tag{3.6}$$

and we have $r_- = 0$, $r_+ = r_{\text{erg}} = M^{1/2}l$.

In order to have a clearer picture of the causal structure of the BTZ geometry, it is useful to transform to Kruskal-like coordinates [42]

$$r_h \leq r < \infty \begin{cases} U = \left(\frac{r-r_h}{r+r_+}\right)^{1/2} \cosh\left(\frac{M^{1/2}t}{l}\right), \\ V = \left(\frac{r-r_h}{r+r_+}\right)^{1/2} \sinh\left(\frac{M^{1/2}t}{l}\right), \end{cases} \tag{3.7}$$

$$0 < r < r_h \begin{cases} U = \left(\frac{r_h - r}{r_h + r}\right)^{1/2} \sinh\left(\frac{M^{1/2}t}{l}\right), \\ V = \left(\frac{r_h - r}{r_h + r}\right)^{1/2} \cosh\left(\frac{M^{1/2}t}{l}\right), \end{cases} \tag{3.8}$$

where we have defined $r_h = r_+ = M^{1/2}l$. In these coordinates the metric Eq. 3.6 is given by

$$ds^2 = \frac{(r + r_h)^2}{M}(-dV^2 + dU^2) + r^2 d\varphi^2. \tag{3.9}$$

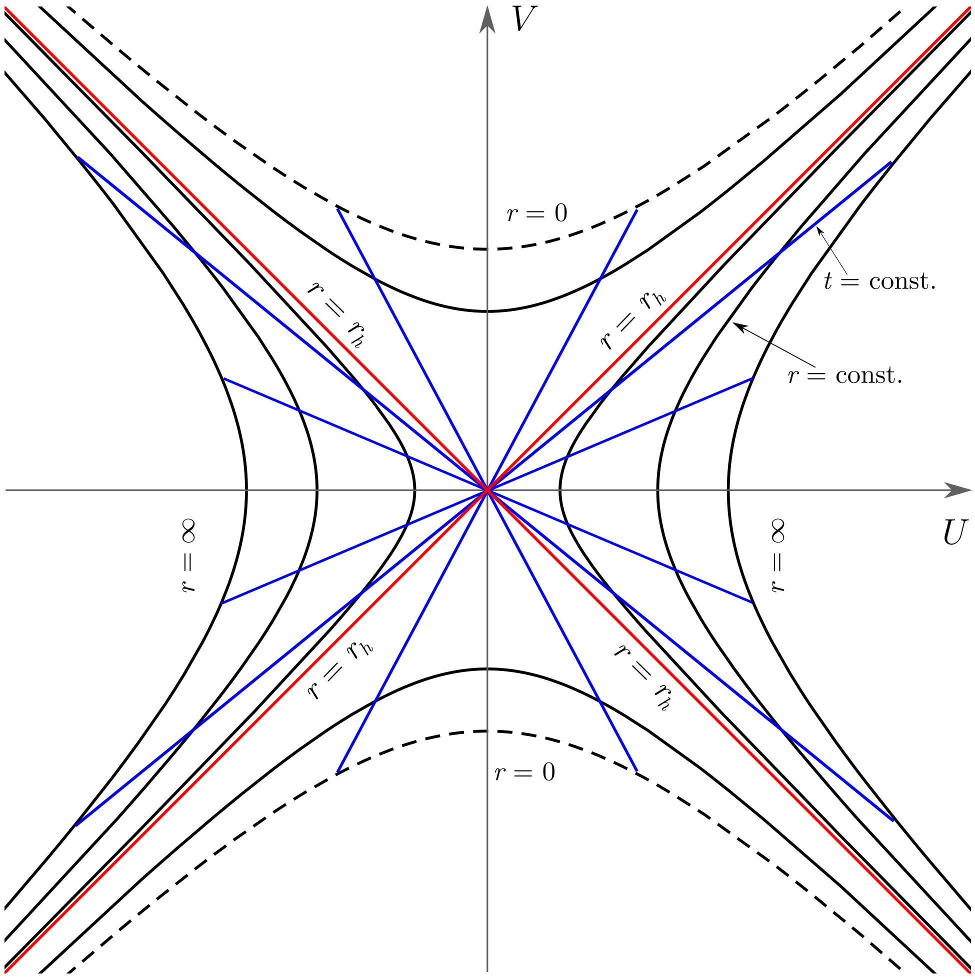

Figure 3.1: Kruskal diagram for the static BTZ black hole.

Figure 3.1 shows the Kruskal diagram for the BTZ static black hole. We note that null geodesics (i.e., those with $ds^2 = 0$) travel along straight lines with slope 45°. Note that we have suppressed the angular coordinate so that each point in Fig 3.1 actually represents a circle in the BTZ spacetime.

Let us interpret the diagram in Fig. 3.1. First, when $r > r_h$ the Eq. (3.7) yields

$$U^2 - V^2 = \frac{r - r_h}{r + r_h}, \tag{3.10}$$

from where it follows that $r = \infty$ is mapped onto the hyperbola $U^2 - V^2 = 1$. Similarly, the lines $r =$ const. correspond to hyperbolas in the (U, V) plane, and as r decreases, the hyperbolas degenerate to the lines $V = \pm U$ at the event horizon $r = r_h$. On the other hand, since

$$\frac{V}{U} = \tanh\left(\frac{M^{1/2}t}{l}\right), \tag{3.11}$$

we see that lines $t =$ const. correspond to straight lines in the (U, V) plane. Thus the exterior of the BTZ black hole corresponds to the set $A = \{(U, V) \,|\, U > V \text{ and } U > -V\}$.

Analogously, when $r < r_h$, we see from Eq. (3.8) that lines $r =$ const. are mapped onto the hyperbolas

$$V^2 - U^2 = \frac{r_h - r}{r_h + r}. \tag{3.12}$$

In particular, the singularity $r = 0$ is mapped onto the hyperbola $V^2 - U^2 = 1$. On the other hand, from Eq. (3.8), we now have

$$\frac{U}{V} = \tanh\left(\frac{M^{1/2}t}{l}\right), \tag{3.13}$$

and $t =$ const. lines are still mapped onto straight lines in the (U, V) plane. The interior of the BTZ black hole corresponds to the set $B = \{(U, V) \,|\, V > U \text{ and } V > -U\}$ in the (U, V) plane.

The set $C = \{(U, V) \,|\, V > U \text{ and } V < -U\}$ corresponds to an exterior region of BTZ disjoint from A, and can be covered by the coordinate patch

$$r_h \leq r < \infty \begin{cases} U = & -\left(\frac{r - r_h}{r + r_+}\right)^{1/2} \cosh\left(\frac{M^{1/2}t}{l}\right), \\ V = & \left(\frac{r - r_h}{r + r_+}\right)^{1/2} \sinh\left(\frac{M^{1/2}t}{l}\right). \end{cases} \tag{3.14}$$

The set $D = \{(U, V) \,|\, V < U \text{ and } V < -U\}$ corresponds to a white hole, and can be covered by the coordinate patch

$$0 < r < r_h \begin{cases} U = & \left(\frac{r_h - r}{r_h + r}\right)^{1/2} \sinh\left(\frac{M^{1/2}t}{l}\right), \\ V = & -\left(\frac{r_h - r}{r_h + r}\right)^{1/2} \cosh\left(\frac{M^{1/2}t}{l}\right). \end{cases} \tag{3.15}$$

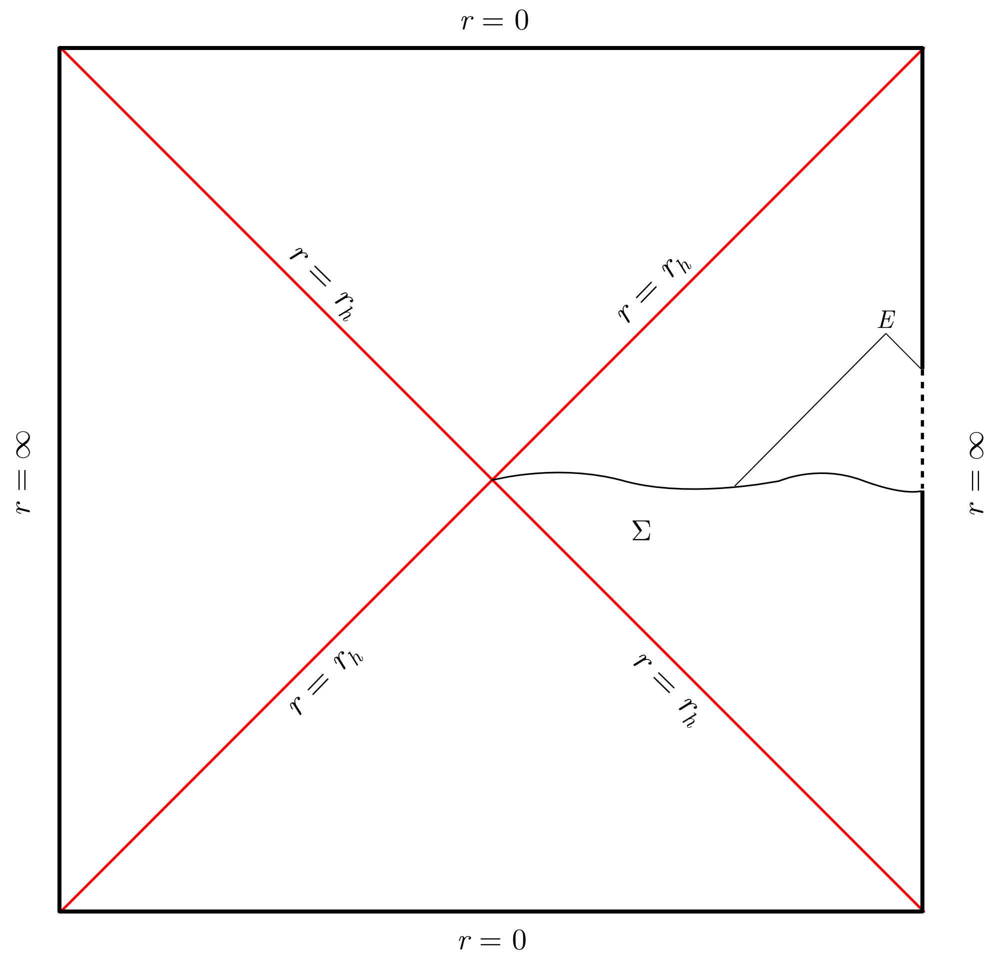

Figure 3.2: Penrose diagram for the static BTZ black hole.

By the same argument used to interpret the lines r = const. and t = const. in regions A and B, one can see that we have again lines r = const. corresponding to hyperbolas and lines t = const. corresponding to straight lines.

The diagram of Fig. 3.1 can be further simplified if we consider the transformation

$$\begin{aligned} U+V &= \tan\left(\tfrac{p+q}{2}\right), \\ U-V &= \tan\left(\tfrac{p-q}{2}\right), \end{aligned} \tag{3.16}$$

with $p, q \in (-\pi, \pi)$, which leads us to the Penrose diagram represented in figure 3.2.

Let us now interpret this diagram. Since $r = \infty$ corresponds to the hyperbola $U^2 - V^2 = 1$, we have that

$$1 = U^2 - V^2 = \tan\left(\frac{p+q}{2}\right)\tan\left(\frac{p-q}{2}\right) = \frac{\cos q - \cos p}{\cos q + \cos p}, \tag{3.17}$$

which implies $\cos p = 0$, and we conclude that $r = \infty$ is mapped onto the lines $p = \pm\pi/2$ in the (p, q) plane. We will refer to $p = \pm\pi/2$ (or, equivalently, to $r = \infty$) as the *conformal boundary* of the BTZ spacetime. By similar reasoning, we conclude that $r = 0$ is mapped onto the lines $q = \pm\pi/2$, and the horizon is mapped onto $p = \pm q$.

The Penrose diagram of fig. 3.2 allows us to illustrate the lack of global hiperbolicity of the BTZ spacetime in a very intuitive way. Indeed, let us suppose we have given smooth initial data on a spacelike hypersurface Σ at the exterior region of the BTZ spacetime. The state of an observer at the event E will depend not only on the information coming from the intersection of his/her past light cone with Σ. In fact, to determine the state of the observer at E, we need to know what happens at the conformal boundary during the time interval indicated by the dashed line in Fig. 3.2.

The indetermination of the dynamics in this static nonglobally hyperbolic spacetime can be overcome by prescribing proper boundary conditions at $r = \infty$. The details of the process of implementing boundary conditions in such spacetimes are not trivial since the equation of motion usually leads to a singular Sturm-Liouville problem [68]. One way to circumvent such dificulties is to apply Wald and Ishibashi's formalism [69, 70, 71]. In this case, one can recover unique deterministic time evolution for the dynamics. In Appendix B, we present a brief introduction to this formalism and its application to the propagation of a scalar field in the BTZ spacetime.

We present Appendix B for the sake of completeness since it will not be fundamentally essential to the discussion on the forthcoming chapters. In fact, in Chapter 4, we emulate the dynamics of a massless scalar field, for which only Dirichlet boundary conditions at infinity are allowed. On the other hand, in Chapter 5, we consider a conformally coupled field, for which general Robin boundary conditions are allowed. Nevertheless, since the effective potential on the radial equation is regular in this case, we can implement Robin boundary conditions in the traditional way of solving regular Sturm-Liouville problems [72].

3.2 Quasinormal Modes

When an isolated system (such as a finite string, a membrane or a cavity filled with electromagnetic radiation) is perturbed, its internal degrees of freedom are excited, and the resulting dynamical evolution is described by a superposition of characteristic vibrations known as *nor-*

mal modes [73, 74, 75]. The frequencies of these modes do not depend on the configuration of the initial perturbation and are, therefore, intrinsic properties of the system. Moreover, they completely describe the dynamics since, at any time, the state of the system is given by a superposition of such normal modes.

On the other hand, in the case of a field propagating in the vicinity of a black hole, energy will always leak out from the system through the horizon (and possibly through infinity), which means that we cannot, in general, treat a black hole as a conservative system. The characteristic modes of oscillation, in this case, are the *quasinormal modes* (QNMs) [45, 76, 46, 47]. The corresponding frequencies, the *quasinormal frequencies*, are complex numbers with a real part corresponding to an actual frequency of oscillation and an imaginary part corresponding to a damping factor accounting for the energy leaking out from the system.

Similarly to what happens in conservative systems, the quasinormal frequencies will in general depend only on the black hole parameters (mass, angular momentum, charge) but not on the particular form of the initial perturbation. Nevertheless, an important distinction between normal modes and QNMs is that the latter, in general, do not describe the dynamics completely at any time [77]. In fact, the usual response of a black hole after a perturbation undergoes three stages [78]: (i) the prompt response, determined by the initial perturbation; followed by (ii) the intermediate phase, which is dominated by the QNMs; and (iii) the final phase, usually governed by a power-law tail.

As an example of how QNMs arise in the description of oscillations on a black hole background, let us make some comments on the characterization of QNMs as solutions to an eigenvalue problem. To keep things simpler, we consider a scalar field propagating on a spherically symmetric spacetime.

After separating time and angular variables, the problem can be reduced to the equation

$$-\frac{d^2\psi(r)}{dr_*^2} + V(r)\psi(r) = \omega^2\psi(r), \tag{3.18}$$

where ψ is the radial component of the field Ψ, $V(r)$ is the effective potential, r_* is the tortoise coordinate, and ω is the eigenfrequency. For instance, in the case of the Schwarzschild black hole, the effective potential is given by [79]

$$V(r) = \left(1 - \frac{2M}{r}\right)\left[\frac{\ell(\ell+1)}{r^2} + \frac{2M}{r^3} + \mu^2\right], \tag{3.19}$$

where M is the black hole mass, μ is the field mass, ℓ is the angular quantum number, and the tortoise coordinate is

$$r_* = r + 2M \ln\left(\frac{r}{2M} - 1\right). \tag{3.20}$$

We are interested in studying wave propagation in the exterior region of the black hole. For the Schwarzschild spacetime, this corresponds to the region $r_h < r < \infty$, where $r_h = 2M$ is the Schwarzschild radius. In terms of the tortoise coordinate, Eq. (3.20), this region corresponds to $-\infty < r_* < \infty$.

To determine the eigenmodes of Eq. (3.18), we need to impose some conditions at the boundaries of the system (i. e. at the horizon and spatial infinity). On the horizon, we have $V = 0$, and the field behaves as $\psi \sim e^{\pm i\omega r_*}$. Since QNMs correspond to waves that take energy out from the system, we should impose the boundary condition

$$\psi \sim e^{-i\omega r_*}, \qquad r_* \to -\infty \quad (r \to r_+), \tag{3.21}$$

which is referred to as an *ingoing* boundary condition, meaning that the wave goes into the black hole. Notice that we are assuming a Fourier mode decomposition such that $\Psi = e^{-i\omega t} \times$ (spatial variables), which indeed implies an ingoing wave at the horizon, $\Psi \sim e^{-i\omega(r_*+t)}$.

In the Schwarzschild case (and for asymptotically-flat spacetimes in general), we have $V = 0$ at spatial infinity, and again the plane wave behavior $\psi \sim \pm e^{\pm i\omega r_*}$. Now the appropriate boundary condition is

$$\psi \sim e^{i\omega r_*}, \qquad r_* \to \infty \quad (r \to \infty), \tag{3.22}$$

which corresponds to *outgoing* waves at infinity, $\Psi \sim e^{i\omega(r_*-t)}$.

The boundary conditions (3.21) and (3.22) determine a discrete infinity set of QNMs, $\{\Psi_\omega\}$, with complex eigenfrequencies $\{\omega_n\,;\ n = 0,\ 1,\ 2,\ \dots\}$. The real part of ω gives the actual frequency of oscillation, and the imaginary part gives the inverse damping time of the corresponding mode. The quasinormal frequencies are usually sorted by the magnitude of their imaginary part. We use an integer label n, called the *overtone number*, and take the least-damped mode (or fundamental mode) corresponding to $n = 0$.

In the case of the BTZ black hole (and for asymptotically-curved spacetimes in general), one does not have $V = 0$ at spatial infinity, so that outgoing boundary conditions are not available there [48, 49]. This issue can be addressed by prescribing appropriate boundary conditions at the BTZ spatial infinity, as we will see in the next section.

For a comprehensive treatment of the many important features of QNMs we refer the reader to the review articles [45, 76, 46, 47], thesis [80, 81, 82], and references therein.

3.3 QNMs of the Scalar Field in the BTZ Black Hole

In this section, we calculate the QNMs of the scalar field Ψ propagating on the BTZ background. We first consider generalized Robin boundary conditions at spatial infinity, and then show that for the particular cases of Dirichlet and Neumann conditions, we can obtain the QNMs exactly.

The equation of motion for the scalar field is

$$(\Box - m_\xi^2)\Psi = 0, \tag{3.23}$$

where the d'Alembert operator, $\Box = \nabla_\mu \nabla^\mu$, is calculated with respect to the BTZ metric Eq. (3.6), and the effective mass squared is given by

$$m_\xi^2 = \mu^2 + \xi\mathcal{R}, \tag{3.24}$$

with μ being the mass of the field and ξ being the coupling constant with the Ricci scalar $\mathcal{R} = -6/l^2$.

Separating variables by the ansatz

$$\Psi(t, r, \varphi) = \frac{\psi(r)}{r^{1/2}} e^{-i\omega t} e^{im\varphi}, \tag{3.25}$$

and transforming to the tortoise coordinate

$$r_* = -\frac{l}{M^{1/2}} \operatorname{arcoth}\left(\frac{r}{M^{1/2} l}\right), \tag{3.26}$$

and substituting into Eq. (3.23), the equation of motion reduces to the radial equation

$$-\frac{d^2\psi(r_*)}{dr_*^2} + V_{\text{eff}}(r_*)\psi(r_*) = \omega^2\psi(r_*), \tag{3.27}$$

where the effective potential is given by

$$V_{\text{eff}}(r_*) = M\left(\frac{3}{4l^2} + m_\xi^2\right)\operatorname{csch}^2\left(\frac{M^{1/2}r_*}{l}\right) + \left(\frac{4m^2 + M}{4l^2}\right)\operatorname{sech}^2\left(\frac{M^{1/2}r_*}{l}\right). \tag{3.28}$$

Note that the transformation Eq. (3.26) maps the horizon $r_h = lM^{1/2}$ to $r_* = -\infty$, and the spatial infinity $r = \infty$ to $r_* = 0$. We also notice that for generic values of m_ξ^2 the potential blows up at the conformal boundary, which, in turn, leads to a singular Sturm-Liouville problem [68], so that boundary conditions cannot be directly imposed at $r_* = 0$. On the other hand, when $m_\xi^2 = -3/4l^2$ the potential is regular, and one can impose boundary conditions by the usual procedure prescribed by the theory of regular Sturm-Liouville problems. This case corresponds to a conformally coupled field ($\mu^2 = 0$, $\xi = 1/8$), and we will be particularly interested in considering it in Chapter 5. However, for now, let us keep things as general as possible and proceed with the calculation of the QNMs with generic m_ξ^2.

As shown in Appendix B [1], one can impose generalized Robin boundary conditions at infinity for ψ when $-1/l^2 < m_\xi^2 < 0$, so we will assume this is the case hereafter in this section. The general solution to Eq. 3.27 can be written as a linear combination of the linearly independent fundamental solutions $\{\psi_\omega^D, \psi_\omega^N\}$,

$$\psi_\omega(r_*) = N_\omega\left[\cos\zeta\,\psi_\omega^D(r_*) + \sin\zeta\,\psi_\omega^N(r_*)\right], \tag{3.29}$$

where $\zeta \in [0,\pi]$ parametrizes the generalized Robin boundary conditions [83, 67] and ψ_ω^D is chosen as the *principal solution*, i.e., the unique solution (up to scalar multiples) such that $\lim_{r_*\to 0}\psi_\omega^D/\phi = 0$, for every solution ϕ that is not a multiple of ψ_ω^D. We say that the other linearly independent solution ψ_ω^N is a *non-principal solution.* Note that a non-principal solution is not unique since, for any constant k, the function $\psi_\omega^D + k\psi_\omega^N$ is also a non-principal solution.

Let us now find ψ_ω^D and ψ_ω^N. It is convenient to choose units such that

$$\hat{r}_* = \frac{M^{1/2}}{l}r_*, \qquad\qquad \hat{\omega} = \frac{l}{M^{1/2}}\omega, \tag{3.30}$$

so that the radial equation becomes

$$-\frac{d^2\psi(\hat{r}_*)}{d\hat{r}_*^2} + \hat{V}_{\text{eff}}(\hat{r}_*)\psi(\hat{r}_*) = \hat{\omega}^2\psi(\hat{r}_*), \tag{3.31}$$

[1] See the case (ii) in section B.1.2 and note that $\nu = 1 + l^2 m_\xi^2$.

where the nondimensional effective potential is given by

$$\hat{V}_{\text{eff}}(\hat{r}_*) = \left(\frac{3}{4} + l^2 m_\xi^2\right) \operatorname{csch}^2 \hat{r}_* + \left(\frac{4m^2 + M}{4M}\right) \operatorname{sech}^2 \hat{r}_* \tag{3.32}$$

Changing to the new coordinate and wave function

$$z = \operatorname{sech}^2 \hat{r}_* \tag{3.33}$$

$$\psi_\omega(z) = z^\alpha (1-z)^\lambda (1-z)^{-1/4} F_\omega(z), \tag{3.34}$$

and substituting these into Eq. (3.31), we find

$$z(1-z)\frac{d^2 F_\omega}{dz^2} + [(1+2\alpha) - (2\alpha + 2\lambda + 1)z]\frac{dF_\omega}{dz} + \left[\frac{A}{z(1-z)} + \frac{B}{1-z} - C\right] F_\omega(z) = 0, \tag{3.35}$$

where

$$A = -\alpha^2 - \frac{\hat{\omega}^2}{4}, \tag{3.36}$$

$$B = \alpha^2 - \lambda^2 + \lambda + \frac{l^2 m_\xi^2}{4} + \frac{\hat{\omega}^2}{4}, \tag{3.37}$$

$$C = \frac{m^2}{4M} + (\alpha + \lambda)^2. \tag{3.38}$$

If we take α and λ so that $A = B = 0$, i.e.,

$$\alpha = -\frac{i\hat{\omega}}{2}, \qquad \lambda = \frac{1}{2}\left(1 + \sqrt{1 + l^2 m_\xi^2}\right), \tag{3.39}$$

and further define the auxiliar quantities

$$a = \alpha + \lambda + \frac{im}{2M^{1/2}}, \qquad b = \alpha + \lambda - \frac{im}{2M^{1/2}}, \qquad c = 1 + 2\alpha, \tag{3.40}$$

the Eq. (3.35) can be rewritten as

$$z(1-z)\frac{d^2 F_\omega}{dz^2} + [c - (a+b+1)z]\frac{dF_\omega}{dz} - abF_\omega(z) = 0, \tag{3.41}$$

which is the known hypergeometric differential equation [84].

When none of c, $c-a-b$, $a-b$ is an integer[2], a convenient pair of linearly independent solutions for Eq. (3.41) is

$$F^D_\omega(z) = {}_2F_1(a,b;a+b+1-c;1-z), \tag{3.42}$$

$$F^N_\omega(z) = (1-z)^{c-a-b}\,{}_2F_1(c-a,c-b;c-a-b+1;1-z), \tag{3.43}$$

where ${}_2F_1$ stands for the standard hypergeometric function

$${}_2F_1(a,b;c;z) = \sum_j^\infty \frac{(a)_j(b)_j}{(c)_j\, j!} z^j, \tag{3.44}$$

and $(x)_j$ indicates the Pochhammer symbol

$$(x)_j = x(x+1)\dots(x+j-1). \tag{3.45}$$

The corresponding solutions for Eq. (3.31) are

$$\psi^D_\omega(z) = z^\alpha(1-z)^\lambda(1-z)^{-1/4}\,{}_2F_1(a,b;a+b+1-c;1-z), \tag{3.46}$$

$$\psi^N_\omega(z) = z^\alpha(1-z)^{1-\lambda}(1-z)^{-1/4}\,{}_2F_1(c-a,c-b;c-a-b+1;1-z), \tag{3.47}$$

which behave near $r=\infty$ ($z=1$) as

$$\psi^D_\omega(z\to 1) \approx (1-z)^\lambda, \tag{3.48}$$

$$\psi^N_\omega(z\to 1) \approx (1-z)^{1-\lambda}, \tag{3.49}$$

so that

$$\lim_{z\to 1} \frac{\psi^D_\omega(z)}{\psi^N_\omega(z)} \approx (1-z)^{2\lambda-1}. \tag{3.50}$$

Since we assumed $m_\xi^2 > -1/l^2$, it follows that $\lambda > 1/2$ and hence

$$\lim_{z\to 1} \frac{\psi^D_\omega(z)}{\psi^N_\omega(z)} = 0, \tag{3.51}$$

[2]The other cases can be treated similarly, and we will not pursue them here. The reader interested in the this case is referred to [83].

which implies

$$\lim_{z\to 1}\frac{\psi_\omega^D(z)}{c_1\psi_\omega^D(z)+c_2\psi_\omega^D(z)}=0, \tag{3.52}$$

for $c_2 \neq 0$, and shows that $\psi_\omega^D(z)$ is the principal solution.

Before imposing the ingoing boundary condition at the horizon, it is convenient to express the general solution in terms of another set of independent solutions, that is,

$$\begin{aligned}\psi_\omega(z) =&c_1\, z^{\alpha}(1-z)^{\lambda}(1-z)^{-1/4}\,{}_2F_1(a,b;c;z)\\ &+c_2\, z^{-\alpha}(1-z)^{\lambda}(1-z)^{-1/4}\,{}_2F_1(a-c+1,b-c+1;2-c;z).\end{aligned} \tag{3.53}$$

From this, it follows that

$$\psi_\omega(\hat{r}_*\to-\infty)\propto c_1 e^{-i\hat{\omega}\hat{r}_*}+c_2 e^{+i\hat{\omega}\hat{r}_*}, \tag{3.54}$$

and in order to have only ingoing waves at the horizon, we should take $c_2 = 0$. If we additionally use the transformation [85]

$$\begin{aligned}{}_2F_1(a,b;c;z) =&\frac{\Gamma(c)\Gamma(c-a-b)}{\Gamma(c-a)\Gamma(c-b)}\,{}_2F_1(a,b;a+b-c+1;1-z)\\ &+(1-z)^{c-a-b}\frac{\Gamma(c)\Gamma(a+b-c)}{\Gamma(a)\Gamma(b)}\,{}_2F_1(c-a,c-b;c-a-b+1;1-z),\end{aligned} \tag{3.55}$$

the solution becomes

$$\psi_\omega(z)=c_1\times\left\{\frac{\Gamma(c)\Gamma(c-a-b)}{\Gamma(c-a)\Gamma(c-b)}\psi_\omega^D(z)+\frac{\Gamma(c)\Gamma(a+b-c)}{\Gamma(a)\Gamma(b)}\psi_\omega^N(z)\right\}. \tag{3.56}$$

Comparing this expression with Eq. (3.29), we find

$$\cos(\zeta)\frac{\Gamma(a+b-c)}{\Gamma(a)\Gamma(b)}=\sin(\zeta)\frac{\Gamma(c-a-b)}{\Gamma(c-a)\Gamma(c-b)}. \tag{3.57}$$

For each $\zeta \in [0,\pi]$, the solutions of Eq. (3.57) will determine a discrete set of quasinormal frequencies. We note that, in general, this equation cannot be analytically solved so that in most cases, one has to rely on numerical methods. However, when $\zeta = 0$ or $\zeta = \pi/2$, we can solve Eq. (3.57) exactly. Indeed, since the gamma function has poles on negative integers, for

$\zeta = 0$, we have that

$$a = -n \qquad \text{or} \qquad b = -n, \qquad (n = 0, 1, 2, 3 \dots), \tag{3.58}$$

solve Eq. (3.57) and yield the frequencies

$$\omega = \pm\frac{m}{l} - i\frac{M^{1/2}}{l}\left(2n + 1 + \sqrt{1 + l^2 m_\xi^2}\right), \qquad (\zeta = 0). \tag{3.59}$$

Similarly, we find that for $\zeta = \pi/2$, the poles of the gamma function correspond to

$$c - a = -n \qquad \text{and} \qquad c - b = -n, \qquad (n = 0, 1, 2, 3 \dots), \tag{3.60}$$

which gives the frequencies

$$\omega = \pm\frac{m}{l} - i\frac{M^{1/2}}{l}\left(2n + 1 - \sqrt{1 + l^2 m_\xi^2}\right), \qquad \left(\zeta = \frac{\pi}{2}\right). \tag{3.61}$$

We note that the obtained frequencies Eqs. (3.59) and (3.61) agree with the results of [66] and [67]. The boundary conditions $\zeta = 0$ and $\zeta = \pi/2$ are usually referred to as *generalized Dirichlet* and *Neumann boundary conditions.* This terminology is motivated by the case of the conformally coupled field, for which we have

$$\mu^2 = 0, \qquad \xi = \frac{1}{8}, \tag{3.62}$$

so that $m_\xi^2 = -3/4l^2$. One can see this by using Eqs. (3.46) and (3.47) to calculate

$$\left.\frac{d\psi_\omega/d\hat{r}_*}{\psi_\omega}\right|_{\hat{r}_*=0} = -\cot\zeta := \beta, \tag{3.63}$$

where we defined the parameter $-\infty < \beta < \infty$. Notice that Eq. (3.63) is the usual Robin boundary condition imposed at the boundary of a regular Sturm-Liouville problem. Besides, we have that $\zeta = 0$ corresponds to $\beta = -\infty$, so that $\psi_\omega(\hat{r}_* = 0) = 0$, which is the known regular Dirichlet boundary condition. By the same reasoning, we see that $\zeta = \pi/2$ ($\beta = 0$) corresponds to the regular Neumann boundary condition, $(d\psi_\omega/d\hat{r}_*)|_{\hat{r}_*=0} = 0$.

Inspired by this discussion, in the general case (non-conformally coupled field), we say that a solution with $\zeta = 0$ ($\zeta = \pi/2$) obeys a *generalized Dirichlet (Neumann)* boundary condition at spatial infinity. In the same way, the other values of $\zeta \in [0, \pi]$ correspond to solutions obeying *generalized Robin boundary conditions* at infinity.

Before ending this section, we note that, for the conformally coupled field, Eqs. (3.57) and (3.63) yield

$$\beta = -\frac{\Gamma(c-a-b)}{\Gamma(c-a)\Gamma(c-b)}\frac{\Gamma(a)\Gamma(b)}{\Gamma(a+b-c)}, \tag{3.64}$$

which after using Eqs. (3.39) and (3.40) reduces to

$$\beta = \frac{2\Gamma\left(\frac{3}{4} - \frac{i\hat{\omega}}{2}\right)^2}{\Gamma\left(\frac{1}{4} - \frac{i\hat{\omega}}{2}\right)^2}, \tag{3.65}$$

for a mode with zero angular momentum, $m = 0$. This result will be used to check the consistency of the analog model of the conformally coupled field introduced in Chapter 5.

Chapter 4

Hydrodynamical Analog Model of the BTZ Black Hole

In this chapter, we present an analog model for the Bañados, Teitelboim, Zanelli (BTZ) black hole based on a hydrodynamical flow. We numerically solve the fully nonlinear hydrodynamic equations of motion and observe the excitation and decay of the analog BTZ quasinormal modes in the process. We consider both a small perturbation in the steady state configuration of the fluid and a large perturbation; the latter could be regarded as an example of formation of the analog (acoustic) BTZ black hole. The material in this chapter is based on our work [54].

4.1 Introduction

In the work [58], we have proposed a hydrodynamical analog model for a class of spherically symmetric metrics (which include the Schwarzschild and Reissner-Nordström spacetimes). That model was based on the propagation of acoustic waves in the bulk of an inviscid fluid and governed by the effective metric Eq. (2.22). Besides, that model required a careful fine-tuning of the physical parameters of the flow, namely its local velocity and sound speed. The local fluid velocity can be directly set up, in principle, by applying a suitable external force to the fluid. However, the local speed of sound is much less amenable to external control since it is determined by the relevant equation of state, which describes the internal forces in the flow and depends on the nature of the fluid.

In this chapter, we apply the method introduced in [58], but now we do not start by fixing the spacetime we want to emulate. Instead, we start by assuming that the equation of state for the fluid is as simple as it gets so that the local speed of sound is constant throughout the fluid (see Eq. (4.13)). Interestingly enough, the curved spacetime that results from this procedure is the celebrated BTZ spacetime introduced by Bañados, Teitelboim and Zanelli in [40].

As mentioned in Chapter 3, an important characterizing property of black holes is how they respond to perturbations in the metric. Upon perturbation, a black hole goes, in general, through a transient stage that depends on the source of the perturbation. After that, the system can be characterized by a spectrum of complex quasinormal frequencies that depend only on the black hole parameters [45, 46, 47]. The corresponding QNMs describe the characteristic ringdown that occurs as a response to the perturbation. As noted in the previous chapter, the QNMs are usually defined as the modes satisfying ingoing boundary conditions at the black hole horizon and outgoing boundary conditions at infinity. This definition works perfectly fine for asymptotically flat spacetimes (Schwarzschild and Kerr black holes, for instance). However, the situation is subtler in the case of asymptotically curved spacetimes. In part, this results from the difficulty in distinguishing ingoing and outgoing waves at infinity. Moreover, for an asymptotically anti-de Sitter spacetime, the lack of global hyperbolicity gives rise to another issue: the initial conditions are not sufficient to uniquely determine the time evolution of a field, and extra boundary conditions at spatial infinity are required [69, 70, 71] (see also the Appendix B). These boundary conditions influence all types of wave phenomena [56, 67, 86], including, in particular, the quasinormal modes.

In this chapter, we are interested in analyzing the characteristic quasinormal decay of the BTZ black hole in terms of the analog nonlinear phenomenon that takes place in the fluid as a response to perturbing its flow. Our goal is, therefore, to use an ideal fluid to probe the quasinormal decay of a scalar field in BTZ via the observation of the decay rate of sound waves.

The next sections are organized as follows. In Sec. 4.2, we find the flow background parameters corresponding to the emulation of the BTZ spacetime by an effective metric. In Sec. 4.3, we numerically solve the equations of fluid dynamics for a small perturbation in the velocity field propagating on the background found in Sec. 4.2. Using the known BTZ quasinormal frequencies [66], we show that the field intermediate-time and the late-time behaviors are well described by a superposition of QNMs. After that, we consider an example of the formation of an analog BTZ black hole and use this fully nonlinear process to observe the excitation and decay of the analog BTZ quasinormal modes.

4.2 Analog BTZ Black Hole

Let us consider an inviscid barotropic fluid flowing in two spatial dimensions. Let x, y, and t be the spatial and time coordinates with respect to an inertial frame of reference in the laboratory. Following [58], we start with a stationary one-dimensional velocity profile given by

$$\vec{v}(x, y) = v(x)\hat{x}. \tag{4.1}$$

The equation of continuity (2.1) then implies that

$$\rho(x) = \frac{k}{|v(x)|}, \tag{4.2}$$

where k is a constant.

Substituting the expression for the density profile Eq. (4.2) into the (2+1)-dimensional version of Eq. (2.22), the effective metric can be written as

$$ds^2 = \frac{\alpha^2 k^2}{c^2 v^2}\left[-(c^2 - v^2)dt^2 - 2v dt dx + dx^2 + dy^2\right], \tag{4.3}$$

where c is the local speed of sound. Note that the metric Eq. (4.3) is fully determined by the background flow configuration. The constant α was introduced for convenience in order to make the factor $(\alpha^2 k^2/c^2 v^2)$ dimensionless.

Let us define a new timelike coordinate

$$T = t + \int \frac{v(x')}{c^2(x') - v^2(x')} dx', \tag{4.4}$$

so that the metric becomes diagonal

$$ds^2 = \frac{\alpha^2 k^2}{c^2(x) v^2(x)}\left\{-\left[c^2(x) - v^2(x)\right] dT^2 + \frac{c^2(x)}{c^2(x) - v^2(x)} dx^2 + dy^2\right\}. \tag{4.5}$$

Following [58], we define an angular coordinate $\Theta = y/L \pmod{2\pi}$, where L is a characteristic length of the analog model, and a radial coordinate[1]

$$R(x) = \pm\frac{\alpha k L}{c(x)\, v(x)}, \tag{4.6}$$

[1] Since the velocity $v(x)$ can be positive or negative, we choose the sign in (4.6) so that $R(x)$ is always positive.

which was chosen as the function that multiplies the resulting $d\Theta^2$ in Eq. (4.5). In terms of the new coordinates (T, R, Θ), the metric now reads

$$ds^2 = -\left[-\frac{\alpha^2 k^2}{c^4(x)} + \frac{R^2(x)}{L^2}\right] dT^2 + \frac{R^2(x)/L^2}{\left[1 - \frac{\alpha^2 k^2 L^2}{c^4(x) R^2(x)}\right] R'^2(x)} dR^2 + R^2(x) d\Theta^2, \tag{4.7}$$

where $R'(x) = dR/dx$. We now demand that this metric be in the Schwarzschild gauge so that $g_{11} = -\kappa^2/g_{00}$. This requires that $R(x)$ obey the differential equation

$$R'^2(x) = \frac{c^2(x) R^4(x)}{\kappa^2 L^4}. \tag{4.8}$$

Up to here, the argument is valid for a generic (position-dependent) speed of sound. However, in contrast with [58], where we considered position-dependent speed of sound configurations (with their ensuing contrived equations of state), here we will analyze the simpler case of a constant speed of sound. In this case, Eq. (4.8) can be immediately integrated to yield (up to a trivial translation in x)

$$R(x) = -\frac{L^2}{x}, \tag{4.9}$$

where we took, for simplicity, $\kappa = c$ and we chose the negative sign at the right-hand side so that $R(x)$ is positive and increasing for $x \in (-\infty, 0)$.

As a result, the effective metric takes the form

$$ds^2 = -\left(-\frac{\alpha^2 k^2}{c^4} + \frac{R^2}{L^2}\right) dT^2 + \left(-\frac{\alpha^2 k^2}{c^4} + \frac{R^2}{L^2}\right)^{-1} dR^2 + R^2 d\Theta^2. \tag{4.10}$$

We recognize (4.10) as the metric of a static BTZ black hole, Eq. (3.6), with mass $M = \alpha^2 k^2/c^4$ and curvature radius $l = L$. We note that the horizon ($R = R_h := l\sqrt{M}$) and conformal boundary ($R = \infty$) of the BTZ spacetime are realized at $x = -L/\sqrt{M}$ and $x = 0$, respectively, in this model. We will denote the boundary $x = 0$ of the laboratory by $\mathcal{E}$. Notice that the constant M is dimensionless in this spacetime.

4.3 Time Evolution and Analog Quasinormal Decay

As we have seen in chapter 2, the equations of motion for an inviscid fluid subjected to an externally imposed body force are given by Eqs. (2.1) and (2.2). For convenience, we rewrite these equations as

$$\frac{\partial \rho}{\partial t} + \nabla \cdot \left(\rho \vec{v}\right) = 0, \quad \text{(continuity equation)} \tag{4.11}$$

$$\rho \left[\frac{\partial \vec{v}}{\partial t} + \left(\vec{v} \cdot \nabla\right) \vec{v}\right] = -\nabla p + \vec{f}, \quad \text{(Euler equation)} \tag{4.12}$$

where $\vec{f}$ denotes the external force applied upon a volume element of the fluid, and the pressure p now satisfies the equation of state

$$p = c^2 \rho, \tag{4.13}$$

with constant c, as discussed above.

We are concerned with two-dimensional flows with physical quantities varying along x only. More explicitly, density and pressure will depend only on x [i.e., $\rho = \rho(x)$, $p = p(x)$], the velocity $\vec{v}$ will be given by (4.1), and the external force density will be given in terms of a driving potential $\Phi(x)$,

$$\vec{f}(x) = -\rho \nabla \Phi = -\rho \partial_x \Phi \, \hat{x}. \tag{4.14}$$

The external potential is taken to be fixed, which means that it is insensitive to backreaction, as in [1, 8]. Therefore, the discussion of [87] does not apply to the present work[2] (nor to [58]). With the assumptions made above, the equations of motion simplify to

$$\partial_t \rho + \partial_x \left(\rho v\right) = 0, \tag{4.15}$$

$$\rho \left(\partial_t + v \partial_x\right) v = -\partial_x p - \rho \partial_x \Phi. \tag{4.16}$$

The fluid configuration that implements the results of the previous section can be obtained from Eqs. (4.2), (4.6) and (4.9), which determine the background velocity

$$v_0(x) = \left(\frac{\alpha k}{cL}\right) x, \tag{4.17}$$

[2]For a discussion concerning the issues of implementing an external force upon a flowing fluid, we refer the reader to [88].

and the background density

$$\rho_0(x) = -\left(\frac{cL}{\alpha}\right)\frac{1}{x}. \tag{4.18}$$

From the Euler equation (4.16), we find the external potential

$$\Phi(x) = c^2 \log\left(\frac{x}{L}\right) - \left(\frac{\alpha^2 k^2}{c^2 L^2}\right)\frac{x^2}{2}. \tag{4.19}$$

We now consider perturbations of the above steady-state configuration of the fluid and follow the evolution of the relevant physical quantities in time. In order to do that, we numerically solve the nonlinear fluid equations and compare the result with what would have been the corresponding evolution on the BTZ black hole. As we show in the following, the propagation of the fluid in this regime allows one to recover the mechanism of excitation of quasinormal modes at the black hole level. We do this for both a small perturbation and a large perturbation; the latter could be regarded as an example of the process of formation of an acoustic BTZ black hole.

We note that since the effective geometry described by Eq. (4.3) couples to a massless scalar field, it follows from the discussion in Appendix B that only generalized Dirichlet boundary conditions are allowed to be imposed at $x = 0$. This, in turn, implies that the acoustic black hole will have quasinormal modes given by Eq. (3.56) with $m_\xi^2 = 0$, which means that

$$\psi_\omega(z) \propto \psi_\omega^D(z) = z^\alpha (1-z)^\lambda (1-z)^{-1/4}\, {}_2F_1(a, b; a+b+1-c; 1-z), \tag{4.20}$$

where

$$z = 1 - R_h^2/R^2, \qquad \alpha = -\frac{i\hat{\omega}}{2}, \qquad \lambda = 1, \tag{4.21}$$

and a, b, c, are given by (3.40). The corresponding frequencies will be

$$\omega = \pm\frac{m}{l} - 2i\frac{M^{1/2}}{l}\,(n+1), \qquad m, n = 0, 1, 2, 3\ldots \tag{4.22}$$

From Eq. (4.20), we can show that the field Ψ satisfy

$$\Psi\Big|_{R=\infty} = 0, \qquad \left.\frac{\partial\Psi}{\partial R}\right|_{R=\infty} = 0. \tag{4.23}$$

From $\vec{v} = -\nabla\Psi$ and Eq. (2.13), we see that on the analog model end, these boundary conditions correspond to vanishing perturbation in the velocity and density profiles at $x = 0$.

A nice feature of our model is that it maps the black hole spatial infinity to the physical (finite) boundary $\mathcal{E}$ of the system at the laboratory, at $x = 0$. Hence, the boundary conditions at $x = 0$ that are required by the sound propagation in the fluid can be naturally chosen to emulate the massless scalar field in the BTZ spacetime. For the fluid motion, these boundary conditions ensure that the energy flux across the boundary $\mathcal{E}$ is zero. At the spacetime level, these boundary conditions mean that information can neither escape to nor come from the spatial infinity.

4.3.1 Small perturbation and QNM excitation

Let us consider as initial conditions a configuration for which v is slightly perturbed from the steady state configuration v_0 at a given point x_0:

$$v(t = 0, x) = v_0(x) + \delta v(x), \tag{4.24}$$

$$\rho(t = 0, x) = \rho_0(x) + \delta\rho(x), \tag{4.25}$$

with

$$\delta v(x) = A\, e^{-\frac{(x-x_0)^6}{2\sigma^2}}, \tag{4.26}$$

$$\delta\rho(x) = 0. \tag{4.27}$$

We choose units such that $\alpha = k = c = 1$; the black hole mass then becomes $M = 1$. For simplicity, we also choose the width L as $L = 1$. The exterior region of the black hole is then mapped into the interval $-1 < x < 0$, with $x = -1$ corresponding to the horizon, and $x = 0$ corresponding to spatial infinity.

To simulate Dirichlet boundary conditions at infinity, we should impose that the disturbance vanishes at $x = 0$,

$$\delta v(x = 0) = 0, \tag{4.28}$$

$$\delta\rho(x = 0) = 0. \tag{4.29}$$

In order to avoid numerical difficulties, we impose boundary conditions at $x = -\epsilon$, with $\epsilon > 0$ being a sufficiently small parameter instead of at $x = 0$. More explicitly, we require

$$v(t, x = -\epsilon) = v_0(-\epsilon), \tag{4.30}$$

$$\rho(t, x = -\epsilon) = \rho_0(-\epsilon). \tag{4.31}$$

We solved the system given by Eqs. (4.15) and (4.16) for $v(t, x)$ and $\rho(t, x)$ with the software *Mathematica* [89].[3] Figure 4.1 shows the obtained time evolution of a perturbation initially centered at $x_0 = -0.5$. We see that the initial disturbance splits into two portions: one goes towards the horizon and falls into the supersonic region ($x < -1$). The other goes towards $x = 0$ and, around $t \sim 0.6$, is reflected at the boundary and redirected towards the horizon. Although the expression of the analog metric is degenerate at the horizon (as it occurs for a Schwarzschild black hole, for instance), the fluid physical quantities and their corresponding perturbations are both well defined there. We see that these physical quantities are also well defined in the supersonic region ($x < -1$).

[3] We used its NDSolve routine with a MaxStepSize set to 0.001. Our calculations showed good numerical convergence, with the same results for values of ϵ ranging from 10^{-3} to 10^{-7}.

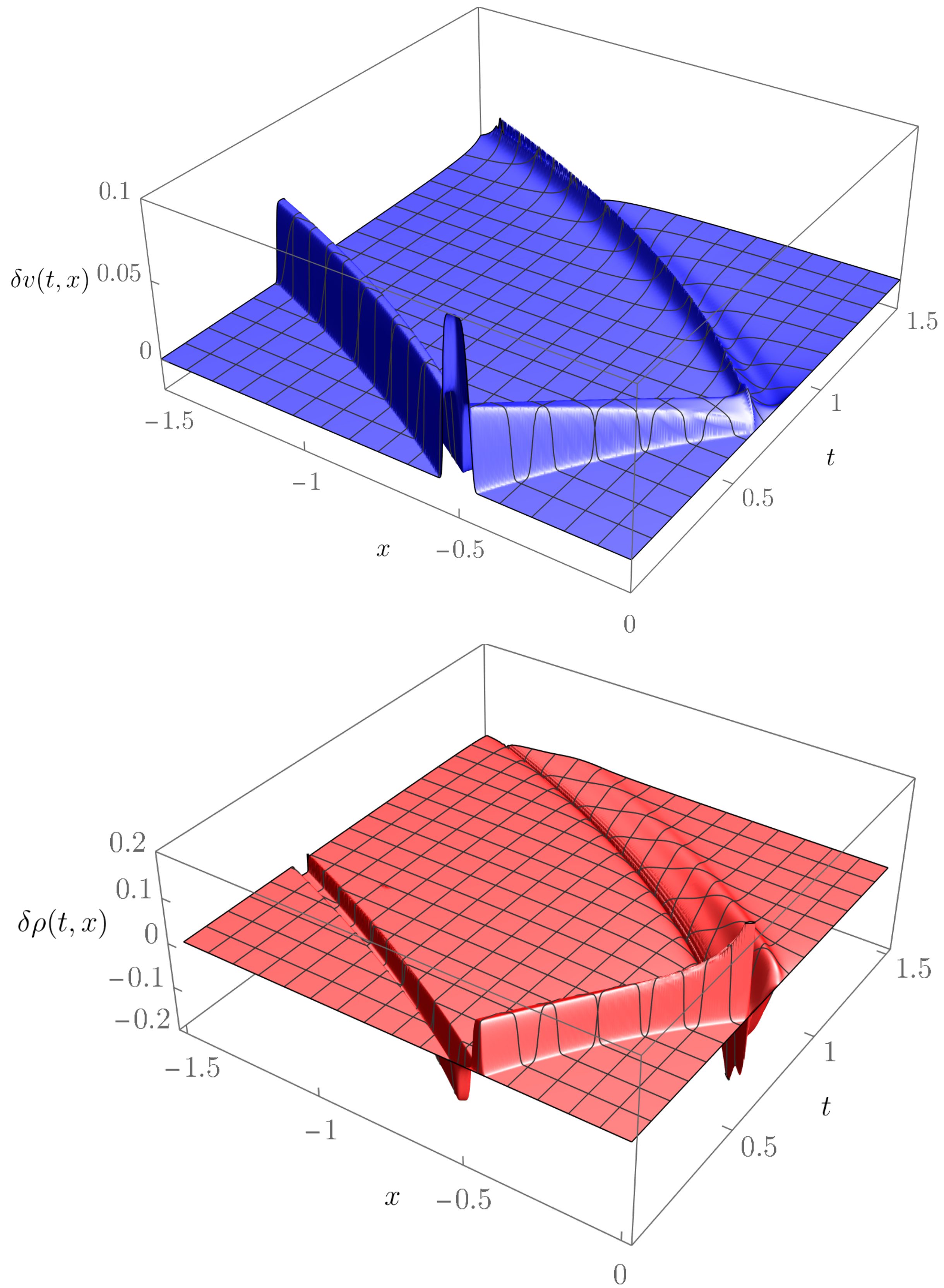

Figure 4.1: Time evolution of an initial perturbation in the background velocity (top) and density (bottom) given by Eqs. (4.26) and (4.27). The parameters were chosen as $\epsilon = 10^{-7}$, $A = 0.1$, $\sigma = 0.00005$, and $x_0 = -0.5$. The perturbation splits into two portions. One goes towards $x = 0$ and is reflected at time $t \sim 0.6$. The other goes towards the horizon and falls into the supersonic region ($x < -1$).

Quasinormal decay

As discussed in Chapter 3, it follows from the general theory of wave propagation on black hole spacetimes that the response to a perturbation on the background geometry has, in general, three distinct stages [78, 90]: (i) the early time response, which depends highly on the initial conditions; (ii) the intermediate-time regime, which is dominated by a QNM ringing; and (iii) the late-time regime, which is governed by a power law tail. Mathematically, the quasinormal modes arise from the poles of the Green's function associated with the wave equation, and the power law tail comes from a branch cut on the Green's function domain.

However, differently from the Schwarzschild and Kerr black holes, where a branch cut on the Green's function frequency domain gives rise to a late-time power law tail [78, 91, 92], the Green's function associated with wave propagation on the BTZ black hole has no branch cut on the ω-complex plane. One can see this by noting that the Green's function in this case is given by

$$G(r_*, r_*'; \omega) = \begin{cases} \frac{\psi_h(r_*',\omega)\psi_\infty(r_*,\omega)}{W(\omega;\psi_h,\psi_\infty)} & \text{if} \quad r_*' < r_*, \\ \\ \frac{\psi_h(r_*,\omega)\psi_\infty(r_*',\omega)}{W(\omega;\psi_h,\psi_\infty)} & \text{if} \quad r_* < r_*', \end{cases} \tag{4.32}$$

where $\psi_h(r_*, \omega)$ and $\psi_\infty(r_*, \omega)$ are linearly independent solutions of the radial equation Eq. (3.31) for the massless field behaving as

$$\psi_h(r_*, \omega) \sim e^{-i\omega r_*}, \qquad \text{at the horizon} \quad (r_* \to -\infty) \tag{4.33}$$

and

$$\begin{aligned} \psi_\infty(r_*, \omega) &\sim \psi^D(z(r_*)) \\ &\sim z^\alpha (1-z)^\lambda (1-z)^{-1/4} \, {}_2F_1(a, b; a+b+1-c; 1-z), \end{aligned} \tag{4.34}$$

with $z(r_*) = \operatorname{sech}^2 r_*$, at spatial infinity $r_* = 0$. The $W(\omega; \psi_h, \psi_\infty)$ stands for the Wronskian of the solutions $\psi_h(r_*)$ and $\psi_\infty(r_*)$, that is,

$$W(\omega; \psi_h, \psi_\infty) = \psi_h(r_*, \omega)\frac{\partial \psi_\infty}{\partial r_*} - \psi_\infty(r_*, \omega)\frac{\partial \psi_h}{\partial r_*}. \tag{4.35}$$

From the discussion in Chapter 3, we see that possible choices for $\psi_h(r_*, \omega)$ and $\psi_\infty(r_*, \omega)$ obeying conditions (4.33) and (4.34) are

$$\psi_h(r_*, \omega) = z^\alpha (1-z)^\lambda (1-z)^{-1/4} \, {}_2F_1(a, b; c; z), \tag{4.36}$$

$$\psi_\infty(r_*, \omega) = \psi^D(z(r_*)) = z^\alpha (1-z)^\lambda (1-z)^{-1/4} \, {}_2F_1(a, b; a+b+1-c; 1-z), \tag{4.37}$$

where z should be seen as a function of r_* given by $z = \operatorname{sech}^2 r_*$. Thus, because neither ψ_h nor ψ_∞ has a branch cut on the ω-complex plane, it follows that the Green's function in Eq. (4.32) also does not have a branch cut. As a result, the late-time behavior of the solution for the field Ψ is governed by a quasinormal (exponential) decay.[4]

In the following, we fit the intermediate and late-time behavior of our numerical solution, at a fixed position of observation x_{obs}, to a linear superposition of the first N quasinormal modes [50]. We take

$$u(\mathbf{C}; t) = v_0(x_{obs}) + \sum_{n=0}^{N} C_n e^{-i\omega_{n0}(t-t_1)}, \tag{4.38}$$

where ω_{n0} are the frequencies given by Eq. (4.22) (with $M = l = 1$) and $\mathbf{C} = (C_0, C_1, C_2, \ldots, C_N)$ are fitting parameters. We note that only frequencies with $m = 0$ are excited since nothing depends on the analog angular coordinate $y = \Theta L$.[5] We find the quasinormal approximation by minimizing the integral

$$E(\mathbf{C}) = \int_{t_1}^{t_2} [v(t, x_{obs}) - u(\mathbf{C}; t)]^2 \, dt. \tag{4.39}$$

The time interval (t_1, t_2) should be chosen within the time domain where the numerical solution $v(t, x)$ is dominated by the QNM decay.

Figure 4.2 shows the numerical velocity profile (solid curve) at fixed position $x = x_{obs} = -0.3$ as a function of time. We see the initial perturbation passing through the observation point around $t \sim 0.3$. The reflected pulse comes around $t \sim 0.85$. After $t \sim 1$ the quasinormal modes govern the signal decay. We also see in Fig. 4.2 the quasinormal fitting obtained from Eq.(4.38) for $N = 0$ (red dashed curve), $N = 1$ (green dotted curve), and $N = 3$ (blue dot-dashed curve). The corresponding parameters C_n are listed in Table 4.1.

[4] For a thorough discussion on this point, we refer the reader to [93, 90].

[5] We note that modes with nontrivial angular dependence ($m \neq 0$) cannot be considered in this model unless we impose periodic boundary conditions identifying the lines $y = 0$ and $y = L$.

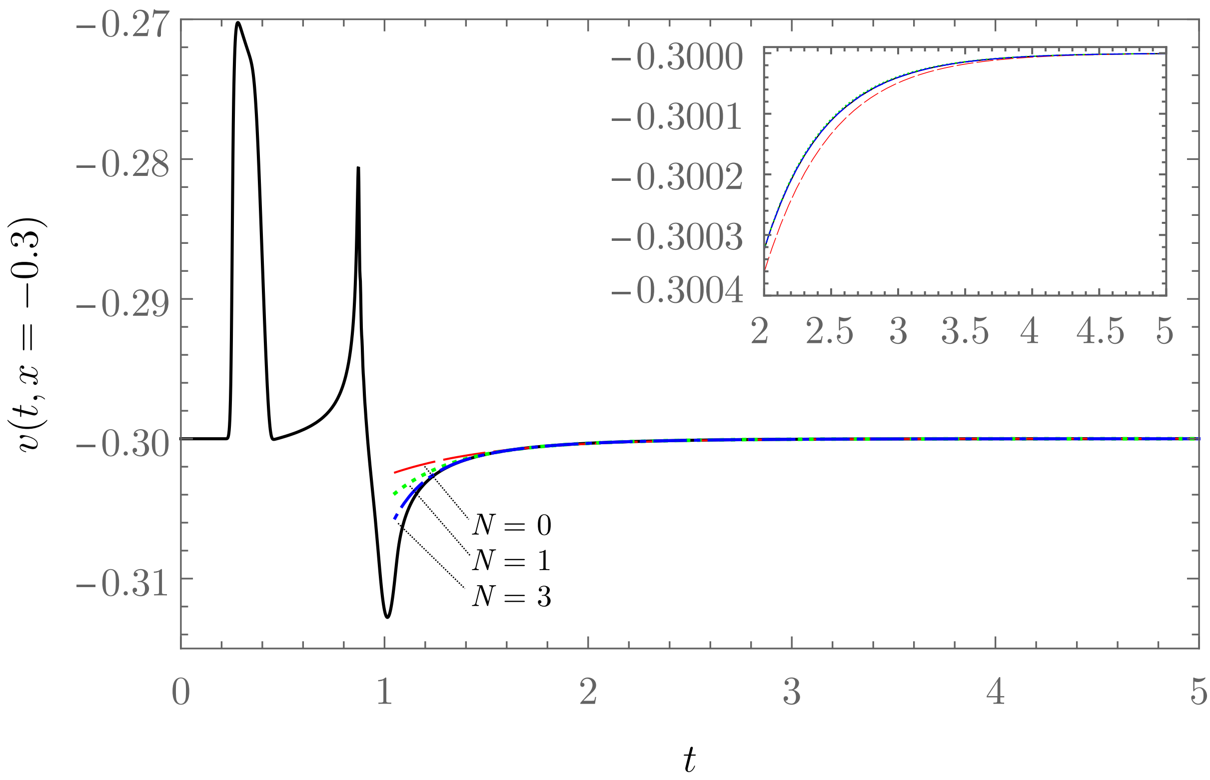

Figure 4.2: Numerical waveform $v(t, x = -0.3)$ (black solid curve) and quasinormal modes for a perturbation on the analog BTZ background. The parameter ϵ was chosen as 10^{-7}. **Top right:** quasinormal approximation to late-time behavior. The red dashed curve represents the least-damped mode ($N = 0$), the green dotted curve represents the sum of the first two modes ($N = 1$), and the blue dot-dashed curve represents the sum of the first four modes ($N = 3$). The integral (4.39) was calculated with $t_1 = 1.5$ and $t_2 = 5$.

Table 4.1: Parameters C_n for the quasinormal approximation in the scenario of a small perturbation on a steady background flow.

	$N = 0$	$N = 1$	$N = 3$
C_0	-0.000983912	-0.000757182	-0.00078922
C_1		-0.000340095	-0.000230737
C_2			-0.0000441535
C_3			-0.0000469776

4.3.2 Large perturbation: acoustic black hole formation

As another example of excitation of quasinormal modes, we now consider a possible scenario for the formation of the acoustic BTZ black hole. As an initial state for the system, we set a particular configuration where the fluid starts with zero velocity everywhere and let it evolve while subjected to the same external potential given by Eq. (4.19). Here it is worth recalling that the analog gravity framework can only probe kinematical aspects of GR, as opposed to dynamical aspects emerging from the Einstein field equations. As such, the model presented in this section does not emulate the actual dynamical evolution of the BTZ spacetime metric. The purpose of this example is to illustrate one possible formation process for the analog BTZ black hole and to analyze the corresponding excitation of its quasinormal modes.

To simulate this scenario numerically, we have taken the initial conditions

$$v(t = 0, x) = 0, \tag{4.40}$$

$$\rho(t = 0, x) = \rho_0(x), \tag{4.41}$$

and solved the fluid equations (4.15) and (4.16) with the software *Mathematica* [89].[6] Figure 4.3 shows the velocity profile at the observation point $x = -0.3$. We again found the contribution of the quasinormal modes to the waveform by using the fitting function (4.38). The values found for C_n are listed in Table 4.2.

We observe from Fig. 4.3 that the initial phase of the transition takes place roughly between $t \sim 0.8$ and $t \sim 1.6$. After that, the quasinormal modes govern the signal. We also see the late-time behavior of the velocity field (black solid curve) together with quasinormal profiles for the least-damped mode, $N = 0$ (red dashed curve), a superposition of the first two modes, $N = 1$ (green dotted curve), and of the first four modes, $N = 3$ (blue dot-dashed curve). After the quasinormal regime, $t \gtrsim 4$, the flow approximately reaches equilibrium at the steady state configuration of the acoustic BTZ black hole.

[6] The boundary conditions were again given by Eqs. (4.30) and (4.31), with the results being the same for values of ϵ ranging from 10^{-3} to 10^{-7}. This time we used the routine NDSolve with a MaxStepSize set to 0.005.

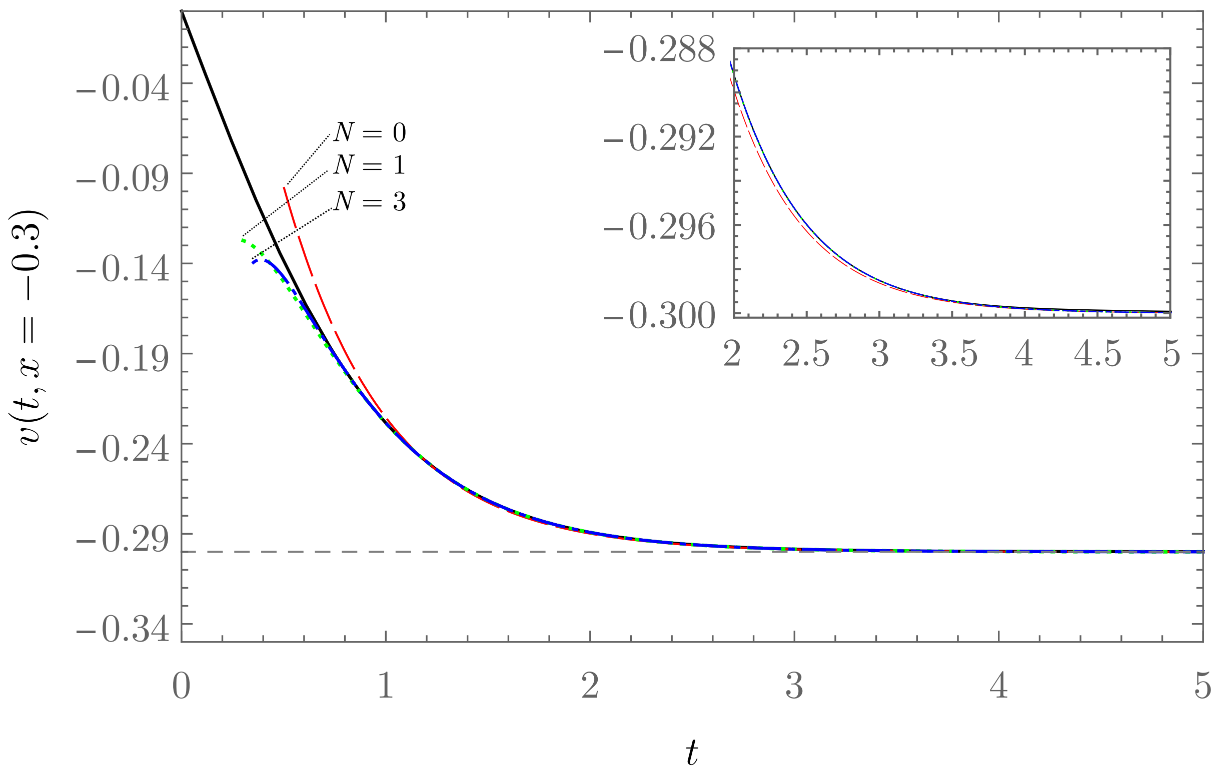

Figure 4.3: Numerical waveform $v(t, x = -0.3)$ (black solid curve) and quasinormal modes for an example of the formation of the acoustic BTZ black hole. The parameter ϵ was again chosen as 10^{-7}. The first phase of the transition occurs roughly between $t \sim 0.8$ and $t \sim 1.6$. After that, the quasinormal modes govern the signal. **Top right:** quasinormal approximation to late-time behavior. The red dashed curve represents the least-damped mode ($N = 0$), the green dotted curve represents the sum of the first two modes ($N = 1$), and the blue dot-dashed curve represents the sum of the first four modes ($N = 3$). The integral (4.39) was calculated with $t_1 = 1$ and $t_2 = 5$.

Table 4.2: Parameters C_n for the quasinormal approximation on the scenario of formation of the analog BTZ black hole.

	$N = 0$	$N = 1$	$N = 3$
C_0	0.074547	0.0808317	0.0812623
C_1		-0.00942706	-0.0113435
C_2			0.00208244
C_3			-0.000485368

Chapter 5

BTZ Black Hole in a Laval Nozzle

In this chapter, we introduce an analog model for the conformally coupled scalar field on the BTZ black hole. The model is based on the propagation of acoustic waves in a Laval nozzle. Since the BTZ black hole is not a globally hyperbolic spacetime, the dynamics of the scalar field is not well defined until extra boundary conditions are prescribed at its spatial infinity. We show that quasinormal modes satisfying Dirichlet, Neumann, and Robin boundary conditions in the BTZ black hole can be interpreted in terms of ordinary QNMs defined with respect to an appropriately extended nozzle. We also discuss the stability of our model with respect to small perturbations. The material in this chapter is strongly based on our work [55].

5.1 Introduction

In this chapter, we introduce an analog model for the conformally coupled scalar field on a BTZ black hole based on a Laval nozzle, which is a convergent-divergent nozzle with a throat in the middle, usually employed to accelerate air [51]. By establishing a sufficiently strong difference of pressure between the nozzle ends, a transonic flow regime can be achieved. On one side of the nozzle, there is a subsonic flow; on the other side, a supersonic flow is established. The sonic point (where air velocity equals sound velocity) is located at the nozzle throat.

We find that the obtained nozzle has a finite length, with its end corresponding to the spatial infinity of the BTZ spacetime, so that our analog model effectively maps the exterior region of the BTZ black hole into a finite region of the Laval nozzle. Since the effective potential governing the wave propagation does not vanish at the nozzle end (which corresponds to the BTZ spatial infinity), we still cannot impose plane wave outgoing boundary conditions to find QNMs. In order to circumvent this problem, we consider a family of extensions for the nozzle. We choose the extensions in such a way that the corresponding effective potentials go to zero in the new end. By doing this, we recover the plane wave behavior, and we can thus impose outgoing boundary conditions and find the ordinary QNMs of the extended nozzle (corresponding to BTZ spacetime + extension). In this way, we interpret the QNMs of the conformally coupled scalar field on the BTZ black hole (which do not obey outgoing boundary conditions at spatial infinity) in terms of ordinary QNMs of acoustic waves in the nozzle (which do obey the usual outgoing boundary conditions). We find that the ordinary QNMs can be sorted according to their parity and show that odd ordinary QNMs correspond to QNMs in the black hole which satisfy a Dirichlet boundary condition, and even ordinary QNMs correspond to black hole QNMs obeying Neumann or Robin boundary conditions.

Finally, we use a result from the dynamics of the scalar field in the BTZ black hole [67] to discuss the stability of our model under linear perturbations.

This chapter is organized as follows. In Sec. 5.2, we briefly review the equations of acoustics in the Laval nozzle and apply the method of [52] to find the nozzle for which acoustic waves correspond to those of a conformally coupled field on the BTZ black hole. In Sec. 5.3, we consider continuations of the effective potential of Sec. 5.2 to find extensions for the nozzle previously obtained. We also show how one may use the ordinary QNMs of acoustic waves to emulate QNMs obeying Dirichlet, Neumann and Robin boundary conditions at BTZ spatial infinity. After that, we discuss the stability of our model under small perturbations.

5.2 The Nozzle Analog to the BTZ Black Hole

5.2.1 Conformally coupled field propagating on the BTZ black hole

The equation of motion for the scalar field Ψ conformally coupled to the static BTZ geometry is obtained taking $\mu^2 = 0$ and $\xi = 1/8$ in Eq. (3.24) so that Eq. (3.23) becomes [94, 95]

$$\left(\Box + \frac{3}{4l^2}\right)\Psi = 0, \tag{5.1}$$

where the d'Alembertian operator, $\Box = \nabla_\mu \nabla^\mu$, is calculated with respect to the spacetime metric Eq. (3.6).

The radial equation in this case is given by Eq. (3.31) with the effective potential

$$\hat{V}_{\mathrm{BTZ}}(\hat{r}_*) = \left(\frac{4m^2 + M}{4M}\right) \operatorname{sech}^2 \hat{r}_*, \tag{5.2}$$

Note that we have rescaled r_* and ω so that $\hat{r}_* = (M^{1/2}/l)r_*$ and $\hat{\omega} = (l/M^{1/2})\omega$, as in Eq. (3.30).

We intend to simulate the scalar field propagation determined by the effective potential $\hat{V}_{\mathrm{BTZ}}(\hat{r}_*)$ in terms of acoustic waves propagating in an appropriately designed Laval nozzle. In order to achieve this, we need to know how the shape of the nozzle determines the wave propagation. In what follows, we review the fundamental equations of fluid dynamics in the Laval nozzle and show how the cross-sectional area determines the effective potential for acoustic waves.

5.2.2 Wave propagation in the Laval nozzle

Let us take the x coordinate along the axial direction of the nozzle. We consider air as a perfect fluid flowing in a quasi-one-dimensional regime [51], where physical quantities vary along the x axis only. The equations of motion are then the continuity and Euler's equations,

$$\partial_t (\rho A) + \partial_x (\rho v A) = 0, \tag{5.3}$$

$$\rho (\partial_t + v\partial_x) v = -\partial_x p, \tag{5.4}$$

where ρ is the air density, p is the pressure, v is the air velocity, and A is the nozzle cross-sectional area. Furthermore, we shall assume the gas is isentropic

$$p \propto \rho^\gamma, \tag{5.5}$$

where $\gamma = 7/5$ stands for the heat capacity ratio of air.

Assuming an irrotational flow, $v = \partial_x \Phi$, and defining the specific enthalpy $h(\rho) = \int \rho^{-1} dp$, Eq. (5.4) reduces to the Bernoulli's equation

$$\partial_t \Phi + \frac{1}{2} (\partial_x \Phi)^2 + h(\rho) = 0. \tag{5.6}$$

To derive the linearized wave equation for sound, we first rewrite (ρ, Φ) as the sum of a contribution corresponding to the background flow $(\bar{\rho}, \bar{\Phi})$ and a contribution corresponding to the acoustic disturbance $(\delta\rho, \phi)$. The background and perturbation satisfy

$$\begin{aligned} \rho =& \quad \bar{\rho} + \delta\rho, & \bar{\rho} \gg |\delta\rho|, \\ \Phi =& \quad \bar{\Phi} + \phi, & |\partial_x\bar{\Phi}| \gg |\partial_x\phi|. \end{aligned} \tag{5.7}$$

Following [50], we define the auxiliary quantities

$$g = \frac{\bar{\rho}A}{c_s} = \frac{\bar{\rho}A}{\sqrt{\gamma\bar{p}/\bar{\rho}}}, \tag{5.8}$$

$$f(x) = \int \frac{|v|dx}{c_s^2 - v^2}, \tag{5.9}$$

$$H_\omega = g^{1/2} \int dt e^{i\omega[t-f(x)]}\phi(t,x), \tag{5.10}$$

$$x_* = c_{s0} \int \frac{dx}{c_s(1-\mathcal{M}^2)}, \tag{5.11}$$

where $c_s = \sqrt{\partial p/\partial\rho} = \sqrt{\gamma\bar{p}/\bar{\rho}}$ is the local sound speed, c_{s0} is the stagnation sound speed, constant over the isentropic flow, and $\mathcal{M} = |v|/c_s$ is the Mach number. In terms of these quantities, the wave equation reduces to

$$-\frac{d^2H_\omega}{dx_*^2} + V(x_*)H_\omega = \kappa^2 H_\omega, \tag{5.12}$$

where

$$\kappa = \frac{\omega}{c_{s0}}, \tag{5.13}$$

and the effective potential is given by

$$V(x_*) = \frac{1}{g^2}\left[\frac{g}{2}\frac{d^2g}{dx_*^2} - \frac{1}{4}\left(\frac{dg}{dx_*}\right)^2\right]. \tag{5.14}$$

The effective potential $V(x_*)$ characterizes the dynamics of acoustic waves in the gas flow. For a transonic flow in a Laval nozzle, all the nondimensional quantities (ρ/ρ_0, p/p_0, $\mathcal{M}, \dots$) are uniquely determined by the function $A(x_*)/A_{th}$, where A_{th} is the cross-sectional area at the throat of the nozzle [51, 50]. In particular, the function $g(x_*)$ and the effective potential $V(x_*)$ are also completely determined by $A(x_*)/A_{th}$. On the other hand, A (and hence all other physical quantities) can be fully determined in terms of g by the equations relating the physical variables in the nozzle.

Let us see more closely how one can express the physical quantities in terms of g. First, we note that it follows from Eqs. (5.5) and (5.8) that

$$g \propto \frac{\bar{\rho}A}{\bar{\rho}^{(\gamma-1)/2}}, \tag{5.15}$$

and from [51], we have

$$\left(\frac{A}{A_{th}}\right)^{-1} = \frac{1}{\eta_\gamma}\left[1-\left(\frac{\bar{\rho}}{\rho_0}\right)^{(\gamma-1)}\right]^{1/2}\frac{\bar{\rho}}{\rho_0}, \tag{5.16}$$

where ρ_0 is the stagnation density and

$$\eta_\gamma = \sqrt{\frac{\gamma-1}{2}}\left(\frac{2}{\gamma+1}\right)^{\frac{\gamma+1}{2(\gamma-1)}}. \tag{5.17}$$

Since Eq. (5.12) is invariant under rescaling of g, we take the coefficient in Eq. (5.15) so that

$$g = \frac{\frac{A}{\eta_\gamma A_{th}}\frac{\bar{\rho}}{\rho_0}}{2\left(\frac{\bar{\rho}}{\rho_0}\right)^{(\gamma-1)/2}}. \tag{5.18}$$

With the assumptions above, we can implement the same reasoning of [52] to find the physical variables in terms of g:

$$\frac{A}{A_{th}} = \frac{\eta_\gamma\sqrt{2}\left[2g^2\left(1-\sqrt{1-g^{-2}}\right)\right]^{1/(\gamma-1)}}{\sqrt{1-\sqrt{1-g^{-2}}}}, \tag{5.19}$$

$$\left(\frac{\bar{\rho}}{\rho_0}\right)^{1-\gamma} = 2g^2\left(1-\sqrt{1-g^{-2}}\right), \tag{5.20}$$

$$c_s = \frac{c_{s0}}{\sqrt{2g^2\left(1-\sqrt{1-g^{-2}}\right)}}, \tag{5.21}$$

$$\mathcal{M}^2 = \frac{2}{\gamma-1}\left(2g^2\left(1-\sqrt{1-g^{-2}}\right)-1\right). \tag{5.22}$$

For convenience, we rescale x_* and ω to dimensionless quantities $\hat{x}_*$ and $\hat{\omega}$ such that

$$\hat{x}_* = \frac{x_*}{L}, \tag{5.23}$$

and

$$\kappa = \frac{\omega}{c_{s0}} = \frac{\hat{\omega}}{c_{s0}T} = \frac{\hat{\omega}}{L}, \tag{5.24}$$

where L is a characteristic length in the nozzle and a characteristic time interval was chosen as $T = L/c_{s0}$. Equation (5.12) then yields

$$-\frac{d^2 H_\omega}{d\hat{x}_*^2} + \hat{V}(\hat{x}_*)H_\omega = \hat{\omega}^2 H_\omega, \tag{5.25}$$

where the dimensionless effective potential is given by

$$\hat{V}(\hat{x}_*) = \frac{1}{g^2}\left[\frac{g}{2}\frac{d^2 g}{d\hat{x}_*^2} - \frac{1}{4}\left(\frac{dg}{d\hat{x}_*}\right)^2\right]. \tag{5.26}$$

5.2.3 Inverse problem

The calculations above show how the nozzle shape, given by $A(x_*)$, determines the wave propagation in the nozzle by means of the effective potential $\hat{V}(x_*)$. We now want to find a nozzle shape which mimics the effective potential $\hat{V}_{\mathrm{BTZ}}$ for perturbations in the BTZ black hole background.

As mentioned before, all physical quantities describing the flow in the Laval nozzle can be determined from the cross section A. On the other hand, given an effective potential, say $\hat{V} = \hat{V}_{\mathrm{BTZ}}$, we should be able to find g by solving Eq. (5.26). This, in turn, determines the shape of the nozzle by means of Eq. (5.19). A boundary condition for g is given by imposing that the air and sound velocities are equal at the acoustic horizon, $|v| = c_s$, so that, from Eq. (5.22),

$$g|_{\mathrm{horizon}} = \frac{\gamma + 1}{2\sqrt{2}\sqrt{\gamma - 1}} = \frac{3}{\sqrt{5}}. \tag{5.27}$$

Before equating $\hat{V}_{\mathrm{BTZ}}$ to the effective potential in the nozzle, we need to relate the radial coordinate r of the BTZ spacetime to the coordinate along the nozzle x. In order to achieve this, we identify the respective tortoise coordinates, $d\hat{r}_* = d\hat{x}_*$. From Eqs. (5.11), (5.21) and (5.22), we have

$$d\hat{r}_* = d\hat{x}_* = \frac{c_{s0}d\hat{x}}{c_s(1-\mathcal{M}^2)} = \frac{\sqrt{2g^2\left(1-\sqrt{1-g^{-2}}\right)}d\hat{x}}{1-\frac{2}{\gamma-1}\left[2g^2\left(1-\sqrt{1-g^{-2}}\right)-1\right]}, \tag{5.28}$$

so that

$$\frac{d\hat{x}}{d\hat{r}_*} = \frac{1 - \frac{2}{\gamma - 1}\left[2g^2\left(1 - \sqrt{1 - g^{-2}}\right) - 1\right]}{\sqrt{2g^2\left(1 - \sqrt{1 - g^{-2}}\right)}}, \tag{5.29}$$

where $\hat{x}$ is the nondimensional coordinate related to the coordinate along the nozzle by $\hat{x} = x/L$.

Since the tortoise coordinates for the nozzle and for the BTZ spacetime were made identical, we can now equate the effective potentials, Eqs. (5.26) and (5.2), to obtain

$$\frac{g''(\hat{r}_*)}{2g(\hat{r}_*)} - \frac{g'(\hat{r}_*)^2}{4g(\hat{r}_*)^2} = \hat{V}_{\text{BTZ}}(\hat{r}_*), \tag{5.30}$$

where the prime indicates differentiation with respect to $\hat{r}_*$, $g' = dg/d\hat{r}_*$. This equation can be simplified by the substitution [53]

$$g(\hat{r}_*) = h^2(\hat{r}_*) \tag{5.31}$$

so that

$$-h''(\hat{r}_*) + \hat{V}_{\text{BTZ}}(\hat{r}_*)h(\hat{r}_*) = 0. \tag{5.32}$$

To obtain the configuration of the nozzle corresponding to the effective potential in Eq. (5.2), we have to solve Eq. (5.32) and use Eq. (5.31) and the boundary condition Eq. (5.27) to determine g. Then, by Eqs. (5.19) and (5.29), we can find the cross section A as a function of the coordinate x along the nozzle, such that the sound propagation now mimics a scalar field propagating on the BTZ spacetime.

5.2.4 The Laval nozzle for the conformal scalar field propagating on the BTZ black hole

To keep the calculations as simple as possible, we are going to consider the mode solution with angular momentum $m = 0$ (the case $m \neq 0$ can be treated in a similar fashion and is briefly discussed at the end of Sec. 5.3.3). In order to solve Eq. (5.32), we change to the new variable

$$u = \tanh \hat{r}_*, \tag{5.33}$$

which turns the differential equation Eq. (5.32) into

$$(1-u^2)\frac{d^2h}{du^2} - 2u\frac{dh}{du} + \nu(\nu+1)h = 0, \tag{5.34}$$

where we have defined $\nu = -1/2$. The differential equation Eq. (5.34) is the well-known Legendre's equation and has the linearly independent solutions [84]

$$h_1(u) = P_\nu(u), \qquad h_2(u) = Q_\nu(u), \tag{5.35}$$

which are known as Legendre functions of the first and second kinds, respectively.

Returning to the coordinate r_* [1], we have that the general solution to the differential equation (5.32) can be expressed as a linear combination

$$h(r_*) = c_1 h_1(r_*) + c_2 h_2(r_*), \tag{5.36}$$

where c_1, c_2, are constants and

$$h_1(r_*) = P_{-\frac{1}{2}}(\tanh r_*), \qquad h_2(r_*) = Q_{-\frac{1}{2}}(\tanh r_*). \tag{5.37}$$

Since $h_1(r_*)$ diverges at the horizon ($r_* \to -\infty$), we take $c_1 = 0$. The boundary condition Eq. (5.27) then determines c_2 so that

$$h(r_*) = \frac{2}{\pi}\sqrt{\frac{3}{\sqrt{5}}}\, Q_{-\frac{1}{2}}(\tanh r_*). \tag{5.38}$$

Having obtained $h(r_*)$, we use Eqs. (5.31), (5.19) and (5.29) to find the cross section A as a function of the coordinate along the nozzle. The lateral section of the resulting nozzle is represented by the black solid curve in Fig. 5.1, where we also plotted the effective potential (red dashed curve). The exterior region of the BTZ black hole corresponds to the subsonic region ($x > 0$).

Figure 5.2 shows the relation between the x coordinate along the nozzle and the radial coordinate r of the BTZ black hole. We observe that x has a finite upper limit, at $x_{\text{end}} \cong 0.417306$. Hence the obtained nozzle has a finite length, with the upper limit of x being mapped into the spatial infinity of the BTZ black hole. In other words, this means that the exterior

[1] Hereafter, we will drop the hat in $\hat{r}_*$ to keep the notation simpler.

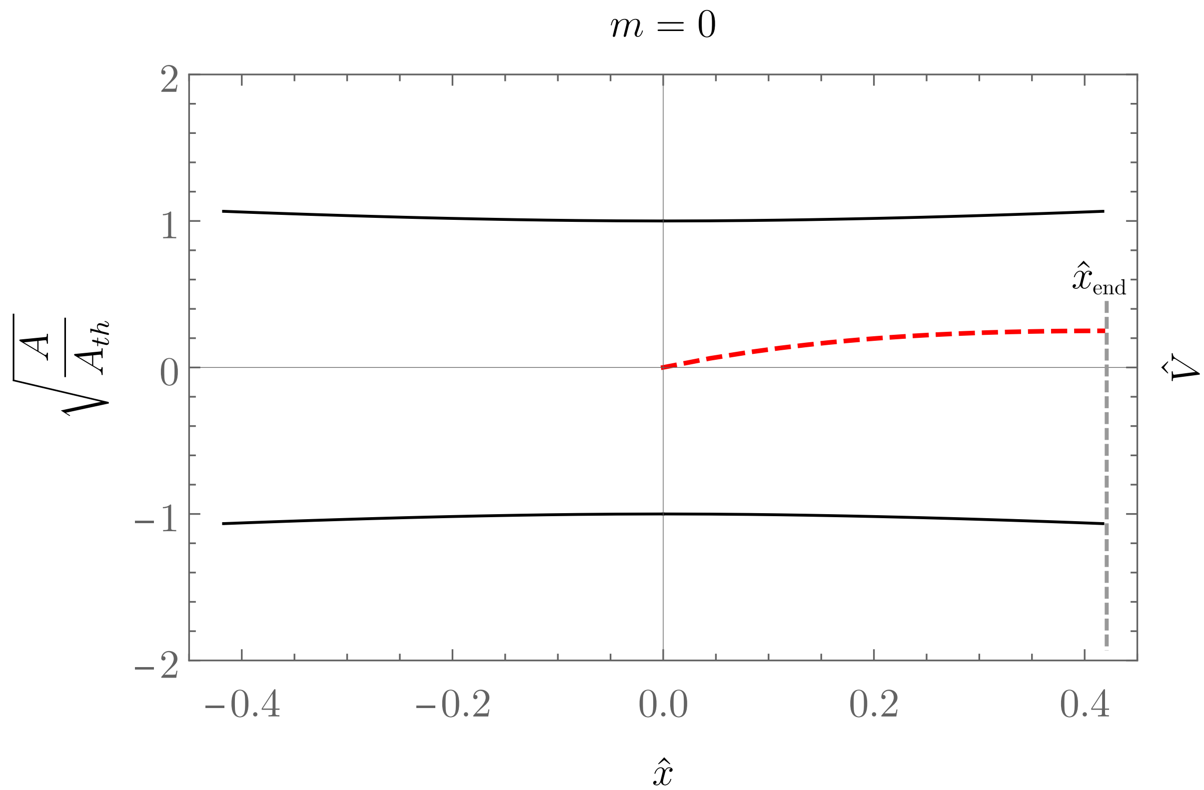

Figure 5.1: (Black curve) Lateral section of the Laval nozzle corresponding to the conformally coupled scalar field. The region $\hat{x} > 0$ ($\hat{x} < 0$) corresponds to subsonic (supersonic) flow. The sonic point (where the fluid velocity equals the sound velocity) is located at the throat $\hat{x} = 0$. (Red dashed line) Nondimensional effective potential for acoustic waves in the subsonic region.

region of the BTZ black hole is mapped into a finite region in the laboratory, with the spatial infinity of the BTZ spacetime being mapped into the right end of the nozzle.

It follows that, in order to determine the acoustic wave propagation in the nozzle completely, it is necessary to prescribe a boundary condition at its right end. At the BTZ spacetime level, the necessity for a boundary condition at spatial infinity comes from its lack of global hyperbolicity [95, 69, 70, 71], as we already mentioned in Chapter 3. Therefore, via the correspondence found above, our model simulates the needed boundary conditions at the conformal boundary of the BTZ spacetime by appropriate boundary conditions at the nozzle (finite) right end.

The boundary conditions that are compatible with sensible dynamics for the scalar field propagating in the BTZ spacetime were studied in [95] and are also presented in Appendix B. In particular, for the conformally coupled scalar field, we have that Robin boundary conditions

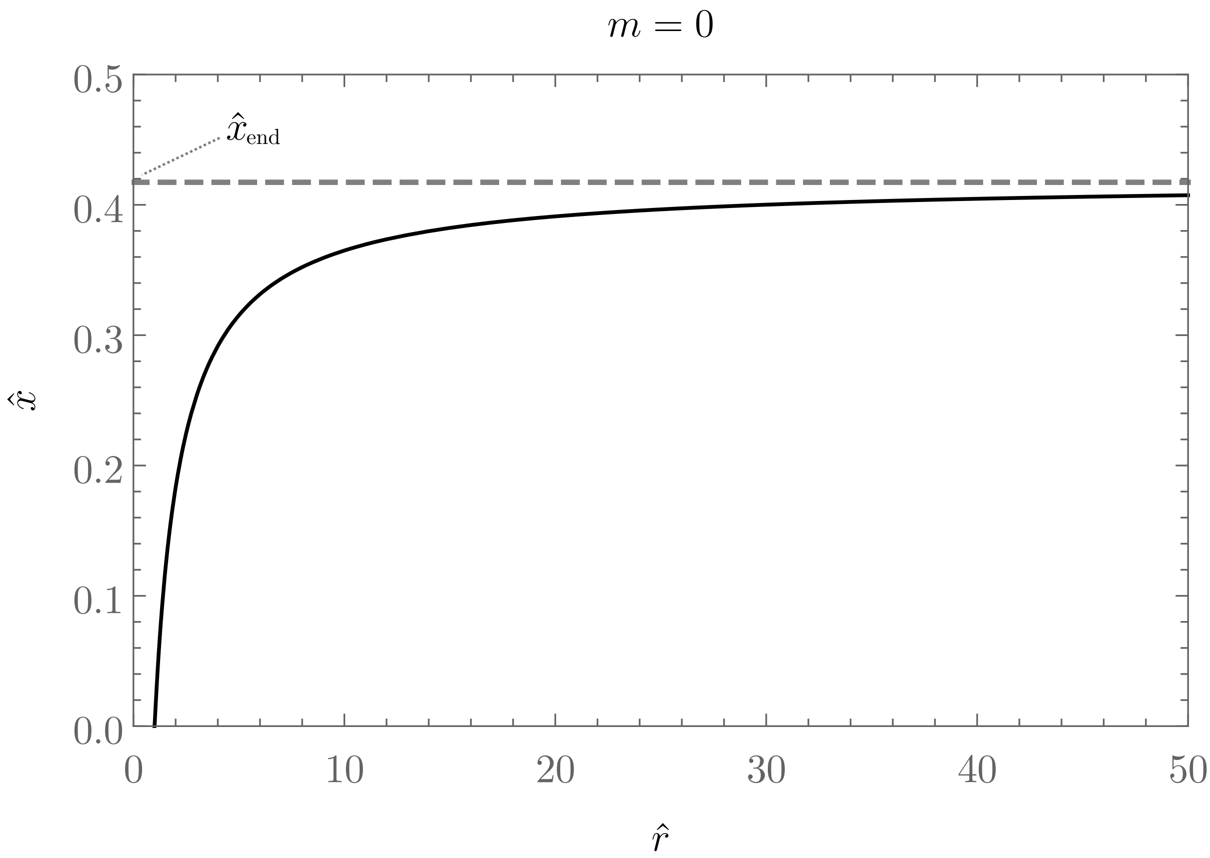

Figure 5.2: The nondimensional coordinate along the nozzle $\hat{x}$ as a function of the nondimensional radial coordinate $\hat{r}$ of the BTZ spacetime. The coordinate $\hat{x}$ has a finite upper limit, $\hat{x}_{\text{end}} \cong 0.417306$, which means that the corresponding nozzle has a finite length. The upper limit in the coordinate $\hat{x}$ is mapped into the spatial infinity of the BTZ spacetime.

(RBCs),

$$\left.\frac{d\psi/dr_*}{\psi}\right|_{r_*=0} = \beta, \tag{5.39}$$

lead to an unambiguous time evolution. In this case, $\beta = \pm\infty$ corresponds to the Dirichlet boundary condition at infinity, $\psi|_{r_*=0} = 0$, and $\beta = 0$ corresponds to the Neumann boundary condition, $d\psi/dr_*|_{r_*=0} = 0$. Aside from that, in [67], Dappiaggi *et al.* calculated the effect of RBCs on the quasinormal modes of the scalar field in the BTZ black hole. In the next section, we propose a nozzle configuration appropriate to realize QNMs obeying RBCs in the BTZ black hole.

5.3 Robin Boundary Conditions in the BTZ Analog Nozzle

5.3.1 Nozzle extension

We have seen above that the nozzle, which mimics the BTZ spacetime, would abruptly end at a finite distance from the throat, at $x = x_{\text{end}} \cong 0.417306$. In what follows, we continue the nozzle in such a way that the usual boundary condition for QNMs at its far right, $x \to \infty$, induces RBCs at x_{end}. In the r_* coordinate, this corresponds to extending the potential $V_{\text{BTZ}}(r_*)$ to the region $r_* > 0$ (recall that the original range of the coordinate r_* is from $-\infty$ to 0).

We will consider the following extension of $V_{\text{BTZ}}(r_*)$ for $r_* \geq 0$:

$$V_{\text{eff}}(r_*) = \left[\frac{4m^2 + M}{M}\right] \operatorname{sech}^2 r_* + a\,\delta(r_*), \tag{5.40}$$

where $\delta(r_*)$ is the Dirac delta function, a is a constant, and $-\infty < r_* < \infty$. We note that, for $-\infty < r_* < 0$, this effective potential reduces to Eq. (5.2). Moreover, for $r_* \to \infty$, V_{eff} goes to zero, and we recover the plane wave behavior, typical for asymptotically flat spacetimes, for the field (i.e., $\psi \sim e^{\pm i\omega r_*}$, when $r_* \to \infty$). In particular, this implies that usual outgoing boundary conditions for QNMs can now be imposed in the extended model. The delta function term has the effect of producing a shape change in $A(x)$ at $x = 0$ (see Fig. 5.3), which will be explored in what follows to implement the RBCs in the BTZ spacetime.

Let us calculate the shape of the extended nozzle, which corresponds to the extended potential above. We do this by solving Eq. (5.32) with $V(r_*)$ given by Eq. (5.40).

For $r_* < 0$, the calculations are identical to the case treated in the previous section. Thus, the corresponding solution is given by Eq. (5.38). For convenience, we now denote this solution by $h^{(<)}(r_*)$,

$$h^{(<)}(r_*) = \frac{2}{\pi}\sqrt{\frac{3}{\sqrt{5}}}\, Q_{-\frac{1}{2}}(\tanh r_*). \tag{5.41}$$

For $r_* > 0$, we have

$$h^{(>)}(r_*) = c_1 h_1(r_*) + c_2 h_2(r_*), \tag{5.42}$$

with $h_1(r_*)$ and $h_2(r_*)$ given by Eqs. (5.37). We now have to match these solutions at $r_* = 0$ to find the constants c_1, c_2. First, continuity requires

$$h^{(<)}(r_* \to 0^-) = h^{(>)}(r_* \to 0^+). \tag{5.43}$$

The other boundary condition is obtained by integrating Eq. (5.32) inside an arbitrarily small neighborhood of $r_* = 0$, which leads to

$$\left.\frac{dh^{(>)}}{dr_*}\right|_{r_*=0^+} - \left.\frac{dh^{(<)}}{dr_*}\right|_{r_*=0^-} = a\,h(0). \tag{5.44}$$

This equation shows that a characterizes the shape change of the nozzle at $x = 0$ (see Fig. 5.3).

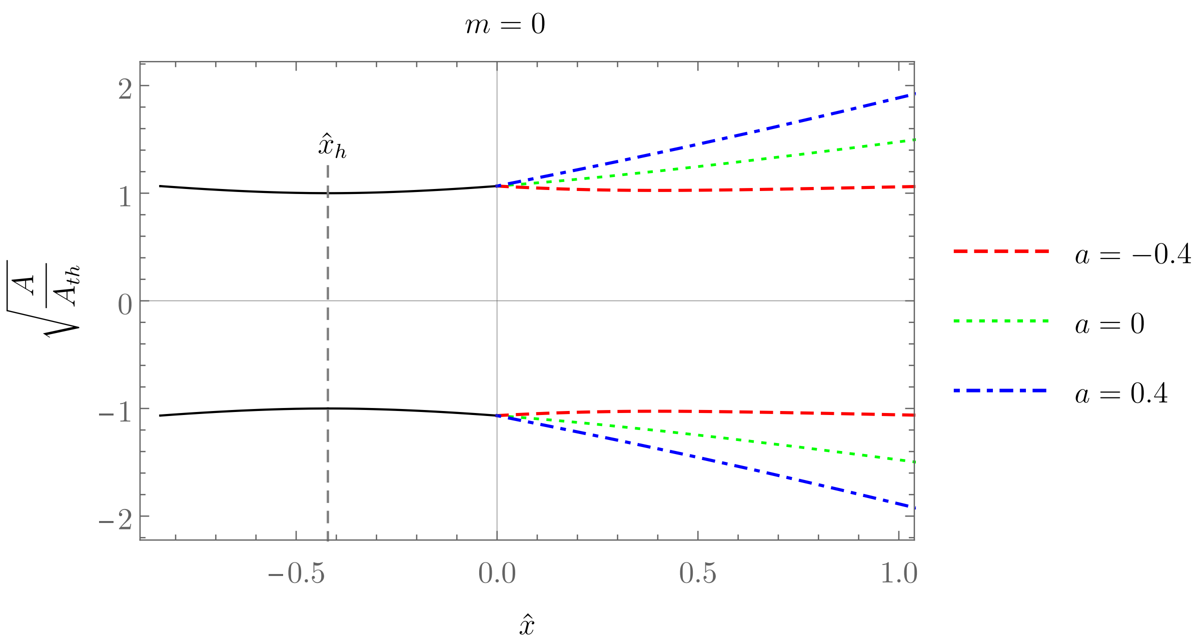

Figure 5.3: Lateral section of the extended Laval nozzle with different values of the parameter a. Each value determines a different extension for the effective potential. Since the wave phenomena is mainly determined by the effective potential, different values of a will lead to different quasinormal spectra. Notice that we have translated the $\hat{x}$ axis by $\hat{x} \to \hat{x} - \hat{x}_{\text{end}}$ so that now the origin $\hat{x} = 0$ corresponds to BTZ spatial infinity, and the horizon corresponds to $\hat{x}_h = -\hat{x}_{\text{end}} \cong -0.417306$.

Using Eqs. (5.43) and (5.44), we find

$$c_1 = -\sqrt{\frac{3}{\sqrt{5}}}\frac{\pi^2 a}{2\,\Gamma\left(\frac{3}{4}\right)^4}, \tag{5.45}$$

$$c_2 = \sqrt{\frac{3}{\sqrt{5}}}\left[\frac{2}{\pi} + \frac{\pi a}{\Gamma\left(\frac{3}{4}\right)^4}\right], \tag{5.46}$$

so that

$$h(r_*) = \sqrt{\frac{3}{\sqrt{5}}}\, Q_{-\frac{1}{2}}(\tanh r_*)\, \theta(-r_*) + \sqrt{\frac{3}{\sqrt{5}}} \left\{ -\frac{\pi^2 a}{2\,\Gamma\left(\frac{3}{4}\right)^4} P_{-\frac{1}{2}}(\tanh r_*) + \left[\frac{\pi a}{\Gamma\left(\frac{3}{4}\right)^4} + \frac{2}{\pi} \right] Q_{-\frac{1}{2}}(\tanh r_*) \right\} \theta(r_*), \tag{5.47}$$

where $\theta(r_*)$ stands for the Heaviside step function. The nozzle shape can then be determined by following the steps discussed in Sec. 5.2. Figure 5.3 shows nozzle extensions obtained for some values of the parameter a.

We note that the diverging behavior of the cross-sectional area as $x \to \infty$ does not spoil the one-dimensional character of the motion because one can always make $A(x)$ vary as slowly as desired by suitably choosing units for x. As pointed out in [52], this is equivalent to "pulling" the nozzle along its axis. In the present case, such a pulling means that we consider a BTZ black hole with a larger ratio $l/M^{1/2}$.

5.3.2 Quasinormal modes of the extended nozzle

Quasinormal modes are characteristic vibrations that describe the energy loss of a system after a perturbation [45, 47, 46]. In principle, they can appear in any physical context involving open systems (not only black holes) [77]. Quasinormal modes in a black hole background are usually defined as mode solutions satisfying ingoing boundary conditions at the horizon ($\psi_\omega \sim e^{-i\omega r_*}$, as $r_* \to -\infty$), and outgoing boundary conditions at spatial infinity ($\psi_\omega \sim e^{i\omega r_*}$, as $r_* \to \infty$). This definition works perfectly well for asymptotically flat spacetimes, since the effective potential coupled to the field vanishes at infinity. However, for asymptotically curved spacetimes, the effective potential is not zero at infinity, and one cannot distinguish ingoing from outgoing modes there [48, 49, 67].

As mentioned before, in contrast with the situation in asymptotically curved spacetimes, the effective potential of our extended nozzle vanishes at $r_* \to +\infty$. Hence one can define QNMs by the usual asymptotic behavior

$$\psi_\omega \sim e^{-i\omega r_*}, \qquad r_* \to -\infty, \tag{5.48}$$

$$\psi_\omega \sim e^{+i\omega r_*}, \qquad r_* \to +\infty. \tag{5.49}$$

The asymptotic conditions (5.48) and (5.49) completely determine the acoustic QNMs in the Laval nozzle. We will refer to modes satisfying Eqs. (5.48) and (5.49) as *ordinary* quasinormal modes.

Quasinormal modes obeying Robin boundary conditions in the BTZ black hole were previously analyzed in [67]. In what follows, we will use the ordinary QNMs of acoustic waves in the nozzle to emulate QNMs of the conformal scalar field obeying RBCs in the BTZ black hole. In order to achieve this, we now calculate the former explicitly.

First, we note that the general solution of Eq. (5.58) can be written in terms of the independent solutions given in Eqs. (3.46) and (3.47) if we take $m_\xi^2 = -3/4l^2$, so that

$$\psi_\omega^D(r_*) = -\tanh r_* \,(\operatorname{sech} r_*)^{-i\omega}\, {}_2F_1\left(\frac{3}{4} - \frac{i\omega}{2}, \frac{3}{4} - \frac{i\omega}{2}; \frac{3}{2}; \tanh^2 r_*\right), \tag{5.50}$$

$$\psi_\omega^N(r_*) = (\operatorname{sech} r_*)^{-i\omega}\, {}_2F_1\left(\frac{1}{4} - \frac{i\omega}{2}, \frac{1}{4} - \frac{i\omega}{2}; \frac{1}{2}; \tanh^2 r_*\right). \tag{5.51}$$

However, for our purposes in this chapter, it is convenient to consider another pair of linearly independent solutions. In order to achieve this, we first write the formulas [84]

$$P_\rho^\sigma(x) = \cos\left(\frac{\pi}{2}(\rho+\sigma)\right) w_1(\rho,\sigma,x) + \sin\left(\frac{\pi}{2}(\rho+\sigma)\right) w_2(\rho,\sigma,x), \tag{5.52}$$

$$Q_\rho^\sigma(x) = -\frac{\pi}{2}\sin\left(\frac{\pi}{2}(\rho+\sigma)\right) w_1(\rho,\sigma,x) + \frac{\pi}{2}\cos\left(\frac{\pi}{2}(\rho+\sigma)\right) w_2(\rho,\sigma,x), \tag{5.53}$$

where $P_\rho^\sigma(x)$ and $Q_\rho^\sigma(x)$ are Legendre functions of the first and second kinds, respectively, and

$$w_1(\rho,\sigma,x) = \frac{2^\sigma \Gamma\left(\frac{\rho}{2}+\frac{\sigma}{2}+\frac{1}{2}\right)}{\sqrt{\pi}\,\Gamma\left(\frac{\rho}{2}-\frac{\sigma}{2}+1\right)}\left(1-x^2\right)^{-\sigma/2} {}_2F_1\left(-\frac{\rho}{2}-\frac{\sigma}{2}, \frac{\rho}{2}-\frac{\sigma}{2}+\frac{1}{2}; \frac{1}{2}; x^2\right), \tag{5.54}$$

$$w_2(\rho,\sigma,x) = \frac{2^{\sigma+1} \Gamma\left(\frac{\rho}{2}+\frac{\sigma}{2}+1\right)}{\sqrt{\pi}\,\Gamma\left(\frac{\rho}{2}-\frac{\sigma}{2}+\frac{1}{2}\right)} x\left(1-x^2\right)^{-\sigma/2} {}_2F_1\left(\frac{1}{2}-\frac{\rho}{2}-\frac{\sigma}{2}, \frac{\rho}{2}-\frac{\sigma}{2}+1; \frac{3}{2}; x^2\right). \tag{5.55}$$

Taking $\rho = -1/2$, $\sigma = i\omega$ and $x = \tanh \hat{r}_*$ in Eqs. (5.54) and (5.55), it follows that

$$w_1(\rho,\sigma,x) \propto \psi_\omega^N(r_*) \qquad \text{and} \qquad w_2(\rho,\sigma,) \propto \psi_\omega^D(r_*). \tag{5.56}$$

Thus, from Eqs. (5.52) and (5.53), we see that one can represent the general solution of Eq. (5.58) in terms of the linearly independent solutions

$$\psi_1(r_*) = P_{-1/2}^{i\omega}(\tanh r_*), \qquad \psi_2(r_*) = Q_{-1/2}^{i\omega}(\tanh r_*). \tag{5.57}$$

Let us now impose the conditions at the boundaries of the system in order to determine the QNMs. First, let us denote by $\psi_\omega^{(<)}$ and $\psi_\omega^{(>)}$ the solutions of

$$-\frac{d^2\psi_\omega(r_*)}{dr_*^2}+V_{\text{eff}}(r_*)\psi_\omega(r_*)=\omega^2\psi_\omega(r_*), \tag{5.58}$$

with effective potential given by Eq. (5.40), for $r_* < 0$ and $r_* > 0$, respectively.

For $r_* < 0$, the boundary condition (5.48) implies

$$\psi_\omega^{(<)}(r_*)=\omega\sinh(\pi\omega)\Gamma(-i\omega)\psi_1(r_*)-\frac{2i\omega}{\pi}\cosh(\pi\omega)\Gamma(-i\omega)\psi_2(r_*). \tag{5.59}$$

For $r_* > 0$, we have

$$\psi_\omega^{(>)}(r_*)=c_1\psi_1(r_*)+c_2\psi_2(r_*). \tag{5.60}$$

Before considering the behavior at $r_* \to \infty$, we match $\psi_\omega^{(<)}$ and $\psi_\omega^{(>)}$ at $r_* = 0$. Continuity requires

$$\psi_\omega^{(<)}(r_*\to 0^-)=\psi_\omega^{(>)}(r_*\to 0^+). \tag{5.61}$$

We also require that

$$\left.\frac{d\psi_\omega^{(>)}}{dr_*}\right|_{r_*=0^+}-\left.\frac{d\psi_\omega^{(<)}}{dr_*}\right|_{r_*=0^-}=a\psi(0), \tag{5.62}$$

which is the condition obtained by integrating Eq. (5.58) inside an arbitrarily small neighborhood of $r_* = 0$.

Solving Eqs. (5.61) and (5.62), we find the constants c_1 and c_2 as functions of the parameter a. After that, we expand $\psi_\omega^{(>)}$ near $r_* \to +\infty$,

$$\psi_\omega^{(>)}(r_*)\sim D(\omega,a)e^{-i\omega r_*}+E(\omega,a)e^{i\omega r_*}. \tag{5.63}$$

The coefficients of the asymptotic expansion Eq. (5.63) are

$$D(\omega,a)=\frac{\pi\operatorname{csch}(\pi\omega)\Gamma(-i\omega)}{2i\Gamma(i\omega)}\left[\frac{2^{2i\omega}\pi a}{\Gamma\left(\frac{3}{4}-\frac{i\omega}{2}\right)^4}+\frac{2}{\Gamma\left(\frac{1}{2}-i\omega\right)^2}\right], \tag{5.64}$$

$$E(\omega, a) = -i\mathrm{csch}(\pi\omega) - \frac{ia}{4}[\mathrm{csch}(\pi\omega) - i]\frac{\Gamma\left(\frac{1}{4} - \frac{i\omega}{2}\right)^2}{\Gamma\left(\frac{3}{4} - \frac{i\omega}{2}\right)^2}. \tag{5.65}$$

Hence the quasinormal frequencies of the extended Laval nozzle are given by solutions of

$$D(\omega, a) = 0. \tag{5.66}$$

From Eq. (5.64), we see that ordinary quasinormal frequencies can be divided into two sets. First, since the Gamma function has poles at negative integers, the frequencies

$$\omega_n = -\frac{i}{2}(4n+3), \quad n = 0,\ 1,\ 2,\ 3,\ \ldots \tag{5.67}$$

satisfy Eq. (5.66) for any value of a. The second set of quasinormal frequencies is given by the solutions of

$$a = -\frac{2^{1-2i\omega}\Gamma\left(\frac{3}{4} - \frac{i\omega}{2}\right)^4}{\pi\Gamma\left(\frac{1}{2} - i\omega\right)^2}. \tag{5.68}$$

In the following, we analyze the resulting quasinormal modes for both cases, Eqs. (5.67) and (5.68). For convenience, we will divide the case of Eq. (5.68) in (i) $a = 0$ and (ii) $a \neq 0$.

Dirichlet quasinormal modes

Let us first consider the QNMs with frequencies given by Eq. (5.67). Using the expressions for $\psi_\omega^{(<)}$ and $\psi_\omega^{(>)}$, Eqs. (5.59) and (5.60), we find

$$\psi_n^{(D)}(r_*) = -\Gamma\left(-2n - \frac{1}{2}\right) P_{-\frac{1}{2}}^{2n+\frac{3}{2}}(\tanh r_*), \tag{5.69}$$

which is defined in $-\infty < r_* < \infty$. From the transformation formula [84]

$$P_{-\frac{1}{2}}^{2n+\frac{3}{2}}(\tanh r_*) = C_n \sinh r_* \cosh^{2n+\frac{1}{2}} r_*\, {}_2F_1\left(-n, -n; \frac{3}{2}; \tanh^2 r_*\right), \tag{5.70}$$

where

$$C_n = \frac{(-1)^n 2^{2n+\frac{5}{2}}\Gamma\left(n+\frac{3}{2}\right)}{\sqrt{\pi}\Gamma\left(-n-\frac{1}{2}\right)}, \tag{5.71}$$

we see that

$$\psi_n^{(D)}(r_* = 0) = 0. \tag{5.72}$$

Since $\psi_n^{(D)}$ is a solution of Eq. (5.58) obeying ingoing boundary conditions at the horizon $r_* = -\infty$, it follows from Eq. (5.72) that, when restricted to $-\infty < r_* \leq 0$, the ordinary QNM $\psi_n^{(D)}$ can be interpreted as a QNM satisfying a Dirichlet boundary condition at BTZ spatial infinity. Moreover, we note that these modes are odd functions with respect to the tortoise coordinate r_*, and do not depend on the value of the parameter a. We also mention that the frequencies given by Eq. (5.67) are the known Dirichlet quasinormal frequencies in the BTZ background given by Eq. (3.59) (with $M = l = 1$, $m = 0$, and $m_\xi^2 = -3/4l^2$). Besides, the QNMs $\psi_n^{(D)}$, Eq. (5.69), are proportional to the Dirichlet solutions found in Chapter 3, Eq. (3.46), with ω given by Eq. (5.67). Figure 5.4 shows $\psi_n^{(D)}$ for $n = 0,\ 1,\ 2$.

Neumann quasinormal modes

For $a = 0$, the frequencies solving Eq. (5.68) are given by

$$\omega_k = -\frac{i}{2}(2k+1), \quad k = 0,\ 1,\ 2,\ 3,\ \ldots \tag{5.73}$$

When k is odd, $k = 2n + 1$, these frequencies reduce to Dirichlet frequencies, Eq. (5.67), and the corresponding modes are given by Eq. (5.69). On the other hand, when k is even, $k = 2n$, we have

$$\omega_n = -\frac{i}{2}(4n+1). \tag{5.74}$$

The mode solutions in this case are given by

$$\psi_n^{(N)}(r_*) = \Gamma\left(\frac{1}{2} - 2n\right) P_{-\frac{1}{2}}^{2n+\frac{1}{2}}\left(\tanh r_*\right), \tag{5.75}$$

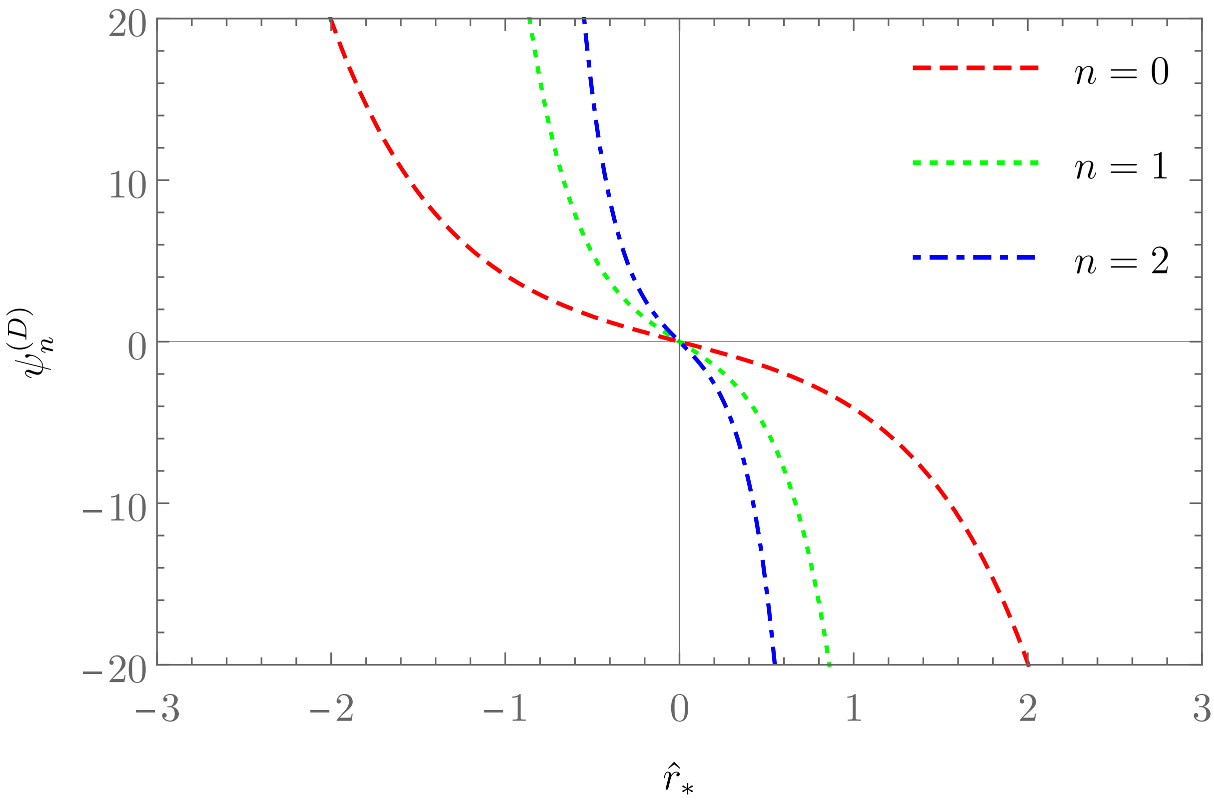

Figure 5.4: The spatial part of the ordinary quasinormal modes of acoustic waves in the extended nozzle as functions of the nondimensional tortoise coordinate, and frequencies given by Eq. (5.67). These QNMs are odd functions with respect to $\hat{r}_*$. For $-\infty < \hat{r}_* \leq 0$, these mode solutions can be interpreted as QNMs of conformally coupled scalar waves obeying a Dirichlet boundary condition at spatial infinity of the BTZ spacetime. Note that these modes do not depend on the parameter a. **Legend**: the red dashed line represents the QNM with $n = 0$, the green dotted line represents the QNM with $n = 1$, and the blue dot-dashed line represents the QNM with $n = 2$.

and are defined in $-\infty < r_* < \infty$. Using the transformation formula [84]

$$P^{2p+\frac{1}{2}}_{-\frac{1}{2}}(\tanh r_*) = C_n \cosh^{2n+\frac{1}{2}} r_* \, F\left(-n, -n; \frac{1}{2}; \tanh^2 r_*\right), \tag{5.76}$$

where

$$C_n = \frac{2^{2n+\frac{1}{2}}\Gamma\left(n+\frac{1}{2}\right)^2}{\pi^{3/2}}, \tag{5.77}$$

we see that $\psi_n^{(N)}$ is an even function with respect to the coordinate r_*. Moreover, from the expressions above, it can be shown that

$$\left.\frac{d\psi_n^{(N)}}{dr_*}\right|_{r_*=0} = 0. \tag{5.78}$$

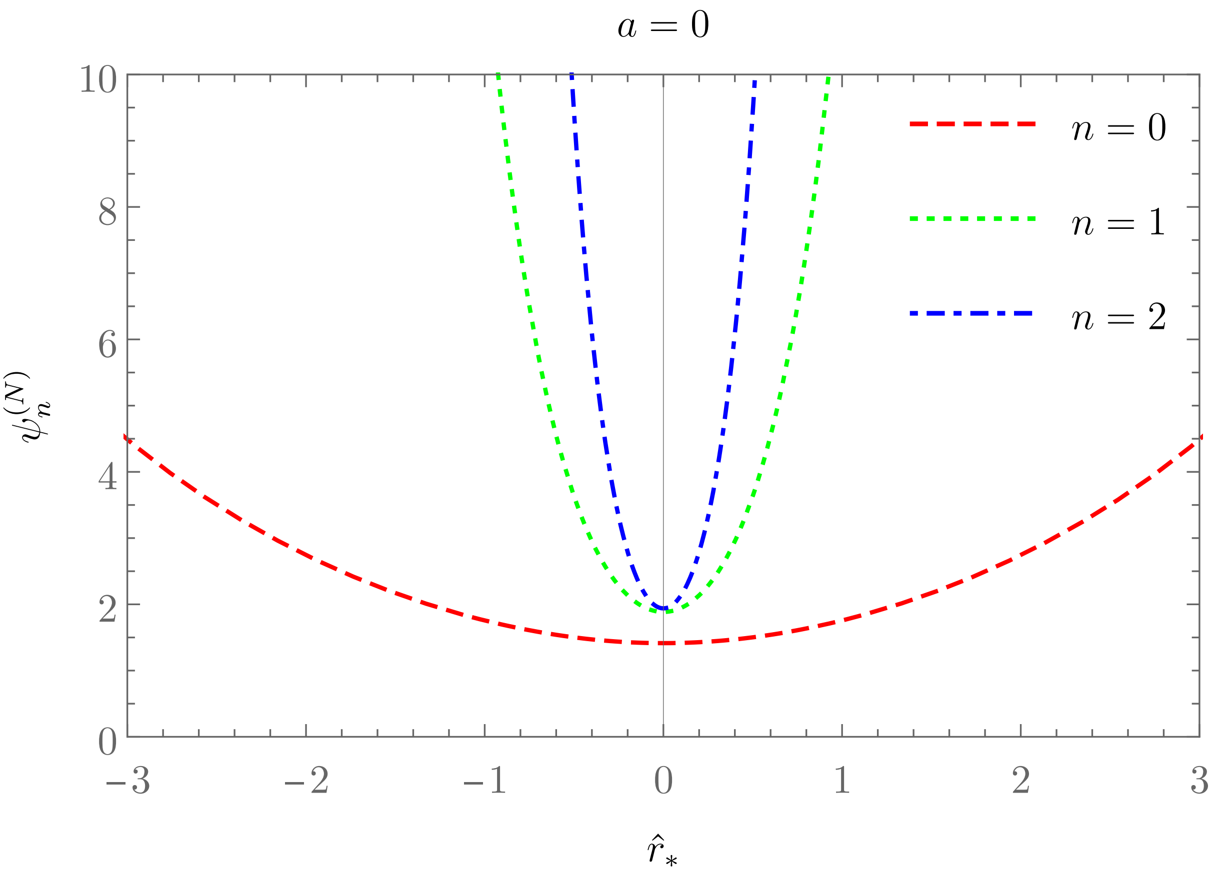

Figure 5.5: The spatial part of the ordinary quasinormal modes of acoustic waves in the extended nozzle as functions of the nondimensional tortoise coordinate, and frequencies given by Eq. (5.74). These QNMs are even functions with respect to $\hat{r}_*$. For $-\infty < \hat{r}_* \leq 0$, these mode solutions can be interpreted as QNMs of conformally coupled scalar waves obeying a Neumann boundary condition at spatial infinity of the BTZ spacetime, $\beta = a = 0$. **Legend**: the red dashed line represents the QNM with $n = 0$, the green dotted line represents the QNM with $n = 1$, and the blue dot-dashed line represents the QNM with $n = 2$.

Hence, when restricted to $-\infty < r_* \leq 0$, the ordinary QNMs, $\psi_n^{(N)}$, correspond to QNMs satisfying a Neumann boundary condition at the spatial infinity of the BTZ black hole. We note that the frequencies given by Eq. (5.74) are the Neumann quasinormal frequencies for the conformally coupled scalar field in the BTZ background found in Chapter 3 (Eq. (3.61) with $M = l = 1$, $m = 0$, and $m_\xi^2 = -3/4l^2$). We also mention that the modes $\psi_n^{(N)}$, Eq. (5.75), are proportional to the solutions given by Eq. (3.47) with ω given by Eq. (5.74). Figure 5.5 shows $\psi_n^{(N)}$ for $n = 0,\ 1,\ 2$.

Robin quasinormal modes

For $a \neq 0$, we cannot exactly solve Eq. (5.68) for ω. Nevertheless, we still can show that the corresponding QNMs are even functions with respect to r_*. Initially, we use Eq. (5.59) and substitute Eq. (5.68) into Eq. (5.60) to find

$$\left.\frac{d\psi_\omega^{(>)}}{dr_*}\right|_{r_*=0^+} = -\left.\frac{d\psi_\omega^{(<)}}{dr_*}\right|_{r_*=0^-} = -\frac{\sqrt{\pi}2^{1+i\omega}\Gamma(1-i\omega)}{\Gamma\left(\frac{1}{4}-\frac{i\omega}{2}\right)^2}. \tag{5.79}$$

Let us define $\phi(r_*)$ in $0 \le r_* < \infty$ by $\phi(r_*) = \psi_\omega^{(<)}(-r_*)$. Since the effective potential is even, it follows that $\phi(r_*)$ is a solution of Eq. (5.58) in $0 \le r_* < \infty$. Moreover, we have

$$\phi(0^+) = \psi_\omega^{(<)}(0^-), \tag{5.80}$$

$$\left.\frac{d\phi}{dr_*}\right|_{r_*=0^+} = -\left.\frac{d\psi_\omega^{(<)}}{dr_*}\right|_{r_*=0^-}. \tag{5.81}$$

Then, by the uniqueness of the solution of Eq. (5.58) obeying conditions (5.80) and (5.81), we conclude that $\psi_\omega^{(<)}(-r_*) = \phi(r_*) = \psi_\omega^{(>)}(r_*)$. The solution in the entire interval $-\infty \le r_* < \infty$ can then be written as

$$\psi_\omega^{(R)}(r_*) = \psi_\omega^{(<)}(r_*)\theta(-r_*) + \psi_\omega^{(<)}(-r_*)\theta(r_*), \tag{5.82}$$

from where it follows directly that $\psi_\omega^{(R)}(r_*)$ is an even function.

Another property of $\psi_\omega^{(R)}$ is found by substituting Eq. (5.79) into Eq. (5.62),

$$\beta = \left.\frac{\left(d\psi_\omega^{(<)}/dr_*\right)}{\psi_\omega^{(<)}}\right|_{r_*=0^-} = -\frac{a}{2}. \tag{5.83}$$

Hence, when restricted to $-\infty < r_* \le 0$, we can interpret the ordinary QNM, $\psi_\omega^{(R)}$, as a QNM in the BTZ black hole satisfying a Robin boundary condition at spatial infinity with $\beta = -a/2$.

Let us analyze Eq. (5.83) more closely. First, using Eq. (5.68), we can rewrite it as

$$\beta = \frac{2^{-2i\omega}\Gamma\left(\frac{3}{4}-\frac{i\omega}{2}\right)^4}{\pi\Gamma\left(\frac{1}{2}-i\omega\right)^2}. \tag{5.84}$$

Taking into account the formula [84]

$$\Gamma(2z) = \pi^{-1/2}2^{2z-1}\Gamma(z)\Gamma\left(z+\frac{1}{2}\right) \tag{5.85}$$

with $z = 3/4 - i\omega/2$, we find

$$\Gamma\left(\frac{1}{2} - i\omega\right) = \pi^{-1/2} 2^{-i\omega-\frac{1}{2}} \Gamma\left(\frac{1}{4} - \frac{i\omega}{2}\right) \Gamma\left(\frac{3}{4} - \frac{i\omega}{2}\right). \tag{5.86}$$

Substituting Eq. (5.86) into Eq. (5.84), it follows that

$$\beta = \frac{2\Gamma\left(\frac{3}{4} - \frac{i\omega}{2}\right)^2}{\Gamma\left(\frac{1}{4} - \frac{i\omega}{2}\right)^2}, \tag{5.87}$$

which agrees with the expression Eq. (3.65) for the frequencies of quasinormal modes obeying RBCs.

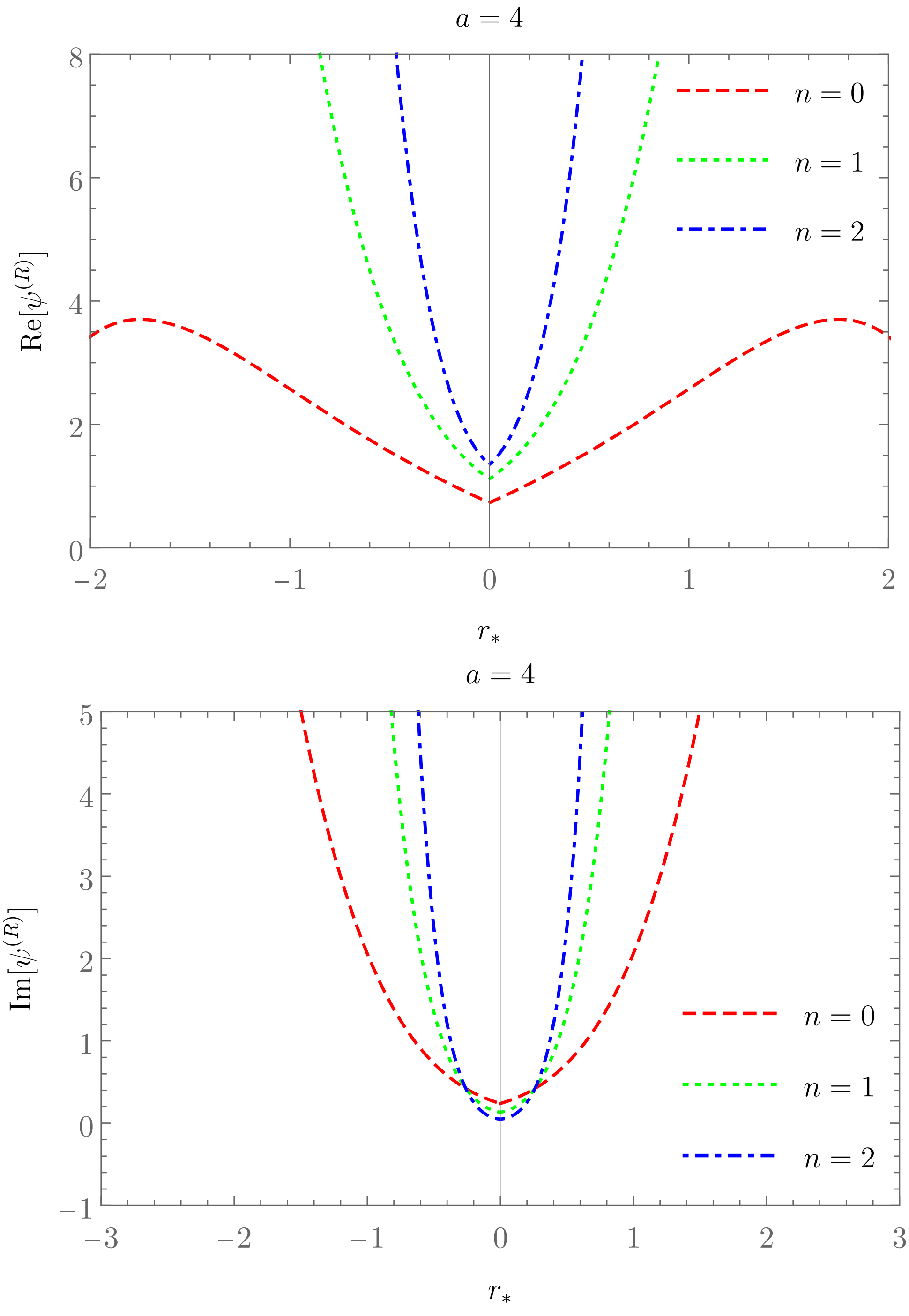

Figure 5.6: Real (Top) and imaginary (bottom) parts of the spatial component of the ordinary quasinormal modes of acoustic waves in the extended nozzle as functions of the nondimensional tortoise coordinate, and with frequencies given by solutions of Eq. (5.68). These QNMs are even functions with respect to $\hat{r}_*$. For $-\infty < \hat{r}_* \leq 0$, these mode solutions can be interpreted as QNMs of conformally coupled scalar waves obeying a Robin boundary condition with $\beta = -a/2 = -2$, at spatial infinity of the BTZ spacetime. The frequencies were calculated numerically and sorted by increasing magnitude of the imaginary parts. **Legend:** the red dashed line represents the least-damped QNM, with the frequency given by $\omega_0 = 0.628244 - 1.21348i$; the green dotted line represents the QNM with the frequency $\omega_1 = 0.711933 - 2.69836i$; the blue dot-dashed line represents the QNM with the frequency $\omega_2 = 0.501734 - 4.54024i$.

Figure 5.6 shows some ordinary QNM modes of the extended nozzle with $a = 4$ and frequencies given by solutions of Eq. (5.68). The quasinormal frequencies are $\omega_0 = 0.628244 - 1.21348i$, $\omega_1 = 0.711933 - 2.69836i$, $\omega_2 = 0.501734 - 4.54024i$. These ordinary QNMs correspond to QNMs satisfying an RBC in the BTZ spacetime with $\beta = -a/2 = -2$.

Summarizing the results in this section, we calculated the ordinary QNMs of acoustic waves in the extended nozzle and showed that all of them have definite parity: odd ordinary QNMs correspond to QNMs in the BTZ black hole satisfying the Dirichlet boundary condition; even ordinary QNMs correspond to QNMs in the BTZ black hole satisfying Neumann or Robin boundary conditions. This provides (at least in principle) a nice way to realize Robin boundary conditions at the conformal boundary of the BTZ black hole by means of an analog model. Notice that, since for arbitrary initial data both types of QNMs (odd and even) allowed by Eq. (5.66) will be excited, in order to observe mode solutions corresponding to QNMs obeying, say, Robin or Neumann boundary conditions, one has to consider time evolution of even initial data.

Hence, we can interpret the QNMs as modes with (complex) frequencies having definite parity. This is expected by the way the nozzle is extended. Such an extension has a resulting even effective potential given by Eq. (5.40) so that, with the asymptotic behavior given by Eqs. (5.48) and (5.49), parity is respected. Moreover, Eqs. (5.80) and (5.81) show that this extension represents two images of the same Cauchy problem with boundary conditions

$$\begin{aligned} &\psi_\omega \sim e^{i\omega r_*}, && r_* \to \infty, \\ &\tfrac{d\psi_\omega}{dn}(r_*) + \tfrac{a}{2}\psi_\omega(r_*) = 0, && r_* \to 0, \end{aligned}$$

where d/dn represents the normal derivative pointing toward $r_* = 0$. In this way, the quasinormal frequencies obtained in such "extended configuration" are precisely the ones found in the BTZ spacetime, Eq. (3.65), with the correspondence $a = -2\beta$.

Before closing this section, we mention that the lack of smoothness at the junction of the extended nozzle, resulting from the Dirac delta in the effective potential, is an idealization that could be removed, for instance, by considering a finite potential barrier in Eq. (5.40). In fact, taking a sufficiently small $\epsilon > 0$, a barrier with width 2ϵ and height $a/2\epsilon$ leads to a smooth nozzle with quasinormal frequencies arbitrarily close to the frequencies calculated via Eqs. (5.67) and (5.68). This means that the Dirac delta in the effective potential and the resulting nonsmooth nozzle do not represent a significant limitation of our model.

5.3.3 Stability

For black holes in asymptotically flat spacetimes, mode solutions growing exponentially in time ($\mathrm{Im}[\omega] > 0$) appear as a result of energy extraction from the background spacetime by the mechanism of *superradiance* [96].

In the case of the rotating BTZ black hole, Dappiaggi *et al.* showed that exponentially growing modes occur for a subset of RBCs [67]. There are two types of such modes: (i) modes corresponding to superradiant instabilities, which extract energy from the black hole; and (ii) modes arising from AdS_3 bulk instabilities [97], which do not extract energy from the black hole. In both cases, angular momentum is extracted from the black hole.

Because our model does not account for black hole rotation, no superradiant modes occur in the quasinormal spectrum determined by Eq. (5.66). On the other hand, since in the analog spacetime there exist exponentially growing modes that are not superradiant, we still have reason to ask if, for some value of a, such modes are allowed in our model.

According to [67], modes with $\mathrm{Im}[\omega] > 0$ occur for RBCs with β greater than a critical value β_c,

$$\beta > \beta_c, \tag{5.88}$$

which, in our case, is given by[2]

$$\beta_c = \frac{2\,\Gamma^2\,(3/4)}{\Gamma^2\,(1/4)}. \tag{5.89}$$

In terms of a, this means that unstable modes are expected to appear when

$$a < -\frac{4\,\Gamma^2\,(3/4)}{\Gamma^2\,(1/4)} = -\frac{2}{\pi^2}\Gamma^4\left(\frac{3}{4}\right), \tag{5.90}$$

where we have used Euler's reflection formula, $\Gamma(z)\Gamma(1-z) = \pi \csc \pi z$, with $z = 3/4$, to establish the last equality.

From the perspective of the Laval nozzle, the expression under the square root in Eq. (5.19) shows that the sectional area is well defined only for $g \geq 1$. One can see that this is, in fact, the case when $r_* \leq 0$ by noting that $h^{(<)}$ is a strictly increasing function in the interval $-\infty < r_* < 0$,

[2]The case of $m = 0$ mode of the conformally coupled scalar field in the static BTZ black hole corresponds to parameters $k = 0$ and $\mu^2 = -3/4$ in [67]. The parameter β for RBCs used here relates to the parameter ζ in [67] by $\beta = -\cot\zeta$.

and has a minimum at $r_* \to -\infty$. Since

$$\lim_{r_* \to -\infty} Q_{-\frac{1}{2}}(\tanh r_*) = \frac{\pi}{2}, \tag{5.91}$$

we see that this minimum is given by

$$\lim_{r_* \to -\infty} h^{(<)}(r_*) = \frac{3}{\sqrt{5}} > 1. \tag{5.92}$$

Thus, we conclude that $g(r_*) > 1$ in $-\infty < r_* \leq 0$, for any value of a.

For $r_* > 0$, there are two cases to consider:

$$\text{(i)} \quad a < -\frac{2}{\pi^2}\Gamma^4\left(\frac{3}{4}\right), \tag{5.93}$$

$$\text{(ii)} \quad a \geq -\frac{2}{\pi^2}\Gamma^4\left(\frac{3}{4}\right). \tag{5.94}$$

In Sec 5.3.4, we show that for the case (i) there always exists $\tilde{r}_*$ such that $g(\tilde{r}_*) < 1$ and, hence, our model is not well defined when a obeys inequality (5.93). On the other hand, we show that when a obeys inequality (5.94), the values of $g(r_*)$ are always greater than 1 so that our model is well defined.

From this discussion, it follows that our model is well defined only for

$$a \geq a_{\min} = -\frac{2}{\pi^2}\Gamma^4\left(\frac{3}{4}\right), \tag{5.95}$$

and, from the discussion before and including Eq. (5.90), we conclude that unstable mode solutions never occur in this model. This result unveils a nice feature, namely that the allowed nozzle configurations automatically reproduce only the boundary conditions that are always consistent with the stability condition in the BTZ spacetime.

As a last comment, we mention that although we have restricted ourselves to mode solutions with zero angular momentum ($m = 0$), the case of $m \neq 0$ can be treated in a similar fashion if we take the black hole mass as $M = m^2$, which turns the effective potential of Eq. (5.2) into $\hat{V}(\hat{r}_*) = (5/4)\,\mathrm{sech}^2\,\hat{r}_*$. As in the case of $m = 0$, the nozzle has a finite length, and one can emulate RBCs by extending it with the addition of a delta function term $a\delta(r_*)$ to the potential. Our other results still hold in this case, namely: the odd (even) ordinary QNMs correspond to QNMs obeying Dirichlet (Neumann or Robin) boundary conditions at the BTZ conformal infinity; and our model is well defined for $a \geq a_{\min}$, for a certain $a_{\min}$. The minimum value $a_{\min}$ still constrains the range of allowed boundary conditions to an interval $-\infty < \beta \leq \beta_{\max}$, but now $\beta_{\max}$ is smaller than the corresponding critical value β_c (and therefore the allowed nozzle configurations again reproduce only the boundary conditions that are consistent with the stability condition in the BTZ spacetime).

5.3.4 Behavior of $g(r_*)$ for a obeying inequalities (5.93) and (5.94)

In this section, we prove the claims made after inequalities (5.93) and (5.94). Initially, let us suppose that a satisfies Eq. (5.93). Noting that

$$\lim_{r_* \to +\infty} Q_{-\frac{1}{2}}(\tanh r_*) = +\infty, \tag{5.96}$$

it follows that

$$\lim_{r_* \to +\infty} h^{(>)}(r_*) = -\infty. \tag{5.97}$$

Hence we conclude that there exists $\tilde{r}_*$ such that $h^{(>)}(\tilde{r}_*) = 0$. For this $\tilde{r}_*$, we have $g(\tilde{r}_*) < 1$, and our model is not well defined for case (i).

Let us now analyze case (ii), given by inequality (5.94). From Eq. (5.47), we have that

$$\begin{aligned} h^{(>)}(r_*) &= \sqrt{\frac{3}{\sqrt{5}}} \left\{ \frac{2}{\pi} Q_{-\frac{1}{2}}(\tanh r_*) + \frac{\pi a}{\Gamma\left(\frac{3}{4}\right)^4} \left[Q_{-\frac{1}{2}}(\tanh r_*) - \frac{\pi}{2} P_{-\frac{1}{2}}(\tanh r_*) \right] \right\} \\ &\geq \sqrt{\frac{3}{\sqrt{5}}} P_{-\frac{1}{2}}(\tanh r_*), \end{aligned} \tag{5.98}$$

where we have used the condition (5.94) and the fact that

$$Q_{-\frac{1}{2}}(\tanh r_*) \geq \frac{\pi}{2} P_{-\frac{1}{2}}(\tanh r_*) \tag{5.99}$$

for $0 \leq r_* < \infty$. Inequality (5.99) follows from the relation [84]

$$Q_{-\frac{1}{2}}(\tanh r_*) = \frac{\pi}{2} P_{-\frac{1}{2}}(-\tanh r_*) \tag{5.100}$$

and the fact that Q_ν^μ is an increasing function in $-\infty < r_* < \infty$.

Since

$$P_{-\frac{1}{2}}(\tanh r_*) \geq 1, \qquad 0 \leq r_* < \infty, \tag{5.101}$$

the result (5.98) implies

$$h^{(>)}(r_*) \geq \sqrt{\frac{3}{\sqrt{5}}} > 1. \tag{5.102}$$

Thus it follows from Eq. (5.31) that $g(r_*) > 1$ whenever the constraint (5.94) is fulfilled, which means that our model is well defined for a in case (ii).

Chapter 6

Conclusion

One of the main insights of the Analog Gravity research program is the realization that the spacetime (effective) description arises as an emergent (low-energy) feature of a much more complex underlying physics. In this sense, studying analog models of gravity (especially based on quantum systems) may provide hints on some of the requirements a Quantum Theory of Gravity should meet. Aside from that, this research program offers lots of ground to investigate and test gravitational effects even at the classical level, as recent experimental observations have shown [34, 35, 36].

On the theoretical side, after introducing some general features of the Analog Gravity program in Chapter 2, we have employed its mathematical machinery to investigate an instance of the very interesting class of nonglobally hyperbolic spacetimes. In such spacetimes, we cannot characterize the solutions of the wave equation only in terms of an initial state so that the conformal boundary of the spacetime plays a fundamental role in the determination of the dynamics in bulk.

In this thesis, we have specifically considered the case of the static BTZ spacetime, which represents a black hole solution of the Einstein field equations of gravity in (2+1) dimensions with a negative cosmological constant, which was briefly introduced in Chapter 3, along with a discussion on its quasinormal modes.

After the introductory discussion in Chapters 2 and 3, in Chapter 4, we introduced a novel analog model for the BTZ black hole based on a unidirectional flow of a nonhomogeneous fluid. Specifically, we have considered a barotropic fluid obeying a simple equation of state, which corresponds to a constant local speed of sound. The physical quantities describing the flow were considered to vary along just one direction. In particular, the flow velocity field pointed to a fixed direction in the laboratory reference frame. The coordinate describing the direction of the flowing fluid was mapped into the radial coordinate of the analog spacetime. Following the steps introduced in [58], we were naturally led to find the effective acoustic metric as that of the well-known static BTZ black hole, Eq. (3.6).

A nice feature of our model is that the outer region of the BTZ black hole is mapped into a finite region in the laboratory. In particular, the BTZ conformal boundary is mapped into the boundary $\mathcal{E}$ at the laboratory, which is at a finite distance from the acoustic horizon. Thus it follows that, on the analog model end, the extra boundary condition (at the conformal boundary) required to determine the time evolution of the field uniquely can be naturally interpreted as a boundary condition (at the boundary $\mathcal{E}$) for the sound propagation in the laboratory.

After that, still in Chapter 4, we considered flow configurations with both small and large deviations from the steady state. In the latter case, we numerically solved the nonlinear equations of fluid dynamics and followed an example of the formation of the acoustic BTZ black hole. In both cases, we examined the excitation and decay of the associated QNMs.

In Chapter 5, we introduced an analog model for the BTZ black hole, which is appropriate to analyze the QNMs resulting from Robin boundary conditions at its corresponding conformal infinity. Applying the procedure first introduced in [52], we found a Laval nozzle configuration for which acoustic waves traveling on the flowing gas mimics a conformally coupled scalar field propagating on the BTZ black hole. We found that the obtained nozzle had a finite length and that the spatial infinity of the BTZ spacetime was mapped into one end of the nozzle. From there on, we considered nozzle extensions corresponding to effective potentials formally extending the BTZ black hole beyond its conformal infinity. We also noticed that, with respect to the tortoise coordinate, the extended model represents two copies of the same initial value problem so that the ordinary QNMs of waves in the nozzle can be obtained by extending the BTZ mode solutions into the region beyond its spatial infinity while preserving parity.

After finding the ordinary QNMs in the extended nozzle, we showed that these modes can be used to simulate QNMs in the BTZ spacetime satisfying Dirichlet, Neumann and Robin boundary conditions at its conformal boundary. Finally, we showed that the range of the parameters for which our model is well defined corresponds precisely to the range of Robin boundary conditions that allow only stable QNMs.

Bibliography

[1] Barceló, C., Liberati, S. & Visser, M. Analogue gravity. *Living reviews in relativity* **14**, 1–159 (2011).

[2] Wald, R. M. *General relativity.* The University of Chicago Press (1984).

[3] Carroll, S. M. *Spacetime and geometry: An introduction to general relativity.* Addison Wesley (2004).

[4] Misner, C. W., Thorne, K. S. & Wheeler, J. A. *Gravitation.* W. H. Freeman and company (1973).

[5] Hawking, S. W. & Ellis, G. F. R. *The large scale structure of space-time, vol. 1.* Cambridge University Press (1973).

[6] Hawking, S. W. Particle creation by black holes. *Communications in Mathematical Physics* **43**, 199–220 (1975).

[7] Unruh, W. G. Experimental black-hole evaporation? *Physical Review Letters* **46**, 1351–1353 (1981).

[8] Visser, M. Acoustic black holes: horizons, ergospheres and Hawking radiation. *Classical and Quantum Gravity* **15**, 1767–1791 (1998).

[9] Visser, M. Hawking radiation without black hole entropy. *Physical Review Letters* **80**, 3436–3439 (1998).

[10] Visser, M. Essential and inessential features of Hawking radiation. *International Journal of Modern Physics D* **12**, 649–661 (2003).

[11] Hawking, S. W. Breakdown of predictability in gravitational collapse. *Physical Review D* **14**, 2460–2473 (1976).

[12] Hooft, G. T. On the quantum structure of a black hole. *Nuclear Physics B* **256**, 727–745 (1985).

[13] Jacobson, T. Black-hole evaporation and ultrashort distances. *Physical Review D* **44**, 1731–1739 (1991).

[14] Unruh, W. G. Sonic analogue of black holes and the effects of high frequencies on black hole evaporation. *Physical Review D* **51**, 2827–2838 (1995).

[15] Brout, R., Massar, S., Parentani, R. & Spindel, P. Hawking radiation without trans-Planckian frequencies. *Physical Review D* **52**, 4559–4568 (1995).

[16] Jacobson, T. A. Introduction to black hole microscopy. *Recent Developments in Gravitation and Mathematical Physics*, 87–114 (1996).

[17] Jacobson, T. On the origin of the outgoing black hole modes. *Physical Review D* **53**, 7082–7088 (1996).

[18] Corley, S. & Jacobson, T. Hawking spectrum and high frequency dispersion. *Physical Review D* **54**, 1568–1586 (1996).

[19] Reznik, B. Origin of the thermal radiation in a solid-state analogue of a black hole. *Physical Review D* **62**, 044044 (2000).

[20] Schützhold, R. & Unruh, W. G. Gravity wave analogues of black holes. *Physical Review D* **66**, 044019 (2002).

[21] Garay, L. J., Anglin, J. R., Cirac, J. I., & Zoller, P. Sonic analog of gravitational black holes in Bose-Einstein condensates. *Physical Review Letters* **85**, 4643–4647 (2000).

[22] Barceló, C., Liberati, S. & Visser, M. Analogue gravity from Bose-Einstein condensates. *Classical and Quantum Gravity* **18**, 1137–1156 (2001).

[23] Liberati, S., Tricella, G., & Trombettoni, A. The information loss problem: an analogue gravity perspective. *Entropy* **21**, 940 (2019).

[24] Liberati, S., Tricella, G., & Trombettoni, A. Back-reaction in canonical analogue black holes. *Applied Sciences* **10**, 8868 (2020).

[25] Novello, M., De Lorenci, V. A., Salim, J. M., & Klippert, R. Geometrical aspects of light propagation in nonlinear electrodynamics. *Physical Review D* **61**, 045001 (2000).

[26] Novello, M., Visser, M., & Volovik, G. E. *Artificial black holes.* World Scientific (2002).

[27] Faccio, D., Belgiorno, F., Cacciatori, S., Gorini, V., Liberati, S., & Moschella, U. *Analogue gravity phenomenology: analogue spacetimes and horizons, from theory to experiment.* Springer (2013).

[28] Rousseaux, G., Mathis, C., Maïssa, P., Philbin, T. G., & Leonhardt, U. Observation of negative-frequency waves in a water tank: a classical analogue to the Hawking effect? *New Journal of Physics* **10**, 053015 (2008).

[29] Weinfurtner, S., Tedford, E. W., Penrice, M. C., Unruh, W. G., & Lawrence, G. A. Measurement of stimulated Hawking emission in an analogue system. *Physical Review Letters* **106**, 021302 (2011).

[30] Euvé, L. P., Michel, F., Parentani, R., Philbin, T. G., & Rousseaux, G. Observation of noise correlated by the Hawking effect in a water tank. *Physical Review Letters* **117**, 121301 (2016).

[31] Steinhauer, J. Observation of quantum Hawking radiation and its entanglement in an analogue black hole. *Nature Physics* **12**, 959–965 (2016).

[32] Muñoz de Nova, J. R., Golubkov, K., Kolobov, V. I., & Steinhauer, J. Observation of thermal Hawking radiation and its temperature in an analogue black hole. *Nature* **569**, 688–691 (2019).

[33] Kolobov, V. I., Golubkov, K., Muñoz de Nova, J. R., & Steinhauer, J. Observation of stationary spontaneous Hawking radiation and the time evolution of an analogue black hole. *Nature Physics* **17**, 362–367 (2021).

[34] Torres, T., Patrick, S., Coutant, A., Richartz, M., Tedford, E. W., & Weinfurtner, S. Rotational superradiant scattering in a vortex flow. *Nature Physics* **13**, 833–836 (2017).

[35] Torres, T., Patrick, S., Richartz, M., & Weinfurtner, S. Analogue black hole spectroscopy; or, how to listen to dumb holes. *Classical and Quantum Gravity* **36**, 194002 (2019).

[36] Torres, T., Patrick, S., Richartz, M., & Weinfurtner, S. Quasinormal mode oscillations in an analogue black hole experiment. *Physical Review Letters* **125**, 011301 (2020).

[37] Jacquet, M. J., Weinfurtner, S., & König, F. The next generation of analogue gravity experiments. *Philosophical Transactions of the Royal Society A* **378**, 20190239 (2020).

[38] Mosna, R. A., Pitelli, J. P. M., & Richartz, M. Analogue model for anti-de Sitter as a description of point sources in fluids. *Physical Review D* **94**, 104065 (2016).

[39] Aruquipa, D. Q., Mosna, R. A., & Pitelli, J. P. M. Analogue gravity and radial fluid flows: The case of AdS and its deformations. *Physical Review D* **97**, 104056 (2018).

[40] Bañados, M., Teitelboim, C., & Zanelli, J. Black hole in three-dimensional spacetime. *Physical Review Letters* **69**, 1849–1851 (1992).

[41] Visser, M. The Kerr spacetime: A brief introduction. *arXiv preprint arXiv:0706.0622*, (2007).

[42] Bañados, M., Henneaux, M., Teitelboim, C., & Zanelli, J. Geometry of the 2 + 1 black hole. *Physical Review D* **48**, 1506–1525 (1993).

[43] Carlip, S. Lectures in (2+1)-dimensional gravity. *arXiv preprint arXiv:gr-qc/9503024*, (1995).

[44] Carlip, S. The (2+1)-dimensional black hole. *Classical and Quantum Gravity* **12**, 2853–2879 (1995).

[45] Kokkotas, K. D. & Schmidt, B. G. Quasi-normal modes of stars and black holes. *Living Reviews in Relativity* **2**, 1–72 (1999).

[46] Berti, E., Cardoso, V., & Starinets, A. O. Quasinormal modes of black holes and black branes. *Classical and Quantum Gravity* **26**, 163001 (2009).

[47] Konoplya, R. A. & Zhidenko, A. Quasinormal modes of black holes: From astrophysics to string theory. *Reviews of Modern Physics* **83**, 793–836 (2011).

[48] Birmingham, D., Sachs, I., & Sen, S. Three-dimensional black holes and string theory. *Physics Letters B* **413**, 281–286 (1997).

[49] Myung, Y. S. & Kim, N. J. Difference between anti-de Sitter and de Sitter spaces: wave equation approach. *Classical and Quantum Gravity* **21**, 63–81 (2003).

[50] Okuzumi, S., & Sakagami, M. A. Quasinormal ringing of acoustic black holes in Laval nozzles: Numerical simulations. *Physical Review D* **76**, 084027 (2007).

[51] Roshko, A. & Liepmann, H. W. *Elements of Gas-dynamics.* Wiley (1957).

[52] Abdalla, E., Konoplya, R. A., & Zhidenko, A. Perturbations of Schwarzschild black holes in laboratories. *Classical and Quantum Gravity* **24**, 5901–5909 (2007).

[53] Cuyubamba, M. A. Laval nozzle as an acoustic analogue of a massive field. *Classical and Quantum Gravity* **30**, 195005 (2013).

[54] de Oliveira, C. C. & Mosna, R. A. Analog model for the BTZ black hole. *Physical Review D* **106**, 064030 (2022).

[55] de Oliveira, C. C., Mosna, R. A., & Pitelli, J. P. M. Robin boundary conditions in acoustic BTZ black holes. *Physical Review D* **107**, 064018 (2023).

[56] de Oliveira, C. C., Mosna, R. A., & Pitelli, J. P. M. Boundary conditions for isolated asymptotically anti-de Sitter spacetimes. *Journal of Mathematical Physics* **63**, 042501 (2022).

[57] Landau, L. D., & Lifshitz, E. M. *Fluid Mechanics, Second Edition: Volume 6 (Course of Theoretical Physics).* Pergamon Press (1987).

[58] de Oliveira, C. C., Mosna, R. A., Pitelli, J. P. M., & Richartz, M. Analogue models for Schwarzschild and Reissner-Nordström spacetimes. *Physical Review D* **104**, 024036 (2021).

[59] Jannes, G. Emergent gravity: the BEC paradigm. *arXiv preprint arXiv:0907.2839*, (2009).

[60] Rindler, W. *Relativity: special, general, and cosmological, Second Edition.* Oxford University Press (2006).

[61] Poisson, E. *A relativist's toolkit: the mathematics of black-hole mechanics.* Cambridge University Press (2004).

[62] Dempsey, D. & Dolan, S. R. Waves and null congruences in a draining bathtub. *International Journal of Modern Physics D* **25**, 1641004 (2016).

[63] Dempsey, D. *Wave propagation on black hole spacetimes.* PhD thesis, University of Sheffield (2017).

[64] Barceló, C., Liberati, S., Sonego, S., & Visser, M. Causal structure of analogue spacetimes. *New Journal of Physics* **6**, 186–186 (2004).

[65] Stone, M. Phonons and forces: momentum versus pseudomomentum in moving fluids. In *Artificial Black Holes*, 335–363. World Scientific (2002).

[66] Cardoso, V. & Lemos, J. P. S. Scalar, electromagnetic, and Weyl perturbations of BTZ black holes: Quasinormal modes. *Physical Review D* **63**, 124015 (2001).

[67] Dappiaggi, C., Ferreira, H. R. C., & Herdeiro, C. A. R. Superradiance in the BTZ black hole with robin boundary conditions. *Physics Letters B* **778**, 146–154 (2018).

[68] Zettl, A. *Sturm–Liouville theory (Mathematical Surveys and Monographs vol. 121).* Providence, RI: American Mathematical Society (2005).

[69] Wald, R. M. Dynamics in nonglobally hyperbolic, static space-times. *Journal of Mathematical Physics* **21**, 2802–2805 (1980).

[70] Ishibashi, A. & Wald R. M. Dynamics in non-globally-hyperbolic static spacetimes: II. General analysis of prescriptions for dynamics. *Classical and Quantum Gravity* **20**, 3815–3826 (2003).

[71] Ishibashi, A. & Wald, R. M. Dynamics in non-globally-hyperbolic static spacetimes: III. Anti-de Sitter spacetime. *Classical and Quantum Gravity* **21**, 2981–3013 (2004).

[72] Vaz Jr, J. & de Oliveira, E. C. *Métodos Matemáticos, vol. 1*, Editora da Unicamp (2016).

[73] Taylor, J. R. *Classical mechanics.* University Science Books (2005).

[74] Goldstein, H., Poole, C. & Safko, J. *Classical Mechanics, Third Edition.* Addison Wesley (2002).

[75] Lemos, N. A. *Mecânica analítica.* Editora Livraria da Física (2007).

[76] Nollert, H. P. Quasinormal modes: the characteristic ‘sound’ of black holes and neutron stars. *Classical and Quantum Gravity* **16**, 159–216 (1999).

[77] Ching, E. S. C., Leung, P. T., Van Den Brink, A. M., Suen, W. M., Tong, S. S., & Young, K. Quasinormal-mode expansion for waves in open systems. *Reviews of Modern Physics* **70**, 1545–1554 (1998).

[78] Leaver, E. W. Spectral decomposition of the perturbation response of the Schwarzschild geometry. *Physical Review D* **34**, 384–408 (1986).

[79] Dolan, S. R. Black holes and wave mechanics. *Lecture Notes* (2008).

[80] Cardoso, V. Quasinormal modes and gravitational radiation in black hole spacetimes. *arXiv preprint gr-qc/0404093* (2004).

[81] Zhydenko, O. *Perturbações lineares de buracos negros: estabilidade, modos quase-normais e caudas.* PhD thesis, Universidade de São Paulo (2009).

[82] Destounis, K. Dynamical behavior of black-hole spacetimes. *arXiv preprint arXiv:1909.08597* (2019).

[83] Bussola, F. *Hadamard states and tunnelling effects for a BTZ black hole.* PhD thesis, Pavia University (2018).

[84] Olver, F. W. J., Lozier, D.W., Boisvert, R.F., & Clark, C.W. *NIST Handbook of Mathematical Functions.* Cambridge University Press (2010).

[85] Abramowitz, M. & Stegun, I. A. *Handbook of mathematical functions with formulas, graphs, and mathematical tables, vol. 55.* US Government printing office (1964).

[86] Ferreira, H. R. C. & Herdeiro, C. A. R. Stationary scalar clouds around a BTZ black hole. *Physics Letters B* **773**, 129–134 (2017).

[87] Bilić, N. Analog Schwarzschild-like geometry in fluids with external pressure. *Physical Review D* **105**, 064052 (2022).

[88] Pitelli, J. P. M., Mosna, R. A., de Oliveira, C. C., & Richartz, M. Comment on “Analog Schwarzschild-like geometry in fluids with external pressure”. *Physical Review D* **106**, 108501 (2022).

[89] Wolfram Research, Inc. Mathematica, Version 12.2. Champaign, IL (2020).

[90] Ching, E. S. C., Leung, P. T., Suen, W. M, & Young, K. Wave propagation in gravitational systems: Late time behavior. *Physical Review D* **52**, 2118–2132 (1995).

[91] Andersson, N. Excitation of Schwarzschild black-hole quasinormal modes. *Physical Review D* **51**, 353–363 (1995).

[92] Andersson, N. Evolving test fields in a black-hole geometry. *Physical Review D* **55**, 468–479 (1997).

[93] Chan, J. S. F. & Mann, R. B. Scalar wave falloff in asymptotically anti–de Sitter backgrounds. *Physical Review D* **55**, 7546–7562 (1997).

[94] Lee, H. W., Kim, N. J., & Myung, Y. S. Probing the BTZ black hole with test fields. *Physics Letters B* **441**, 83–88 (1998).

[95] Garbarz, A., La Madrid, J. & Leston, M. Scalar field dynamics in a BTZ background with generic boundary conditions. *The European Physical Journal C* **77**, 807 (2017).

[96] Brito, R., Cardoso, V., & Pani, P. Superradiance–the 2020 edition. *arXiv preprint arXiv:1501.06570*, (2015).

[97] Dappiaggi, C. & Ferreira, H. R. C. Hadamard states for a scalar field in anti–de Sitter spacetime with arbitrary boundary conditions. *Physical Review D* **94**, 125016 (2016).

[98] Kreyszig, E. *Introductory functional analysis with applications, vol. 1.* Jonh Wiley & Sons (1978).

[99] Reed, M. & Simon, B. *II: Fourier Analysis, Self-Adjointness. Methods of Modern Mathematical Physics.* Academic Press (1975).

[100] Reed, M. & Simon, B. *I: Functional Analysis. Methods of Modern Mathematical Physics.* Academic Press (1980).

[101] Ismail, M. E. H. & Muldoon, M. E. Inequalities and monotonicity properties for gamma and q-gamma functions. In *Approximation and Computation: A Festschrift in Honor of Walter Gautschi, Springer*, 309–323 (1994).

Appendices

Appendix A

Boundary Conditions For Isolated Asymptotically Anti-de Sitter Spacetimes

(Reproduced from [56], with the permission of AIP Publishing)

Journal of Mathematical Physics

Boundary conditions for isolated asymptotically anti-de Sitter spacetimes

Cite as: J. Math. Phys. **63**, 042501 (2022); https://doi.org/10.1063/5.0078118
Submitted: 10 November 2021 • Accepted: 19 March 2022 • Published Online: 05 April 2022

Christyan C. de Oliveira, Ricardo A. Mosna and João Paulo M. Pitelli

Boundary conditions for isolated asymptotically anti-de Sitter spacetimes

Cite as: J. Math. Phys. **63**, 042501 (2022); doi: 10.1063/5.0078118
Submitted: 10 November 2021 • Accepted: 19 March 2022 •
Published Online: 5 April 2022

View Online Export Citation CrossMark

Christyan C. de Oliveira,[1,a] Ricardo A. Mosna,[2,b] and João Paulo M. Pitelli[2,c]

AFFILIATIONS

[1] Instituto de Física "Gleb Wataghin" (IFGW), Universidade Estadual de Campinas, 13083-859 Campinas, SP, Brazil
[2] Departamento de Matemática Aplicada, Universidade Estadual de Campinas, 13083-859 Campinas, SP, Brazil

[a] Author to whom correspondence should be addressed: chris@ifi.unicamp.br
[b] Electronic mail: mosna@unicamp.br
[c] Electronic mail: pitelli@unicamp.br

ABSTRACT

We revisit the propagation of classical scalar fields in a spacetime, which is asymptotically anti-de Sitter. The lack of global hyperbolicity of the underlying background gives rise to an ambiguity in the dynamical evolution of solutions of the wave equation, requiring the prescription of extra boundary conditions at the conformal infinity to be fixed. We show that the only boundary conditions that are compatible with the hypothesis that the system is isolated, as defined by the (improved) energy–momentum tensor, are of Dirichlet and Neumann types.

I. INTRODUCTION

The anti-de Sitter (AdS) spacetime is the classic solution to the vacuum Einstein equations in the presence of a negative cosmological constant. It has the highest possible degree of symmetry since it is maximally symmetric. Despite this apparent geometric simplicity, the AdS spacetime has remarkable properties that make it a particularly interesting background for the study of classical and quantum fields. In particular, it is a non-globally hyperbolic spacetime, implying that the solutions of the wave equation are not fully determined from initial data.[1] This requires the prescription of extra boundary conditions at its spatial infinity in order to have a unique solution for the Cauchy problem.[2] Physically, the lack of global hyperbolicity is related to the fact that information propagating in AdS can reach spatial infinity in finite time, which allows the energy to leak out of the spacetime. As a result, the AdS spacetime does not give rise, in general, to an isolated system.

This problem has been addressed in Refs. 3 and 4 within the context of *supergravity* in $(1 + 3)$-dimensions. Besides analyzing the stability of the anti-de Sitter background with respect to small scalar perturbations, these works show that the boundary conditions that make the improved energy functional positive and conserved are restricted to the Dirichlet and Neumann types.

Given the arbitrariness on the choice of the boundary condition at the conformal boundary, Wald and Ishibashi defined in Refs. 2, 5, and 6 a sensible prescription for obtaining the dynamics of a propagating field on AdS.[7] By requiring that the field propagation respects causality and time translation/reflection invariance and, what is most important, also has a conserved energy functional, it was shown that the non-equivalent types of sensible dynamics are in one-to-one correspondence with the positive self-adjoint extensions of the spatial part of the wave operator. These self-adjoint extensions are obtained by choosing suitable boundary conditions at the conformal infinity. The resulting conserved energy functional, however, is not that extracted from the improved energy–momentum tensor $T_{\mu\nu}$. In fact, it can be shown that it arises from the subtraction of a boundary term from the energy functional coming from $T_{\mu\nu}$.[8] This boundary term vanishes for Dirichlet or Neumann boundary conditions, and in this case, the newly defined (conserved) energy matches the usual energy, which is already conserved. For every other—generalized Robin—boundary condition, there is an effective contribution of the boundary term to the newly defined (conserved) energy functional, showing that there is an effective flux of energy through the conformal boundary of AdS.

In any event, Robin boundary conditions have recently spawned great interest in the context of quantum field theory in asymptotically anti-de Sitter spacetimes and several authors analyzed the consequences implied by these boundary conditions on the quantization of the scalar field (see, for instance, Refs. 9–13 and references therein). As a matter of fact, the introduction of Robin boundary conditions is often motivated by the desire that the system be isolated, as explicitly stated in Refs. 10, 11, and 13. One of the goals of the present work is to clarify this issue and show that generic Robin boundary conditions are incompatible with the requirement that the spacetime be isolated.

More precisely, this paper is concerned with the Cauchy problem associated with the wave equation

$$(\Box - m_\xi^2)\Phi = 0 \tag{1}$$

in an *asymptotically* anti-de Sitter spacetime, where $m_\xi^2 \equiv \mu^2 + \xi\mathscr{R}$ and ξ is a constant, which couples the field to the curvature scalar $\mathscr{R}$. This coupling modifies the usual energy–momentum tensor obtained by the variation of the action with respect to the metric. In what follows, we use the resulting improved energy–momentum tensor to define the energy functional. Our aim is to establish the boundary conditions for which the system *spacetime + field* can be considered as effectively isolated, a point which, as mentioned above, has occasionally been a source of confusion in the literature. It turns out that this is equivalent to finding the boundary conditions for which the conserved energy functional defined by Wald and Ishibashi is equal to the one extracted from the improved energy–momentum tensor. We emphasize that our analysis takes into account only classical fields. In the context of quantum fields in curved spacetimes, the prescription of Wald and Ishibashi leads to a vanishing (renormalized) energy flux $\langle T_{t\rho}\rangle$ (see Ref. 13).

This paper is organized as follows. In Sec. II, we obtain an asymptotic expression for the scalar field at spatial infinity. This is done by means of a Green function that encodes the dependence of the solution on the initial data and boundary conditions. Our analysis differs from that in Refs. 3, 4, and 6 in that we only assume that the spacetime is *asymptotically* AdS; we thus make no assumption (except for certain technicalities to be explained below) about its bulk structure. In Sec. III, we discuss the requirements on the boundary conditions at spatial infinity for the system *spacetime + scalar field* to be effectively isolated. We find that the only boundary conditions that are compatible with this assumption are the (generalized) Dirichlet and Neumann boundary conditions. Finally, in Sec. IV, we discuss our results and make our closing remarks.

II. ASYMPTOTIC BEHAVIOR OF THE FIELD

Let M be a stationary n-dimensional spacetime, which is asymptotically AdS. We choose coordinates $\{t, r, \theta_1, \ldots, \theta_{n-2}\}$ such that the metric on M satisfies

$$ds^2|_{r\to\infty} \approx ds^2_{AdS} = -(1+r^2)dt^2 + \frac{dr^2}{1+r^2} + r^2\, d\Omega^2_{n-2}, \tag{2}$$

where ds^2_{AdS} is the line element in AdS_n and $d\Omega^2_{n-2}$ is the metric on the $(n-2)$-dimensional unity sphere.

We separate variables for the scalar field and consider the *ansatz*

$$\Phi(t,r,\theta) = \sum_{\{\ell\}} \phi_\ell(r,t) Y_\ell(\theta), \tag{3}$$

where $\{\ell\}$ represents the set of integer indices labeling the *hyperspherical harmonics* $Y_\ell(\theta)$. The wave equation (1) can then be written as

$$L_{rt}[\phi] = 0, \tag{4}$$

where L_{rt} is a second order differential operator of the form

$$L_{rt} = u^{ij}(r)\partial_i\partial_j + v^i(r)\partial_i + q(r), \qquad i,j = r,t. \tag{5}$$

When dealing with problems such as (4), it is common practice to consider a time dependence of the form $e^{-i\omega t}$ and then to solve the resulting time-independent problem. However, when considering non-conservative systems (for instance, when energy can flow through the boundaries), with ω being a complex number, such an approach leads to extra mathematical difficulties, which, in turn, make it difficult to physically interpret the resulting solutions.[14–16] When the spacetime bulk contains a black hole, such an approach allows for the determination of the quasinormal mode spectrum of the system. However, the quasinormal modes do not provide a complete set of eigenfunctions, and hence, an arbitrary initial condition cannot be expressed in terms of them.

As discussed in Ref. 14, one can overcome this difficulty by taking the initial conditions into account from the beginning. A suitable mathematical tool for implementing this strategy is the Laplace transform[17]

$$\mathscr{L}\{\phi_\ell(t,r)\} = \hat{\phi}_\ell(\omega,r) = \int_{t_0}^{\infty} \phi_\ell(t,r)e^{i\omega t}dt. \tag{6}$$

Applying the Laplace transform to (4), we obtain an ordinary differential equation,

$$P_2(\omega,r)\frac{\partial^2\hat{\phi}(\omega,r)}{\partial r^2} + P_1(\omega,r)\frac{\partial\hat{\phi}(\omega,r)}{\partial r} + P_0(\omega,r)\hat{\phi}(\omega,r) = \mathscr{I}(\omega,r), \tag{7}$$

for each ω, with $\mathscr{I}(\omega,r)$ taking care of the initial conditions. We omitted the index ℓ to not clutter notation.

Equation (7) can be rewritten as a Schrödinger-type equation,

$$\frac{d^2\hat{\psi}}{dr_*^2} - s(r_*)\hat{\psi} = f(r_*), \tag{8}$$

by using a suitable change of variables

$$\hat{\phi} \to \hat{\psi}, \quad r \to r_*, \tag{9}$$

which maps r into an interval $(r_*^{\min}, r_*^{\max})$. This is to be determined by the specific form of the metric. The solution of Eq. (8) can then be found by the standard Green's function method and can be expressed as

$$\hat{\psi}(\omega,r_*) = \frac{\hat{\psi}_b(\omega,r_*)}{W[\hat{\psi}_b,\hat{\psi}_\infty]}\int_{r_*}^{r_*^{\max}} f(\omega,r'_*)\hat{\psi}_\infty(\omega,r'_*)dr'_* + \frac{\hat{\psi}_\infty(\omega,r_*)}{W[\hat{\psi}_b,\hat{\psi}_\infty]}\int_{r_*^{\min}}^{r_*} f(\omega,r'_*)\hat{\psi}_b(\omega,r'_*)dr'_*. \tag{10}$$

Here, $W[\hat{\psi}_b,\hat{\psi}_\infty]$ is the Wronskian of the solutions $\hat{\psi}_b$ and $\hat{\psi}_\infty$ of the homogeneous equation associated with (8),

$$W_{r_*}[\hat{\psi}_b,\hat{\psi}_\infty] = \hat{\psi}_b\frac{\partial\hat{\psi}_\infty}{\partial r_*} - \frac{\partial\hat{\psi}_b}{\partial r_*}\hat{\psi}_\infty. \tag{11}$$

The function $\hat{\psi}_b$ should be determined after imposing some condition at $r_*^{\min}$, deep into the bulk. This could be a regularity condition at the "origin" $r = 0$ when $M = AdS$ or a condition at the event horizon when M contains a black hole. On the other hand, the function $\hat{\psi}_\infty$ is determined from the boundary conditions at the conformal infinity, $r_*^{\max}$.

Assuming initial data with compact support, we find the following asymptotic approximation:

$$\hat{\psi}(\omega,r_*) \approx \mathscr{A}(\omega)\hat{\psi}_\infty(\omega,r_*) \text{ as } r \to r_*^{\max}, \tag{12}$$

with $\mathscr{A}(\omega) = (1/W[\hat{\psi}_b,\hat{\psi}_\infty])\int_{r_*^{\min}}^{r_*^{\max}} f(\omega,r'_*)\hat{\psi}_b(\omega,r'_*)dr'_*$. Inverting the transformation (9) leads to

$$\hat{\phi}(\omega,r) \approx \mathscr{A}(\omega)\hat{\phi}_\infty(\omega,r) \text{ as } r \to \infty, \tag{13}$$

where $\hat{\phi}_\infty(\omega,r)$ is a solution of the homogeneous equation associated with (7) obeying some boundary condition at spatial infinity. The inverse Laplace transform then yields

$$\phi(t,r) \approx \frac{1}{2\pi}\int_{-\infty+i\varepsilon}^{+\infty+i\varepsilon} \mathscr{A}(\omega)\hat{\phi}_\infty(\omega,r)e^{-i\omega t}d\omega \tag{14}$$

as $r \to \infty$.

We note that the boundary conditions affect the resulting scalar field by means of the solutions of the homogeneous equation, $\hat{\psi}_b(\omega,r_*)$ and $\hat{\psi}_\infty(\omega,r_*)$, while the initial data are encoded in $f(\omega,r*)$. Equivalently, the transformation (9) allows one to interpret the dependence of the solution on the boundary conditions in terms of [the fundamental set of solutions of the homogeneous equation associated with (7)] $\{\hat{\phi}_b,\hat{\phi}_\infty\}$, while its dependence on the initial conditions is given by $\mathscr{I}(\omega,r)$.

Since our aim here is to study the flux of energy at the conformal boundary, we will not fix any specific conditions on the field in the bulk other than requiring the usual regularity conditions, such as initial data with compact support and finiteness of the integrals associated with the asymptotic approximations. As a matter of fact, the convergence of these integrals depends on the analytical structure of the Green's function, which, in turn, depends on the boundary conditions deep inside the spacetime bulk. Hence, the convergence of these integrals must be treated differently for each spacetime. Throughout this work, we will assume that it is always possible to find an approximation such as (14) for the spacetime at hand.

III. ENERGY FLUX IN ASYMPTOTICALLY ANTI-DE SITTER SPACETIMES

We are now ready to study under what conditions the system *spacetime + field* is isolated, in the sense of having no energy flux through the timelike spatial boundary at infinity. As discussed in Sec. II, the asymptotic behavior of the solutions of (1) is encoded in $\hat{\phi}_{\infty,\ell}(\omega,r)$ (we, henceforth, reinsert the ℓ index for definiteness). For each value of ℓ, this function satisfies the homogeneous equation associated with (7) in the limit $r \to \infty$, which is given by

$$\frac{\partial^2}{\partial\rho^2}\hat{\phi}_{\infty,\ell}(\omega,\rho) + (n-2)\sec\rho\,\csc\rho\frac{\partial}{\partial\rho}\hat{\phi}_{\infty,\ell}(\omega,\rho) + \left[\omega^2 - \frac{\ell(\ell+n-3)}{\sin^2\rho} - \frac{m_\xi^2}{\cos^2\rho}\right]\hat{\phi}_{\infty,\ell}(\omega,\rho) = 0, \tag{15}$$

where we have changed the radial coordinate to ρ, with $r = \tan\rho$. Multiplying the last equation by $(\tan\rho)^{n-2}$ and performing the transformation

$$\hat{\phi}_{\infty,\ell}(\omega,\rho) = \frac{Z_\ell(\omega,\rho)}{(\tan\rho)^{\frac{n-2}{2}}}, \tag{16}$$

we find

$$\frac{\partial^2 Z_\ell(\omega,\rho)}{\partial\rho^2} + \left[\omega^2 - V(\rho)\right]Z_\ell(\omega,\rho) = 0, \tag{17}$$

where the effective potencial V is given by

$$V(\rho) = \left[\ell(\ell+n-3) + \frac{1}{4}\left(n^2 - 6n + 8\right)\right]\csc^2\rho + \left[\frac{1}{4}n(n-2) + m_\xi^2\right]\sec^2\rho. \tag{18}$$

We also define

$$d = n-1,\ \nu^2 = \frac{(n-1)^2}{4} + m_\xi^2 \tag{19}$$

and

$$a = \frac{1}{2}\left(\frac{d}{2} + \ell + \nu - \omega\right), \tag{20}$$

$$b = \frac{1}{2}\left(\frac{d}{2} + \ell + \nu + \omega\right). \tag{21}$$

A. A convenient fundamental set of solutions

For the sake of definiteness, let us fix a convenient set $\{Z_\ell^{(D)}, Z_\ell^{(N)}\}$ of linearly independent solutions of (17). Following Ref. 18, we take these functions as follows.

(i) For ν not being an integer,

$$Z_\ell^{(D)}(\omega,\rho) = (\cos\rho)^{\frac{1}{2}+\nu}(\sin\rho)^{l+\frac{d-1}{2}}\,{}_2F_1\left(a,b;1+\nu;\cos^2\rho\right), \tag{22}$$

$$Z_\ell^{(N)}(\omega,\rho) = (\cos\rho)^{\frac{1}{2}-\nu}(\sin\rho)^{l+\frac{d-1}{2}}\,{}_2F_1\left(a-\nu,b-\nu;1-\nu;\cos^2\rho\right). \tag{23}$$

(ii) For $\nu = 0$,

$$Z_\ell^{(D)}(\omega,\rho) = (\cos\rho)^{\frac{1}{2}+\nu}(\sin\rho)^{l+\frac{d-1}{2}}\,{}_2F_1\big(a,b;1;\cos^2\rho\big), \tag{24}$$

$$\begin{aligned}Z_\ell^{(N)}(\omega,\rho) &= (\cos\rho)^{\frac{1}{2}+\nu}(\sin\rho)^{l+\frac{d-1}{2}}\Big\{{}_2F_1\big(a,b;1;\cos^2\rho\big)\ln(\cos^2\rho) + \sum_{k=1}^{\infty}\frac{(a)_k(b)_k}{(k!)^2}(\cos\rho)^{2k}\\ &\times[\psi(a+k)-\psi(a)+\psi(b+k)-\psi(b)-2\psi(k+1)+2\psi(1)]\Big\}.\end{aligned} \tag{25}$$

(iii) For ν being a positive integer,

$$Z_\ell^{(D)}(\omega,\rho) = (\cos\rho)^{\frac{1}{2}+\nu}(\sin\rho)^{l+\frac{d-1}{2}}\,{}_2F_1\big(a,b;1+\nu;\cos^2\rho\big), \tag{26}$$

$$\begin{aligned}Z_\ell^{(N)}(\omega,\rho) &= (\cos\rho)^{\frac{1}{2}+\nu}(\sin\rho)^{l+\frac{d-1}{2}}\Bigg\{{}_2F_1\big(a,b;1+\nu;\cos^2\rho\big)\ln(\cos^2\rho) + \sum_{k=1}^{\infty}\frac{(a)_k(b)_k}{(1+\nu)_k k!}(\cos\rho)^{2k}\\ &\times[h(k)-h(0)] - \sum_{k=1}^{\nu}\frac{(k-1)!(-\nu)_k}{(1-a)_k(1-b)_k}(\cos\rho)^{-2k}\Bigg\},\end{aligned} \tag{27}$$

where

$$\psi(x) = \frac{d}{dx}\ln\Gamma(x), \tag{28}$$

$$h(k) = \psi(a+k)+\psi(b+k)-\psi(1+\nu+k)-\psi(k+1). \tag{29}$$

We note that, depending on the field mass μ and coupling constant ξ, the value of ν^2 can be greater, less, or equal to zero. With no loss of generality, we will consider $\nu > 0$ in the first case and $\nu = i\eta$, $\eta > 0$, in the last case.

The general solution of (17) can be written in terms of the fundamental solutions above as

$$Z_\ell = \mathcal{N}_\ell\Big[\cos\zeta\, Z_\ell^{(D)} + \sin\zeta\, Z_\ell^{(N)}\Big], \tag{30}$$

where $\mathcal{N}_\ell$ does not depend on ρ and $\zeta \in [0,\pi]$ does not depend neither on ρ nor on ℓ. We will refer to the condition $\zeta = 0$ as the *generalized Dirichlet boundary condition* and to the function $Z_\ell^{(D)}$ as the *Dirichlet solution*. The *generalized Neumann boundary condition* will be defined by $\zeta = \pi/2$, and we will refer to $Z_\ell^{(N)}$ as the *Neumann solution*. The other values of $\zeta \in [0,\pi]$ parameterize the *generalized Robin boundary conditions*.

As shown in Ref. 6, the motivation for this terminology comes from the case of a conformally coupled field, for which we have

$$\mu^2 = 0, \qquad \xi = \frac{(n-2)}{4(n-1)}, \quad \nu = \frac{1}{2}. \tag{31}$$

In this case, the effective potencial (18) is non-singular at $\rho = \pi/2$, and the ratio

$$\frac{\partial Z_\ell/\partial\rho}{Z_\ell}\bigg|_{\rho=\frac{\pi}{2}} \tag{32}$$

is well defined. The general solution (30) can be written as

$$Z_\ell(\rho) = G_\nu(\rho)\{\sin\zeta + \cos\zeta(\cos\rho)^{2\nu} + \cdots\} \tag{33}$$

with

$$G_{\nu\ell}(\rho) = \mathcal{N}_\ell\,(\cos\rho)^{-\nu+\frac{1}{2}}(\sin\rho)^{\frac{n-2}{2}+\ell} \tag{34}$$

so that the ratio (32) becomes

$$\left.\frac{\partial Z_\ell/\partial\rho}{Z_\ell}\right|_{\rho=\frac{\pi}{2}} = -\cot\zeta. \tag{35}$$

We note that $\zeta = 0$ and $\zeta = \pi$ correspond to $Z_\ell|_{\rho=\pi/2} = 0$, which is the usual Dirichlet boundary condition. On the other hand, $\zeta = \pi/2$ corresponds to $\partial Z_\ell/\partial\rho|_{\rho=\pi/2} = 0$, the usual Neumann boundary condition. Other choices of $\zeta \in [0,\pi]$ correspond to Robin boundary conditions. In the general case, the effective potential (18) diverges as ρ goes to $\pi/2$, and the ratio $(dZ_\ell/d\rho)/Z_\ell$ is no longer well defined. Despite that, the behavior of $G_{\nu\ell}^{-1}Z_\ell$ as ρ goes to $\pi/2$ is dictated by $\sin\zeta$, while the behavior of $\partial(G_{\nu\ell}^{-1}Z_\ell)/\partial\rho$ is governed by $\cos\zeta$, so it seems natural to define the "generalized Dirichlet boundary condition" as $\zeta = 0$ and the "generalized Neumann boundary condition" by $\zeta = \pi/2$. The other values of $\zeta \in [0,\pi]$ parameterize the "generalized Robin boundary conditions."

B. The flux at infinity

According to Weyl's *limit point* and *limit circle* theory, the allowed boundary conditions at the endpoints of the interval where a Sturm–Liouville problem is defined depend on the integrability of the solutions in the vicinity of these points.[9,19] In the present case, the solutions of (17) provide an approximation for the field near the point $\rho = \pi/2$. The integrability of these solutions depends on the parameter ν.

In what follows, we are going to use the improved energy–momentum tensor of the complex scalar field,[3,8]

$$T_{\alpha\beta} = \frac{1}{2}\big(\partial_\alpha\Phi\,\partial_\beta\Phi^* + \partial_\beta\Phi\,\partial_\alpha\Phi^*\big) - \frac{1}{2}g_{\alpha\beta}\big[g^{\rho\sigma}\partial_\rho\Phi\partial_\sigma\Phi^* + m_\xi^2\Phi\Phi^*\big] + \xi\big(\mathscr{R}_{\alpha\beta} - g_{\alpha\beta}\,\Box - \nabla_\alpha\nabla_\beta\big)\Phi\Phi^*, \tag{36}$$

to calculate the energy flux. The Killing vector field $k = \partial/\partial t$ gives rise to the formally conserved energy $Q^\alpha = |g|^{1/2}T^{\alpha\beta}k_\beta$ $(\partial_\mu Q^\mu = 0)$, and the energy flux across the spatial infinity is given by

$$\mathscr{F}_\infty = -\lim_{\rho\to\pi/2}\int d\theta_1\cdots d\theta_{n-2}\; g^{\rho\rho}\,Q_\rho. \tag{37}$$

The case $\nu^2 \geq 1$

This is a simplest instance to analyze. In this case, $Z_\ell^{(D)}$ is square integrable near $\rho = \pi/2$, while $Z_\ell^{(N)}$ is not. As a result, the generalized Dirichlet boundary condition must be chosen in this case. With this boundary condition, the energy flux across the spatial infinity turns out to be zero. We omit the calculation since it is identical to the case $0 < \nu^2 < 1$, treatedbelow, onceweset once we set $\zeta = 0$.

The case $0 < \nu^2 < 1$

In this case, both solutions are square integrable near $\rho = \pi/2$. The allowed boundary conditions are therefore of Robin type.

For these values of ν, (30) and (16) imply the following asymptotic behavior for $\hat\phi_{\infty,\ell}$:

$$\hat\phi_{\infty,\ell}(\omega,\rho) \approx \mathscr{N}_\ell(\omega)\Big[\cos\zeta\,\hat\phi_\ell^{(D)}(\omega,\rho) + \sin\zeta\,\hat\phi_\ell^{(N)}(\omega,\rho)\Big], \tag{38}$$

where

$$\hat\phi_\ell^{(D)}(\omega,\rho) = \left(\frac{\pi}{2}-\rho\right)^{\frac{d}{2}+\nu} + J_\ell(\omega)\left(\frac{\pi}{2}-\rho\right)^{\frac{d}{2}+\nu+2} + O\left[\left(\frac{\pi}{2}-\rho\right)^{\frac{d}{2}+\nu+4}\right], \tag{39}$$

$$\hat\phi_\ell^{(N)}(\omega,\rho) = \left(\frac{\pi}{2}-\rho\right)^{\frac{d}{2}-\nu} + K_\ell(\omega)\left(\frac{\pi}{2}-\rho\right)^{\frac{d}{2}-\nu+2} + O\left[\left(\frac{\pi}{2}-\rho\right)^{\frac{d}{2}-\nu+4}\right], \tag{40}$$

with

$$J_\ell(\omega) = \frac{a_1(\omega)b_1(\omega)}{1+\nu} - \frac{n-1+6\ell+2\nu}{12}, \tag{41}$$

$$K_\ell(\omega) = \frac{a_2(\omega)b_2(\omega)}{1-\nu} - \frac{n-1+6\ell-2\nu}{12}, \tag{42}$$

as $\rho\to\pi/2$. Upon substitution of (38) into (14), we obtain the following asymptotic expression for ϕ_ℓ:

$$\phi_\ell(t,\rho) \approx \cos\zeta\left(\frac{\pi}{2}-\rho\right)^{\frac{d}{2}+\nu}\mathcal{T}_\ell(t) + \cos\zeta\left(\frac{\pi}{2}-\rho\right)^{\frac{d}{2}+\nu+2}\mathcal{T}_{D,\ell}(t) + \sin\zeta\left(\frac{\pi}{2}-\rho\right)^{\frac{d}{2}-\nu}\mathcal{T}_\ell(t) + \sin\zeta\left(\frac{\pi}{2}-\rho\right)^{\frac{d}{2}-\nu+2}\mathcal{T}_{N,\ell}(t), \tag{43}$$

where

$$\mathcal{T}_\ell(t) = \frac{1}{2\pi}\int_{-\infty+i\varepsilon}^{+\infty+i\varepsilon}\mathcal{A}_\ell(\omega)\mathcal{N}_\ell(\omega)e^{-i\omega t}d\omega, \tag{44}$$

$$\mathcal{T}_{D,\ell}(t) = \frac{1}{2\pi}\int_{-\infty+i\varepsilon}^{+\infty+i\varepsilon}\mathcal{A}_\ell(\omega)\mathcal{N}_\ell(\omega)J_\ell(\omega)e^{-i\omega t}d\omega, \tag{45}$$

$$\mathcal{T}_{N,\ell}(t) = \frac{1}{2\pi}\int_{-\infty+i\varepsilon}^{+\infty+i\varepsilon}\mathcal{A}_\ell(\omega)\mathcal{N}_\ell(\omega)K_\ell(\omega)e^{-i\omega t}d\omega. \tag{46}$$

Using the asymptotic form (43), (36), and (37), we get

$$\mathcal{F}_\infty \sim \lim_{\rho\to\pi/2}\sin\zeta\left\{\cos\zeta\, A + \sin\zeta\, B\left(\frac{\pi}{2}-\rho\right)^{-2\nu}\right\}\left(\sum_{\{\ell\}}\frac{d}{dt}|\mathcal{T}_\ell(t)|^2\right), \tag{47}$$

where

$$A = \frac{d}{2} - 2\xi(d+1), \tag{48}$$

$$B = \left(\frac{1}{4}-\xi\right)(d-2\nu) - \xi. \tag{49}$$

We immediately see that by imposing the Dirichlet boundary condition ($\zeta = 0$), the flow of energy across the infinity turns out to be zero.

On the other hand, when $\zeta \neq 0$, we must choose the coupling constant so that $B = 0$ in order that the energy flux be finite. This leads to

$$\mathcal{F}_\infty \sim \sin\zeta\,\cos\zeta\, A\sum_{\{\ell\}}\frac{d}{dt}|\mathcal{T}_\ell(t)|^2. \tag{50}$$

The integrals defining $\mathcal{T}_\ell(t)$, $\ell = 0, 1, 2\ldots$, depend on the singularity structure of the functions $\mathcal{A}_\ell$, which, in turn, depend on the boundary conditions in the spacetime bulk and on the initial conditions of the system. As a result, except for very specific field configurations, we must impose the Neumann condition ($\zeta = \pi/2$) for the system to become effectively isolated. For general Robin conditions ($\zeta \neq 0$ and $\zeta \neq \pi/2$), the energy flux across the conformal boundary is generically not zero.

There is a notable case where the energy flux (50) can be zero without imposing either $\zeta = 0$ or $\zeta = \pi/2$. For the propagation of a single mode of frequency $\omega \in \mathbb{R}$, we have $\mathcal{T}_\ell(t) \sim e^{-i\omega t}$, and then, $d|\mathcal{T}_\ell(t)|^2/dt = 0$, and the energy flux (50) vanishes for every Robin boundary condition $\zeta \in [0,\pi]$. However, for the propagation of two field modes, this conclusion is no longer true. More generally, if the scalar field is composed of a nontrivial superposition of modes of different frequencies, then $d|\mathcal{T}_\ell(t)|^2/dt \neq 0$.

In summary, the boundary conditions that make the system *scalar field* + *spacetime* effectively isolated in this case are as follows:

(i) $\zeta = 0$ (Dirichlet).
(ii) $\zeta = \pi/2$ (Neumann), together with ξ chosen such that $B = 0$.

In particular, for a minimally coupled field ($\xi = 0$), only the Dirichlet boundary condition gives zero energy flux across the spatial infinity since in this case, $B \neq 0$.

The case $\nu^2 = 0$

As in the previous case, both solutions are square integrable near $\rho = \pi/2$ here. The allowed boundary conditions are therefore again of Robin type.

Moreover, the behavior of both $G_{\nu\ell}^{-1}Z_\ell$ and $\partial(G_{\nu\ell}^{-1}Z_\ell))/\partial\rho$ are governed by $\sin\zeta$ for $\nu = 0$. Thus, one can interpret $\zeta = 0$ (or $\zeta = \pi$) as the simultaneous imposition of generalized Neumann and Dirichlet boundary conditions. Following the same steps as in the previous case, we find that the condition of zero flux again requires $\zeta = 0$ together with $\xi = (n-1)/4n$.

The case $\nu^2 < 0$

We now consider the case when $\nu^2 < 0$, i.e., $\nu = i\eta$ with $\eta > 0$. Once again, both solutions are square integrable near $\rho = \pi/2$ here. The energy flow across the spatial infinity is now given by

$$\mathscr{F} \approx \lim_{\rho\to\pi/2} \sum_{\{\ell\}} (A_\ell \cos 2\zeta + B_\ell \sin 2\zeta + C_\ell), \tag{51}$$

where

$$A_\ell = \eta\,\mathrm{Im}\left\{\mathscr{T}_\ell^*(t)\frac{d\mathscr{T}_\ell(t)}{dt}\right\}, \tag{52}$$

$$B_\ell = \frac{1}{2}Re\left\{[(n+2i\eta)(4\xi-1)+1]\left(\frac{\pi}{2}-\rho\right)^{2i\eta}\right\}Re\left\{\mathscr{T}_\ell^*(t)\frac{d\mathscr{T}_\ell(t)}{dt}\right\}, \tag{53}$$

$$C_\ell = \frac{1}{2}[1+n(4\xi-1)]Re\left\{\mathscr{T}_\ell^*(t)\frac{d\mathscr{T}_\ell(t)}{dt}\right\}. \tag{54}$$

Since the functions $\sin 2\zeta$ and $\cos 2\zeta$ are linearly independent, we conclude that, in general, the system cannot be treated as isolated for $\nu^2 < 0$.

Once again, a notable exception is given by the propagation of a single mode with frequency $\omega \in \mathbb{R}$. In this case, we have $\mathscr{T}(t) \sim e^{i\omega t}$, and therefore, $Re\{\mathscr{T}^*(t)[d\mathscr{T}(t)/dt]\} = 0$, which implies that the coefficients B and C in (51) both vanish. Then, by choosing the boundary condition as $\zeta = \pi/4$, we can cancel out the energy flux through the conformal boundary.

It is worth mentioning that when M is not only *asymptotically* AdS, but $M = AdS$, the differential operator associated with Eq. (17) is unbounded below for $\nu^2 < 0$. As a result, one cannot find positive self-adjoint extensions of it[6] so that it is not possible to define a physically "reasonable" time evolution in this case.[20] In general, one cannot make assertions concerning the positivity of the differential operator associated with the correspondent radial equation without detailed information about the bulk structure of spacetime. Indeed, the positivity of the differential operator may be somewhat subtle to be rigorously established even when the bulk structure is fully known.[21]

Finally, we note that the calculations in this section could be performed using the canonical (non-improved) energy–momentum tensor,

$$\widetilde{T}_{\alpha\beta} = \frac{1}{2}\left(\partial_\alpha\Phi\,\partial_\beta\Phi^* + \partial_\beta\Phi\,\partial_\alpha\Phi^*\right) - \frac{1}{2}g_{\alpha\beta}\left[g^{\rho\sigma}\partial_\rho\Phi\partial_\sigma\Phi^* + m_\xi^2\Phi\Phi^*\right]. \tag{55}$$

In this case, we find that (i) for $\nu^2 > 0$, only the Dirichlet boundary condition yields a zero energy flux across infinity and (ii) for $\nu^2 \le 0$, the flux is generically nonzero even for the Dirichlet choice. These results are also what one would obtain by formally substituting $\xi = 0$ in the above calculations for the improved energy–momentum tensor.

C. Mode analysis

To conclude this section, we discuss how our results fit with the existing literature. A common approach consists in considering a time dependence given by $e^{-i\omega t}$ and to impose boundary conditions on the radial part for each field mode of frequency ω.[9–13] For simplicity and in order to make the discussion clearer, let us consider the specific case of $n = 3$, i.e., of a spacetime, which is asymptotically AdS$_3$.

The allowed values of ω for the field eigenfunctions are determined from the boundary conditions in the bulk and at infinity, with $\omega \in \mathbb{R}$ or $\omega \in \mathbb{C}$, depending on the specific conditions imposed. In the following, we will consider both the energy flow due to the propagation of a single frequency mode ω_1 and the flux due to the propagation of a superposition of modes with frequencies ω_1 and ω_2. Since we are not imposing any boundary condition on the spacetime bulk, we will allow ω to be complex and then specialize to the case of a real ω.

Let us consider the case when $0 < \nu < 1$. Let Φ_1 be a mode with frequency $\omega_1 \in \mathbb{C}$,

$$\Phi_1(t,\rho,\varphi) = \phi_{\omega_1\ell}(\rho)\,e^{-i\omega_1 t}e^{i\ell\varphi}. \tag{56}$$

A straightforward calculation shows that the energy flux across infinity for this specific solution is given by

$$\mathscr{F}^{(1)} \sim \lim_{\rho\to\pi/2} e^{2\,\mathrm{Im}(\omega_1)\,t}\,\mathrm{Im}(\omega_1)\sin\zeta\left\{\cos\zeta\,(1-6\xi) + \sin\zeta\,B\left(\frac{\pi}{2}-\rho\right)^{-2\nu}\right\}, \tag{57}$$

where

$$B = \left[\left(\frac{1}{2}-2\xi\right)(1-\nu) - \xi\right]. \tag{58}$$

We immediately see that when $\mathrm{Im}(\omega_1) \neq 0$, only the Dirichlet and Neumann boundary conditions cancel the flux (the latter with ξ chosen such that $B = 0$ as usual). On the other hand, when $\omega \in \mathbb{R}$, the energy flux is null for any Robin boundary condition $(0 \le \zeta < \pi)$, regardless of the coupling constant ξ. However, this is only a result of the very particular situation of a single mode solution. Considering the superposition of even just two modes, Φ_1 and Φ_2, with frequencies $\omega_1,\ \omega_2 \in \mathbb{R}$, we obtain the corresponding flux given by

$$\mathscr{F}^{(1,2)} \sim \lim_{\rho\to\pi/2} \sin(\Delta\omega t)\ \sin\zeta\left\{\cos\zeta\,(1-6\xi)+\sin\zeta\, B\left(\frac{\pi}{2}-\rho\right)^{-2\nu}\right\}, \tag{59}$$

where $\Delta\omega = \omega_1 - \omega_2$. Therefore, once again, only the Dirichlet and Neumann boundary conditions are compatible with the hypothesis that the system is isolated (the latter with ξ chosen such that $B = 0$ as usual).

The analysis of the other cases of ν leads to the same conclusion. A single mode of real frequency can have zero flux at infinity while obeying Robin boundary conditions. However, as soon as we consider a superposition of modes of different real frequencies (or even a single mode of complex frequency), generic Robin boundary conditions are not compatible with zero flux at infinity and the results of Subsection III B are recovered.

For the sake of completeness, we repeat this analysis for the case of a real scalar field in Appendix B. The results are essentially the same, the only difference being that general Robin boundary conditions are not compatible with zero energy flux at infinity even in the case of a single mode.

We conclude this section by noting that our results do not depend on the bulk structure of the spacetime. Regardless of the bulk, the only boundary conditions at infinity that make the system effectively isolated are those of Dirichlet and Neumann types. Some particular field configurations may, of course, have zero flux without conforming to this rule. This is the case of a single mode of a complex scalar field with real frequency, for which the flux is zero irrespective of the choice of ζ.

IV. DISCUSSION

We have studied the asymptotic behavior of scalar fields in spacetimes, which are asymptotically anti-de Sitter. We determined the boundary conditions at the spatial infinity for which there is no flow of energy at the conformal boundary. We showed that the only allowed choices that are consistent with this requirement are the generalized Dirichlet and Neumann boundary conditions (the latter with a specific choice of the coupling constant). This happens regardless of the theory in the spacetime bulk. The energy flux was calculated using the improved energy–momentum tensor (36). If we had used the canonical energy–momentum tensor (55) instead, only the Dirichlet boundary conditions would be compatible with zero flux at the conformal boundary.

In particular, Robin mixed boundary conditions, as considered, for instance, in Refs. 6 and 9–13 (although physically reasonable since they provide a fully deterministic dynamics), are not compatible with the requirement that the spacetime is an isolated system.

The case of an asymptotically AdS_2 spacetime can be treated in a similar manner. The fundamental difference is that in this case, the spatial infinity has two distinct components so that, in order for the system to be isolated, one must demand the energy flow to be (separately) zero at each of the boundaries. We must then impose two independent conditions at each of the two boundaries. The zero flux condition constrains those to be, again, of Dirichlet and Neumann types.

ACKNOWLEDGMENTS

R.A.M. acknowledges discussions with L. de Souza Campos. C.C.d.O. acknowledges support from the Conselho Nacional de Desenvolvimento Científico e Tecnológico (CNPq, Brazil), Grant No. 142529/2018-4. R.A.M. was partially supported by Conselho Nacional de Desenvolvimento Científico e Tecnológico under Grant No. 310403/2019-7. J.P.M.P. was partially supported by Conselho Nacional de Desenvolvimento Científico e Tecnológico under Grant No. 311443/2021-4.

AUTHOR DECLARATIONS

Conflict of Interest

The authors have no conflicts to disclose.

DATA AVAILABILITY

Data sharing is not applicable to this article as no new data were created or analyzed in this study.

APPENDIX A: PRINCIPAL AND NON-PRINCIPAL SOLUTIONS

For $\nu \in \mathbb{R}$, the function $Z_\ell^{(D)}$ defined in Sec. III A is the only solution (up to a multiplicative factor) such that $\lim_{\rho\to\pi/2}\left[Z_\ell^{(D)}(\rho)/Z_\ell(\rho)\right] = 0$ for any solution Z_ℓ not proportional to $Z_\ell^{(D)}$. A solution satisfying this condition is called a *principal* solution (at the endpoint $\rho = \pi/2$). Solutions that are not proportional to $Z_\ell^{(D)}$ are called *non-principal* (at the endpoint $\rho = \pi/2$).

We note that non-principal solutions are not unique. In fact, if $\tilde{Z}_\ell$ is a non-principal solution, then $\tilde{Z}_\ell + \alpha Z_\ell^{(D)}$ is also a solution of this type for any $\alpha \in \mathbb{R}$. It is interesting to ask what would change in our analysis if we replace $Z_\ell^{(N)}$ of Sec. III A by another non-principal solution $\tilde{Z}^{(N)} = Z^{(D)} + \gamma Z^{(N)}$, $\gamma \in \mathbb{R}$. In terms of the new set $\{Z^{(D)}, \tilde{Z}^{(N)}\}$, the general solution of (17) can be expressed as

$$Z_\ell = \mathcal{N}_\ell\Big[\cos\zeta\, Z_\ell^{(D)} + \sin\zeta\, \tilde{Z}_\ell^{(N)}\Big], \tag{A1}$$

and the condition $\zeta = \pi/2$ no longer selects the function given in (23). The value of ζ that selects that function is now

$$\cot\bar{\zeta} = -\gamma. \tag{A2}$$

The energy flux calculated in terms of the new set of solutions is given by

$$\mathcal{F}_\infty \sim \lim_{\rho\to\pi/2} \sin\zeta\left\{(\cos\zeta + \gamma\sin\zeta)\, A + \sin\zeta\, B\left(\frac{\pi}{2}-\rho\right)^{-2\nu}\right\}\left(\sum_{\{\ell\}}\frac{d}{dt}|\mathcal{T}_\ell(t)|^2\right). \tag{A3}$$

From (A3), we see that the boundary conditions that cancel the energy flux across the conformal boundary are $\zeta = 0$ (Dirichlet) and $\zeta = \bar{\zeta}$ (along with ξ chosen such that $B = 0$). Therefore, regardless of how the generalized Neumann condition is defined, the boundary conditions associated with zero flux at infinity are those that select the solutions $Z^{(D)}$ and $Z^{(N)}$ of Sec. III A.

APPENDIX B: REAL SCALAR FIELDS

We discuss in this appendix the behavior of the energy flux across the spatial infinity for real scalar fields. The improved energy–momentum tensor in this case is given by

$$T_{\alpha\beta} = \partial_\alpha\Phi\,\partial_\beta\Phi - \frac{1}{2}g_{\alpha\beta}\big[g^{\rho\sigma}\partial_\rho\Phi\partial_\sigma\Phi + m_\xi^2\Phi^2\big] + \xi\big(\mathcal{R}_{\alpha\beta} - g_{\alpha\beta}\,\Box - \nabla_\alpha\nabla_\beta\big)\Phi^2. \tag{B1}$$

The counterparts for real scalar fields of the real and complex frequency cases of the main text are, respectively, given as follows:

(i) $\cos(\omega t + \delta)$ when $\omega \in \mathbb{R}$;
(ii) $e^{\omega_I t}\cos(\omega_R t + \delta)$ when $\omega = \omega_R + i\omega_I \in \mathbb{C}$.

Let us consider case (i) separately. Let Φ_1 be a mode with frequency $\omega_1 \in \mathbb{R}$,

$$\Phi_1(t,\rho,\varphi) = \phi_{\omega_1\ell}(\rho)\cos(\omega_1 t + \delta_1)[C_1\cos\ell\varphi + D_1\sin\ell\varphi]. \tag{B2}$$

This leads to

$$\phi_{\omega_j\ell}(\rho) \approx \cos\zeta\phi_{\omega_j\ell}^{(D)}(\rho) + \sin\zeta\phi_{\omega_j\ell}^{(N)}(\rho), \tag{B3}$$

$j = 1, 2$, as $\rho \to \pi/2$, where

$$\phi_{\omega_j\ell}^{(D)}(\rho) = (\sin\rho)^\ell(\cos\rho)^{1+\nu}\,{}_2F_1\big(a_1, b_1; c_1; \cos^2\rho\big), \tag{B4}$$

$$\phi_{\omega_j\ell}^{(N)}(\rho) = (\sin\rho)^\ell(\cos\rho)^{1-\nu}\,{}_2F_1\big(a_2, b_2; c_2; \cos^2\rho\big) \tag{B5}$$

and

$$a_1 = \frac{1}{2}(1 + \ell + \nu - \omega_1), \tag{B6}$$

$$b_1 = \frac{1}{2}(1 + \ell + \nu + \omega_1), \tag{B7}$$

$$c_1 = 1 + \nu, \tag{B8}$$

$$a_2 = \frac{1}{2}(1 + \ell - \nu - \omega_2), \tag{B9}$$

$$b_2 = \frac{1}{2}(1 + \ell - \nu + \omega_2), \tag{B10}$$

$$c_2 = 1 - \nu. \tag{B11}$$

The energy flux across the spatial infinity is then given by

$$\mathscr{F} \approx \omega_1 \sin[2(\omega_1 t + \delta_1)] \sin\zeta \lim_{\rho\to\pi/2} \left\{\cos\zeta\,(1 - 6\xi) + \sin\zeta\, B\left(\frac{\pi}{2} - \rho\right)^{-2\nu}\right\}, \tag{B12}$$

and we see that this is zero only for the Dirichlet boundary condition ($\zeta = 0$) or the Neumann boundary condition ($\zeta = \pi/2$) with ξ such that $B = 0$. This should be compared to the corresponding result for the complex field, Eq. (57), for which the flux associated with a single mode was found to be zero even for Robin conditions.

Now, consider the superposition of two modes [still in case (i)], Φ_1 and Φ_2, with

$$\Phi_1(t, \rho, \varphi) = \phi_{\omega_1 \ell}(\rho) \cos(\omega_1 t + \delta_1)[C_1 \cos \ell\varphi + D_1 \sin \ell\varphi], \tag{B13}$$

$$\Phi_2(t, \rho, \varphi) = \phi_{\omega_2 \ell}(\rho) \cos(\omega_2 t + \delta_2)[C_2 \cos \ell\varphi + D_2 \sin \ell\varphi], \tag{B14}$$

with $\omega_1, \omega_2 \in \mathbb{R}$. The energy flow across the conformal infinity is now given by

$$\mathscr{F} \sim [\cos(\omega_1 t + \delta_1) + \cos(\omega_2 t + \delta_2)][\omega_1 \sin(\omega_1 t + \delta_1) + \omega_2 \sin(\omega_2 t + \delta_2)] 2 \sin\zeta \lim_{\rho\to\pi/2} \left\{\cos\zeta\,(1 - 6\xi) + \sin\zeta\, B\left(\frac{\pi}{2} - \rho\right)^{-2\nu}\right\}. \tag{B15}$$

Since the functions $\sin \omega_j t$ and $\cos \omega_j t$ are linearly independent, the only boundary conditions that do not violate the isolated system hypothesis are again of the Dirichlet and the Neumann types (the latter with ξ such that $B = 0$).

We end by considering case (ii). The real scalar field mode in this case (the counterpart of the complex mode with complex frequency) is given by

$$\Phi_1(t, \rho, \varphi) = Re[\phi_{\omega_1 \ell}(\rho)] e^{\beta_1 t} \cos(\alpha_1 t + \delta_1)[C_1 \cos \ell\varphi + D_1 \sin \ell\varphi]. \tag{B16}$$

The energy flux through infinity is now

$$\mathscr{F} \approx e^{2t\beta_1}\left[\beta_1 \cos^2(\alpha_1 t + \delta_1) - \alpha_1 \cos(\alpha_1 t + \delta_1) \sin(\alpha_1 t + \delta_1)\right] 2 \sin\zeta \lim_{\rho\to\pi/2} \left\{\cos\zeta(1 - 6\xi) + \sin\zeta\, B\left(\frac{\pi}{2} - \rho\right)^{-2\nu}\right\}, \tag{B17}$$

and we see again that the only conditions compatible with the hypothesis that the system is isolated are those of Neumann and Dirichlet (the latter with ξ such that $B = 0$).

REFERENCES

[1] R. M. Wald, *General Relativity* (University of Chicago Press, 1984).
[2] R. M. Wald, J. Math. Phys. **21**, 2802 (1980).
[3] P. Breitenlohner and D. Z. Freedman, Phys. Lett. B **115**, 197 (1982).
[4] P. Breitenlohner and D. Z. Freedman, Ann. Phys. **144**, 249 (1982).
[5] A. Ishibashi and R. M. Wald, Classical Quantum Gravity **20**, 3815 (2003).
[6] A. Ishibashi and R. M. Wald, Classical Quantum Gravity **21**, 2981 (2004).
[7] In fact, Refs. 2 and 5 deal with a general non-globally hyperbolic spacetime, where the lack of global hyperbolicity arises due to a conformal boundary or a naked singularity. Reference 6 worked, specifically, with the AdS spacetime.
[8] S. J. Avis, C. J. Isham, and D. Storey, Phys. Rev. D **18**, 3565 (1978).
[9] C. Dappiaggi and H. R. C. Ferreira, Phys. Rev. D **94**, 125016 (2016).
[10] C. Dappiaggi, H. R. C. Ferreira, and C. A. R. Herdeiro, Phys. Lett. B **778**, 146 (2018).
[11] H. R. C. Ferreira and C. A. R. Herdeiro, Phys. Lett. B **773**, 129 (2017).
[12] T. Morley, P. Taylor, and E. Winstanley, Classical Quantum Gravity **38**, 035009 (2021).
[13] V. S. Barroso and J. P. M. Pitelli, Gen. Relativ. Gravitation **52**, 29 (2020).
[14] H.-P. Nollert and B. G. Schmidt, Phys. Rev. D **45**, 2617 (1992).
[15] N. Andersson, Phys. Rev. D **51**, 353 (1995).

[16]E. Berti and V. Cardoso, Phys. Rev. D **74**, 104020 (2006).
[17]We take the parameter of the Laplace transform as $s = -i\omega$, in accordance with Refs. 15 and 16. The Laplace transform $\hat{f}(\omega)$ of $f(t)$, defined in a certain interval $t_0 < t < \infty$, is well defined if there exists λ, ε, and τ, such that

$$f(t) < \lambda e^{\varepsilon\tau}, \quad \forall t > \tau.$$

Under these assumptions, $\hat{f}(\omega)$ exists for all $\omega \in \mathbb{C}$ such that $\mathrm{Im}(\omega) > \varepsilon$. For a rigorous approach regarding the existence and unicity of the Laplace transform in Schwarzschild spacetime, we refer to Refs. 14 and 15.
[18]I. S. Gradshteyn and I. M. Ryzhik, *Table of Integrals, Series, and Products* (Academic Press, 2014).
[19]A. Zettl, *Sturm–Liouville Theory*, Mathematical Surveys and Monographs Vol. 121 (American Mathematical Society, Providence, RI, 2005).
[20]By "reasonable," we mean precisely the conditions given in Refs. 2 and 5.
[21] A. Garbarz, J. La Madrid, and M. Leston, Eur. Phys. J. C **77**, 807 (2017).

Appendix B

Scalar Field Propagation in Nonglobally Hyperbolic Spacetimes

B.1 Self-Adjoint Operators

In this section, we present the fundamental definitions and theorems needed to characterize the self-adjoint extensions of symmetric linear operators in Hilbert spaces. We will not prove the theorems, (the reader is referred to [98, 99, 100] for the proofs). The positive self-adjoint extensions of symmetric operators play a central role in the framework introduced in [69].

Initially, we will establish some notation and definitions. Let $\mathcal{H}$ be a complex Hilbert space endowed with an inner product denoted by $\langle \cdot, \cdot \rangle_{\mathcal{H}}$, and $A : D(A) \subseteq \mathcal{H} \to \mathcal{H}$ be a linear operator, with $D(A)$ being its domain.

Definition B.1.1 (Closure of a set) *Let $S \subset \mathcal{H}$.*

1. *The function $\psi \in \mathcal{H}$ is said to be a* ***point of closure*** *of S if for every $\epsilon > 0$ there exists some $\phi \in S$ such that $\| \phi - \psi \| < \epsilon$.*

2. *The* ***closure*** *of S is the set of all of its points of closure. We denote it by $\overline{S}$.*

It is clear from definition that $S \subseteq \overline{S}$.

Definition B.1.2 *The operator A is said to be* ***densily defined*** *in $\mathcal{H}$ if $\mathcal{D}(A)$ is dense in $\mathcal{H}$, i.e., $\overline{\mathcal{D}(A)} = \mathcal{H}$.*

Definition B.1.3 (Closed Operator) *Let* $\{\phi_n\}$, $\phi_n \in \mathcal{D}(A)$, *be a sequence in* $\mathcal{D}(A)$. *The operator* A *is said to be **closed** if*

$$\lim_{n\in\mathbb{N}} \phi_n = \phi \quad \textit{and} \quad \lim_{n\in\mathbb{N}} A\phi_n = \psi$$

together imply that

$$\phi \in \mathcal{D}(A) \quad \textit{and} \quad A\phi = \psi.$$

Definition B.1.4 (Closure of a linear operator) *The linear operator* A *is said to be **closable** if it has an extension which itself is a closed operator. If there exists a minimal closed extension, such extension is called the **closure** of* A, *and we denote it by* $\bar{A}$.

Definition B.1.5 (Adjoint operator) *Let* $A : \mathcal{D}(A) \to \mathcal{H}$ *be a linear operator densily defined in* $\mathcal{H}$. *Let us consider the set*

$$\mathcal{D}(A^\dagger) = \{\psi \in \mathcal{H} \,\big|\, \exists\ \psi^\dagger \in \mathcal{H}\ \textit{s.t.}\ \langle A\phi, \psi\rangle = \langle \phi, \psi^\dagger\rangle,\ \forall \phi \in \mathcal{H}\}. \tag{B.1}$$

We define the adjoint $A^\dagger : \mathcal{D}(A^\dagger) \to \mathcal{H}$ *of* A *by*

$$\psi^\dagger = A^\dagger \psi. \tag{B.2}$$

Definition B.1.6 *A linear operator* $A : \mathcal{D}(A) \to \mathcal{H}$ *densely defined in* $\mathcal{H}$ *is said to be **symmetric** if*

$$\langle A\phi, \psi\rangle = \langle \phi, A\psi\rangle, \quad \forall \phi, \psi \in \mathcal{D}(A). \tag{B.3}$$

It follows from this definition that if A is symmetric, then $\mathcal{D}(A) \subset \mathcal{D}(A^\dagger)$ and $A^\dagger\big|_{\mathcal{D}(A)} = A$ [1].

Definition B.1.7 (Self-adjoint operator) *A linear operator* $A : \mathcal{D}(A) \to \mathcal{H}$ *is said to be **self-adjoint** if:*

(i) *A is symmetric,*

(ii) $\mathcal{D}(A) = \mathcal{D}(A^\dagger)$

[1] The notation $A^\dagger\big|_{\mathcal{D}(A)}$ stands for the operator $A^\dagger$ with domain restricted to the set $\mathcal{D}(A)$.

In other words, A is self-adjoint if $A = A^{\dagger}$.

It is worth to notice that a self-adjoint operator is necessarily symmetric, but the converse may not be true.

Definition B.1.8 (Essentially self-adjoint operator) *A symmetric operator $A : \mathcal{D}(A) \to \mathcal{H}$ is **essentially self-adjoint** if its closure $\bar{A}$ is self-adjoint.*

At this stage, we may ask if it is possible to turn a symmetric operator into a self-adjoint operator. In fact, in some cases, this can be achieved by a suitable enlargement of the domain of the symmetric operator. In particular, if the operator is symmetric and positive, then there exists at least one self-adjoint extension, which is the so-called Friedrichs extension [100].

Before we present the theorems establishing the criteria that a given symmetric operator needs to match in order to have a self-adjoint extension, we remark a simple important property of self-adjoint operators. Let the linear operator $A : \mathcal{D}(A) \to \mathcal{H}$ be self-adjoint, and let us assume that $A^{\dagger}\phi = \pm i\phi$, then

$$\mp i\langle\phi,\phi\rangle = \langle\pm i\phi,\phi\rangle = \langle A\phi,\phi\rangle = \langle\phi,A^{\dagger}\phi\rangle = \langle\phi,\pm i\phi\rangle = \pm i\langle\phi,\phi\rangle, \tag{B.4}$$

which implies that $\langle\phi,\phi\rangle = 0$. In other words, if A is self-adjoint, the equation $A^{\dagger}\phi = \pm i\phi$ admits only the trivial solution. This result indicates that when A is not a self-adjoint operator, the spaces generated by the solutions of $A^{\dagger}\phi = \pm i\phi$ play a significant role in the process of determination of its possible self-adjoint extensions. This result motivates the following definition.

Definition B.1.9 (Deficiency subspaces) *We define the **deficiency subspaces** $\mathcal{N}_{\pm}$ and their **deficiency indices** (n_+, n_-) by*

$$\mathcal{N}_{\pm} = \{\phi \in \mathcal{D}(A^{\dagger}) \big| \; A^{\dagger}\phi = \pm i\lambda\phi, \; \lambda > 0\} \tag{B.5}$$

The following theorems show in which cases a symmetric operator A has a self-adjoint extension and provide a method to construct such extensions in the affirmative case.

Theorem B.1.1 *Let $A : \mathcal{D}(A) \to \mathcal{H}$ be a symmetric operator with deficiency indices (n_-, n_+). We have three possible cases*

1. *If $n_- = n_+ = 0$, then A is essentially self-adjoint (indeed, this condition is necessary and sufficient).*

2. *If $n_- = n_+ = n \geq 1$, then A has infinitely many self-adjoint extensions. They are in one-to-one correspondence to the isometries between $\mathcal{N}_+$ and $\mathcal{N}_-$, parametrized by an $n \times n$ unitary matrix U.*

3. *If $n_+ \neq n_-$, then A has no self-adjoint extensions.*

The following theorem gives us a systematic procedure to construct the self-adjoint extensions in the second case above.

Theorem B.1.2 *Let $A : \mathcal{D}(A) \to \mathcal{H}$ be a closable symmetric operator with closure $\bar{A}$ and deficiency indices $n_- = n_+ = n \geq 1$. Let U be the unitary matrix parametrizing the isometries between $\mathcal{N}_-$ and $\mathcal{N}_+$. Let us define the operators $A_E : \mathcal{D}(A_E) \to \mathcal{H}$*

$$A_E \phi = A\phi_0 + i\phi_+ - iU\phi_-, \tag{B.6}$$

where

$$\mathcal{D}(A_E) = \left\{ \phi = \phi_0 + \phi_+ + U\phi_+ \middle| \, \phi_0 \in \mathcal{D}(\bar{A}),\ \phi_+ \in \mathcal{N}_+ \right\}. \tag{B.7}$$

Then, each operator A_E is self-adjoint.

Having the results presented in this section at hand, we now turn to their application on the dynamics of the scalar field in static nonglobally hyperbolic spacetimes.

B.1.1 Prescription for dynamics

Let $(M, g_{\mu\nu})$ be a static spacetime with metric

$$ds^2 = -V^2 dt^2 + h_{ij} dx^i dx^j \tag{B.8}$$

where $V^2 = -\tau_\alpha \tau^\alpha$, and $\tau = \partial/\partial t$ is a hypersurface orthogonal time-like Killing vector field. We wish to consider the Klein-Gordon equation of motion

$$(\Box - m_\xi^2)\phi = 0 \tag{B.9}$$

for a scalar field with effective mass $m_\xi^2 = \mu^2 + \xi R$, where μ stands for the field mass and ξ is the coupling constant with the scalar curvature R. Suppose we specify initial conditions on a hypersurface Σ orthogonal to the static Killing field

$$\begin{aligned} \phi\big|_\Sigma &= \phi_0, \\ \tau^\alpha \nabla_\alpha \phi\big|_\Sigma &= \dot{\phi}_0. \end{aligned} \tag{B.10}$$

If the spacetime is globally hyperbolic, the initial data (B.10) will determine ϕ in the entire spacetime. On the other hand, if the spacetime is not globally hyperbolic, the hypersurface Σ is not a Cauchy Surface and data on Σ will determine ϕ only in the domain of dependence $D(\Sigma)$. In such a case, we need some kind of prescription in order to determine ϕ everywhere in spacetime.

Aiming to overcome this situation, we start by rewriting (B.9) as

$$\frac{\partial^2 \phi}{\partial t^2} = -A\phi, \tag{B.11}$$

where the differential operator $A : \mathcal{D}(A) \to \mathcal{H}$ is formally defined by

$$A = -V h^{ij} D_j \left(V D_i \phi \right) + m^2 V^2. \tag{B.12}$$

The operator A is not precisely defined because we did not specify a Hilbert space $\mathcal{H}$ nor a domain $\mathcal{D}(A)$ where A is supposed to act. In [69], Wald argues that if we define $\mathcal{H}$ as the space of square-integrable functions on Σ with measure given by $d\mu = V^{-1} d\Sigma$, where $d\Sigma$ is the natural volume element on Σ, and the domain of A as the set of smooth functions with compact support, i.e., $\mathcal{D}(A) = C_0^\infty(\Sigma)$, then A will be a positive[2] symmetric (but not necessarily self-adjoint) operator.

If we now replace (B.11) by

$$\frac{d^2 \phi}{dt^2} = -A_E \phi \tag{B.13}$$

where A_E denotes a self-adjoint extension of A, this allows us to write the solution

$$\phi(t) = \cos\left(A_E^{1/2} t\right) \phi_0 + A_E^{-1/2} \sin\left(A_E^{1/2} t\right) \dot{\phi}_0, \tag{B.14}$$

[2]The linear operator $A : \mathcal{D}(A) \to \mathcal{H}$ is said to positive if $\langle \psi, A\psi \rangle \geq 0$, for all $\psi \in \mathcal{H}$.

where the operators $\cos\left(A_E^{1/2}t\right)$ and $\sin\left(A_E^{1/2}t\right)$ are defined using the functional cauculus of self-adjoint operators [98, 99]. We note that the solution (B.14) matches the initial data in Σ and determines ϕ everywhere in spacetime. Besides, it can be shown that (B.14) coincides with the ordinary Cauchy evolution in the domain of dependence of Σ, $D(\Sigma)$, where Cauchy evolution is well defined [69].

The prescription for defining the dynamics of ϕ is then given in terms of a positive, self-adjoint extension A_E of A. The allowed initial data are given by the functions $\phi_0, \dot{\phi}_0 \in \mathcal{D}(A_E)$. In particular, all initial data with compact support $\phi_0, \dot{\phi}_0 \in C_0^\infty(\Sigma)$ are permitted, since $C_0^\infty(\Sigma) = \mathcal{D}(A) \subset \mathcal{D}(A_E)$. If the operator A has only one self-adjoint extension, the dynamics is then unambiguously defined. On the other hand, if A has more than one self-adjoint extension, the dynamics is not completely determined until we pick a specific extension A_E. In the next section, we illustrate how the process of choosing a specific extension of A is related to the prescription of extra boundary conditions on certain regions of spacetime. We will consider specifically the BTZ black hole as an instance of a nonglobally hyperbolic spacetime.

B.1.2 Scalar field in the BTZ black Hole

In this section, we apply the method described in Sec. B.1.1 to the scalar field in the exterior region of the static BTZ black hole. The spcacetime metric is given by Eq. (3.6), which we rewrite here for convenience,

$$ds^2 = -\left(-M + \frac{r^2}{l^2}\right)dt^2 + \frac{dr^2}{\left(-M + \frac{r^2}{l^2}\right)} + r^2 d\varphi^2, \tag{B.15}$$

where the horizon $r_h = l\sqrt{M}$ determines the horizon, M is the mass of the black hole, l is the anti-de Sitter curvature radius.

We start by separating the field variables with the *ansatz*

$$\phi(t, r, \varphi) = \frac{1}{r^{1/2}} \sum_m f_{m,\omega}(r) e^{-i\omega t} e^{im\varphi}. \tag{B.16}$$

Substituting in (B.9) and changing the radial coordinate to

$$x = \operatorname{arcoth}\left(\frac{r}{r_h}\right), \tag{B.17}$$

we find the differeential equation

$$Af_{m,\omega} = -\frac{d^2 f_{m,\omega}}{dx^2} + \frac{f_{m,\omega}}{\sinh^2(x)}\left[\nu^2 - \frac{1}{4}\right] + \frac{f_{m,\omega}}{\cosh^2(x)}\left[\sigma^2 + \frac{1}{4}\right] = \omega^2 f_{m,\omega}, \tag{B.18}$$

where we have defined $\nu^2 = 1 + m_\xi^2$ and $\sigma = ml/r_+$.

Since for eigenfunctions

$$\phi_{1,m} = \frac{1}{r^{1/2}} f_{\omega_1,m} e^{-i\omega_1 t} e^{im\varphi}, \qquad \phi_{2,n} = \frac{1}{r^{1/2}} f_{\omega_2,n} e^{-i\omega_2 t} e^{in\varphi}, \tag{B.19}$$

the inner product is

$$\langle \phi_{1,m}, \phi_{2,n} \rangle = \int \phi^*_{1,m}, \phi_{2,n} V^{-1} d\Sigma \sim \delta_{mn} \int_0^\infty f^*_{\omega_1,m}(x), f_{\omega_2,n}(x) dx, \tag{B.20}$$

we can consider the operator A in each m-subspace separately. Thus, we will study the (closable and densely defined) operator

$$A = -\frac{d^2}{dx^2} + \frac{1}{\sinh^2(x)}\left[\nu^2 - \frac{1}{4}\right] + \frac{1}{\cosh^2(x)}\left[\sigma^2 + \frac{1}{4}\right] \tag{B.21}$$

initially defined on the set of smooth functions with compact support on Σ, i.e., $C_0^\infty(\Sigma)$. The underlying Hilbert space is $L^2([0,\infty), dx)$.

Defining the auxiliar parameters

$$a = \tfrac{1}{2}(1 + \nu + i\sigma + i\omega) \qquad b = \tfrac{1}{2}(1 + \nu + i\sigma - i\omega) \qquad c = 1 + \nu \tag{B.22}$$

the general solution of (B.18) (for $a - b = i\omega \notin \mathbb{Z}$[3]) can be expressed as[4]

$$f_m(x) = B_1 f_{1m}(x) + B_2 f_{2m}(x) \tag{B.23}$$

where[5]

$$f_{1m}(x) = \sinh^{\nu+1/2}(x) \cosh^{-\nu-1/2-i\omega}(x)\ {}_2F_1\left(a, a-c+1; a-b+1; \operatorname{sech}^2 x\right), \tag{B.24}$$

$$f_{2m}(x) = \sinh^{\nu+1/2}(x) \cosh^{-\nu-1/2+i\omega}(x)\ {}_2F_1\left(b, b-c+1; b-a+1; \operatorname{sech}^2 x\right), \tag{B.25}$$

[3]For $a - b = i\omega \in \mathbb{Z}$, see [95].

[4]Hereafter, we suppress the indice ω in $f_{\omega,m}$.

[5]The same process applied to find linearly independent solutions of Eq. (3.31) can be used here.

B_1, B_2 are constants and ${}_2F_1(a,b;c;x)$ is the standard hypergeometric function.

Near the horizon, we have the behavior

$$|f_{1m}(x \to \infty)| \sim e^{x\,\mathrm{Im}(\omega)}, \qquad |f_{2m}(x \to \infty)| \sim e^{-x\,\mathrm{Im}(\omega)}, \tag{B.26}$$

and only one of these functions is square integrable. Which one of f_{1m}, f_{2m} is in $L^2((0,\infty],dx)$ depends on the signal of $\mathrm{Im}(\omega)$. For the root of ω^2 with $\mathrm{Im}(\omega) > 0$ ($\mathrm{Im}(\omega) < 0$) only f_{2m} (f_{1m}) is in $L^2((0,\infty],dx)$. With no loss of generality, we can take the root of ω^2 such that $\mathrm{Im}(\omega) > 0$ and set $B_1 = 0$ in (B.23). Supposing $1+\nu \notin \mathbb{Z}$[6] and using the transformation identities for the hypergeometric functions [85], we can rewrite (B.23) as

$$f_m(x) = B_2\, G_\nu(x) \left[\sinh^{2\nu}(x)\frac{\Gamma(b-a+1)\Gamma(c-a-b)}{\Gamma(1-a)\Gamma(c-a)}\psi_{1m} + \frac{\Gamma(b-a+1)\Gamma(a+b-c)}{\Gamma(b)\Gamma(1+b-c)}\psi_{2m}\right], \tag{B.27}$$

where

$$G_\nu(x) = \sinh^{-\nu+1/2}(x)\cosh^{i\sigma+1/2}(x) \tag{B.28}$$

and

$$\psi_{1m} = {}_2F_1\left(b, a; a+b-c+1; 1-\cosh^2 x\right), \tag{B.29}$$

$$\psi_{2m} = {}_2F_1\left(1-a, 1-b; c-a-b+1; 1-\cosh^2 x\right). \tag{B.30}$$

In order to find self-adjoint extensions of A — by applying the theorems B.1.1 and B.1.2 — it is necessary first to calculate the deficiency indices, n_+, n_-. This amounts to find the square-integrable solutions of $A^\dagger f = \pm i\lambda f$. With no loss of generality, we choose $\lambda = 2$ for convenience. Thus, the searched solutions are given by (B.27) with ω replaced by $\omega_\pm = i \pm 1$.

There are three cases to be considered according to the value of ν^2: (i) $\nu^2 \geq 1$, (ii) $0 < \nu^2 < 1$, (iii) $\nu^2 < 0$. For the case (iii), Garbaz et al. argue in [95] that the operator A is not positive, and since we are interested in positive extensions, this case can be ruled out. For the other cases, we have

[6]The case $1+\nu \in \mathbb{Z}$ can be treated similarly; see [95] for details.

(i) $\nu^2 \geq 1$: There are no square-integrable solutions to $A^\dagger f = \pm 2if$. In this case the deficiency indices are $n_+ = n_- = 0$ and there is only one self-adjoint extension of A according to theorem B.1.1.

(ii) $0 \leq \nu^2 < 1$: There are two square-integrable solutions to $A^\dagger f = \pm 2if$, one for each eigenvalue $\omega_\pm^2 = \pm 2i$. In this case the deficiency indices are $n_+ = n_- = 1$ and, according to theorem B.1.1, there is a one-parameter family of self-adjoint extensions of A. This family is parametrized by a phase $e^{i\alpha}$.

In case (i), the scalar field has an unambiguous time evolution since the self-adjoint extension of A is unique. On the other hand, in case (ii), there are several self-adjoint extensions, and we must pick one such extension to completely determine the dynamics of the field. In what follows, we will describe the relationship between the choice of a self-adjoint extension and the imposition of boundary conditions at the conformal boundary of the BTZ black hole. This will allow us to describe the possible evolutions of the field in bulk in terms of the boundary conditions at the conformal boundary.

Let us focus on the case with $0 < \nu^2 < 1$[7]. A solution f in the extended domain $\mathcal{D}(A_\alpha)$ can be expressed as

$$f_m(x) = f_{0m}(x) + f_+(x) - e^{i\alpha} f_-(x), \tag{B.31}$$

where $f_{0m} \in C_0^\infty(\Sigma)$ and $f_\pm$ are given by (B.27) with ω replaced by $\omega_\pm = i \pm 1$. The asymptotic behavior of f_m as $x \to 0$ ($r \to \infty$) is dictated by $f_m^\alpha = f_+ - e^{i\alpha} f_-$, which is given by

$$f_m^\alpha(x \to 0) = \sinh^{-\nu+1/2}(x) \left[a_\nu + b_\nu \sinh^{2\nu}(x) + \cdots\right], \tag{B.32}$$

where

$$a_\nu = -2\Gamma(\nu)e^{i\frac{\alpha}{2}} \left|\frac{\Gamma(1-i\omega_-)}{\Gamma(b_-)\Gamma(1+\nu-a_-)}\right| \sin\left(\frac{\alpha}{2} - \theta_a\right), \tag{B.33}$$

$$b_\nu = -2\Gamma(-\nu)e^{i\frac{\alpha}{2}} \left|\frac{\Gamma(1-i\omega_-)}{\Gamma(b_- - \nu)\Gamma(1-a_-)}\right| \sin\left(\frac{\alpha}{2} - \theta_b\right), \tag{B.34}$$

[7] The case $\nu = 0$ can be treated similarly.

and

$$\sin\theta_a = -\frac{\mathrm{Re}\left(\frac{\Gamma(1-i\omega_-)}{\Gamma(b_-)\Gamma(1+\nu-a_-)}\right)}{\left|\frac{\Gamma(1-i\omega_-)}{\Gamma(b_-)\Gamma(1+\nu-a_-)}\right|}, \qquad \sin\theta_b = -\frac{\mathrm{Re}\left(\frac{\Gamma(1-i\omega_-)}{\Gamma(b_--\nu)\Gamma(1-a_-)}\right)}{\left|\frac{\Gamma(1-i\omega_-)}{\Gamma(b_--\nu)\Gamma(1-a_-)}\right|}, \tag{B.35}$$

with constants a_- and b_- defined using (B.22) with ω replaced by ω_-. We notice that the values of α are in a one-to-one relation with the values of the ratio b_ν/a_ν, which can be any real number or $\pm\infty$. In order to better interpret these boundary conditions, we consider first the conformally coupled case ($\nu = 1/2$), for which the effective potential term in the expression (B.21) is regular at the boundary $x = 0$ and we have

$$\left.\frac{\left(df_m^\alpha/dx\right)}{f_m^\alpha}\right|_{x=0} = \frac{b_\nu}{a_\nu}. \tag{B.36}$$

We see that the choice $b_\nu/a_\nu = \pm\infty$ corresponds to the Dirichlet boundary condition, $f_m^\alpha\Big|_{x=0} = 0$, whereas the choice $b_\nu/a_\nu = 0$ corresponds to the Neumann boundary condition, $\left(df_m^\alpha/dx\right)_{x=0} = 0$. The other values of b_ν/a_ν correspond to Robin boundary conditions, in which a linear combination of f_m^α and df_m^α/dx is required to vanish at the boundary.

In the general case, $\nu \neq 0$, the potential term in (B.21) is divergent at $x = 0$ and the ratio $\left(df_m^\alpha/dx\right)_{x=0} = 0$ is not well defined. In spite of that, the dominant behavior of $G_\nu^{-1} f_m^\alpha$ as $x \to 0$ is governed by a_ν, whereas the dominant behavior of $d(G_\nu^{-1} f_m^\alpha)/dx$ is governed by b_ν. Thus the condition $a_\nu = 0$ may be defined as the *"generalized Dirichlet boundary condition"*, whereas $b_\nu = 0$ as the *"generalized Neumann boundary condition"*, and the other possible values of b_ν/a_ν define the *"generalized Robin boundary conditions"*.

Having described the possible self-adjoint extensions of the operator A in terms of boundary conditions at $x = 0$, we still have to ensure that these extensions are positive for the Wald's prescription to be well defined. Since the self-adjoint extensions of A are in a one-to-one relationship with the values of b_ν/a_ν, the requirement of positivity will impose some restrictions on b_ν/a_ν. In what follows, we examine what constraint b_ν/a_ν should obey in order to guarantee the positivity of the associated self-adjoint extension A_α.

Initially, we recall that it was already argued that (for $0 < \nu < 1$) A is positive in the set of compactly supported functions defined on Σ. Since the domain of an extension A_α of A is given by the sum (as vector spaces) of $C_0^\infty(\Sigma)$ and the one-dimensional space $\mathrm{Span}\{f_m^\alpha\}$, we have to show that A_α is positive in $\mathrm{Span}\{f_m^\alpha\}$. In the discussion below, we are going to find a sufficient condition for A_α to be positive by finding a necessary condition A_α would satisfy if it was nonpositive. The following discussion will make this point clearer.

Firstly, let us suppose that A_α is not positive in $\mathrm{Span}\{f_m^\alpha\}$, then there exists an eigenfunction $\tilde{f} \in \mathrm{Span}\{f_m^\alpha\}$ such that

$$A_\alpha \tilde{f} = \omega^2 \tilde{f}, \qquad \text{with} \quad \omega^2 < 0. \tag{B.37}$$

Let us take the square root $\omega_\lambda = -i\lambda$, with $\lambda > 0$. The asymptotic behavior of $\tilde{f}$ is given by

$$\tilde{f}(x \to 0) = \sinh^{-\nu+1/2}(x) \left[D\, \psi_{2m}|_{\omega=-i\lambda} + \sinh^{2\nu}(x)\, E\ \psi_{1m}|_{\omega=-i\lambda} \right], \tag{B.38}$$

where

$$D = \frac{\Gamma(1-i\omega_\lambda)\Gamma(\nu)}{\Gamma(b_\lambda)\Gamma(1+\nu-a_\lambda)}, \qquad\qquad E = \frac{\Gamma(1-i\omega_\lambda)\Gamma(-\nu)}{\Gamma(b_\lambda-\nu)\Gamma(1-a_\lambda)}, \tag{B.39}$$

and a_λ, b_λ were defined using (B.22) with ω replaced by $\omega_\lambda = -i\lambda$. Since $\tilde{f} \in \mathrm{Span}\{f_m^\alpha\}$, its asymptotic behavior as $x \to 0$ have to agree with asymptotics (B.31). Hence, we should have $E/D = b_\nu/a_\nu$, which implies

$$\left| \frac{\Gamma(b_\lambda)}{\Gamma(b_\lambda - \nu)} \right|^2 = \frac{\Gamma(\nu)}{\Gamma(-\nu)} \frac{b_\nu}{a_\nu}. \tag{B.40}$$

From the theorem 5.2 in [101] we have that the left hand side of (B.40) has a minimum when $\lambda = 0$, which means

$$\left| \frac{\Gamma(b_0)}{\Gamma(b_0 - \nu)} \right| < \left| \frac{\Gamma(b_\lambda)}{\Gamma(b_\lambda - \nu)} \right|. \tag{B.41}$$

From this inequality and the fact $\Gamma(-\nu)/\Gamma(\nu) < 0$ it follows that a necessary condition for A_α to be nonpositive is

$$\frac{b_\nu}{a_\nu} < -\left| \frac{\Gamma(-\nu)}{\Gamma(\nu)} \right| \left| \frac{\Gamma(b_0)}{\Gamma(b_0 - \nu)} \right|^2. \tag{B.42}$$

Thus we conclude that a sufficient condition for A_α to be positive is

$$\frac{b_\nu}{a_\nu} \geq -\left| \frac{\Gamma(-\nu)}{\Gamma(\nu)} \right| \left| \frac{\Gamma(b_0)}{\Gamma(b_0 - \nu)} \right|^2. \tag{B.43}$$